

AD-A126 048

CUMULATIVE DAMAGE MODEL FOR ADVANCED COMPOSITE
MATERIALS(U) GENERAL DYNAMICS FORT WORTH TX FORT WORTH
DIV K M LIECHTI ET AL JUL 82 F2M-7074

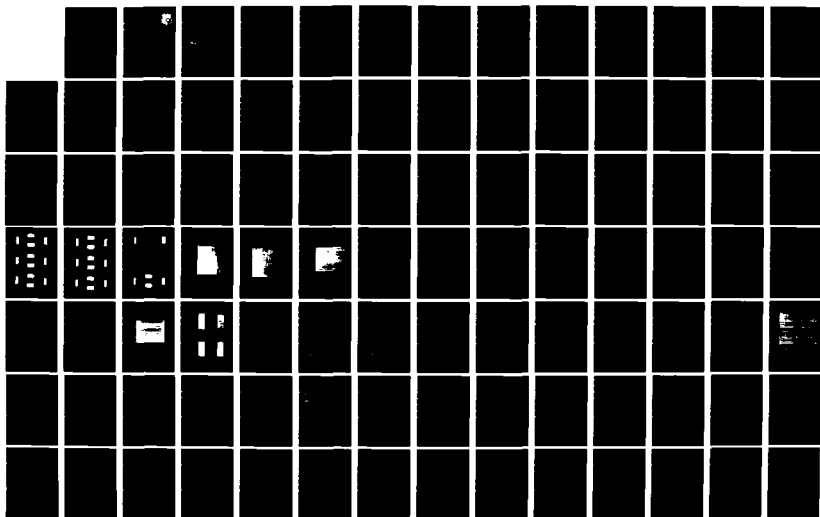
1/2

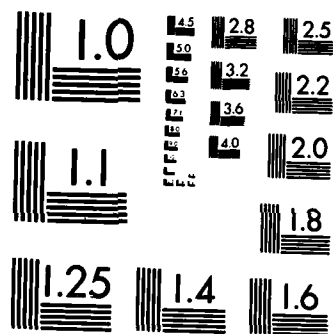
UNCLASSIFIED

AFWAL-TR-82-4094 F33615-81-C-5049

F/G 12/1

NL





MICROCOPY RESOLUTION TEST CHART
NATIONAL BUREAU OF STANDARDS-1963-A

AFWAL-TR-82-4094

CUMULATIVE DAMAGE MODEL FOR
ADVANCED COMPOSITE MATERIALS



GENERAL DYNAMICS
FORT WORTH DIVISION
P. O. BOX 748
FORT WORTH, TEXAS 76101

July 1982

Final Report for Period 23 February 1981 to 23 May 1982

Approved for public release; distribution unlimited.

ADA 126048
DTIC FILE COPY

MATERIALS LABORATORY
AIR FORCE WRIGHT AERONAUTICAL LABORATORIES
AIR FORCE SYSTEMS COMMAND
WRIGHT-PATTERSON AIR FORCE BASE OHIO 45433

DTIC
MAR 24 1983
A

83 03 24 001


NOTE

When Government drawings, specifications, or other data are used for any purpose other than in connection with a definitely related Government procurement operation, the United States Government thereby incurs no responsibility nor any obligation whatsoever; and the fact that the government may have formulated, furnished, or in any way supplied the said drawings, specifications, or other data, is not to be regarded by implication or otherwise as in any manner licensing the holder or any other person or corporation, or conveying any rights or permission to manufacture use, or sell any patented invention that may in any way be related thereto.


This report has been reviewed by the Office of Public Affairs (ASD/PA) and is releasable to the National Technical Information Service (NTIS). At NTIS, it will be available to the general public, including foreign nations.

This technical report has been reviewed and is approved for publication.


M. KNIGHT
Materials Research Engineer
Nonmetallic Materials Division


S. W. TSAI, Chief
Mechanics & Surface Interactions Branch
Nonmetallic Materials Division

FOR THE COMMANDER


F. D. CHERRY, Chief
Nonmetallic Materials Division

"If your address has changed, if you wish to be removed from our mailing list, or if the addressee is no longer employed by your organization please notify AFWAL/MLBM, W-PAFB, OH 45433 to help us maintain a current mailing list".

Copies of this report should not be returned unless return is required by security considerations, contractual obligations, or notice on a specific document.

Unclassified

SECURITY CLASSIFICATION OF THIS PAGE (When Data Entered)

REPORT DOCUMENTATION PAGE		READ INSTRUCTIONS BEFORE COMPLETING FORM
1. REPORT NUMBER AFWAL-TR-82-4094	2. GOVT ACCESSION NO. A126048	3. RECIPIENT'S CATALOG NUMBER
4. TITLE (and Subtitle) Cumulative Damage Model for Advanced Composite Materials		5. TYPE OF REPORT & PERIOD COVERED Technical - Final 23 Feb 81 - 23 May 82
		6. PERFORMING ORG. REPORT NUMBER FZM-7074
7. AUTHOR(s) K. M. Liechti, K. L. Reifsnider, W. W. Stinchcomb, D. A. Ulman		8. CONTRACT OR GRANT NUMBER(s) F33615-81-C-5049
9. PERFORMING ORGANIZATION NAME AND ADDRESS General Dynamics Corp. Fort Worth Division Fort Worth, TX		10. PROGRAM ELEMENT, PROJECT, TASK AREA & WORK UNIT NUMBERS 24190327
11. CONTROLLING OFFICE NAME AND ADDRESS Materials Laboratory Air Force Wright Aeronautical Laboratories AFSC, WPAFB, OH 45433		12. REPORT DATE July 1982
		13. NUMBER OF PAGES 182
14. MONITORING AGENCY NAME & ADDRESS (if different from Controlling Office)		15. SECURITY CLASS. (of this report) Unclassified
		15a. DECLASSIFICATION/DOWNGRADING SCHEDULE
16. DISTRIBUTION STATEMENT (of this Report) Approved for public release; distribution unlimited.		
17. DISTRIBUTION STATEMENT (of the abstract entered in Block 20, if different from Report)		
18. SUPPLEMENTARY NOTES		
19. KEY WORDS (Continue on reverse side if necessary and identify by block number) Cumulative damage, composite materials, stacking sequence, fatigue testing, multiple load histories, NDE, stiffness change, residual strength, environmental effects, models, property degradation.		
20. ABSTRACT (Continue on reverse side if necessary and identify by block number) Test coupons, taken from laminates of structural signifi- cance, have been developed. Their design allowed for one geometry to be used in tensile and compressive testing at strains of importance in engineering design. The response of four laminates, made up of four different laminate stacking sequences, to quasi- static tension and compression and tension-tension, (Continued)		

Unclassified

SECURITY CLASSIFICATION OF THIS PAGE(When Data Entered)

20. (Continued)

compression-compression and tension-compression loading was determined. The different damage modes and their chronologies were investigated using edge replication and X-ray radiography and then related to longitudinal and Poisson (transverse) stiffness and residual strength measurements. The damage was found to occur in a progressive and systematic manner, thus providing a sound basis for the property degradation approach taken in the modeling. At a given strain level, tension-compression fatigue loading was found to be the most critical loading mode as a result of transverse cracks induced under tension reducing the delamination resistance in compression. An initial investigation of environmental effects was undertaken through testing at the 250°F dry condition.

Models for the prediction of strength and life of unnotched laminates under cyclic tensile and compressive loading have been developed. The models for tensile loading are essentially complete, although refinements may be made as the experimental data is interpreted. The models for compressive behavior are postulated but not complete in the sense that competing damage mode concepts have not yet been incorporated. A basic description of the philosophy behind the models, the approach for certain generic cases and some illustrative example calculations are presented.

Unclassified

SECURITY CLASSIFICATION OF THIS PAGE(When Data Entered)

FOREWORD

This technical report describes the research conducted for the Materials Laboratory, Air Force Wright Aeronautical Laboratory, Air Force Systems Command, Wright-Patterson Air Force Base, OH 45433 under contract F33615-81-C-5049, with Mr. M. Knight (AFWAL/MLBM) as Project Engineer.

Dr. K. M. Liechti, GD/FWD Program Manager, acknowledges the work of his predecessor, Dr. J. E. Masters, who laid the foundations for the experimental portion of this work. At GD/FWD, Dr. Liechti was principally assisted by Mr. D. A. Ulman, also from the Materials Research Lab. The analytical work was contributed by Dr. K. Reifsnider of VPI and Dr. W. Stinchcomb, also of VPI, was responsible for experimental effort there.

Thanks also go to Messrs. C. P. Fisher and R. D. Bruner, Materials Research Lab, who conducted portions of the testing and Mr. J. H. Fruit, Chemistry Lab, who was responsible for specimen fabrication. The support of Messrs. R. Simonds and N. P. Black, Research Assistants at VPI, is also acknowledged.



A

TABLE OF CONTENTS

<u>Section</u>	<u>Page</u>
LIST OF ILLUSTRATIONS	vii
LIST OF TABLES	xiii
I INTRODUCTION	1
II SPECIMEN FABRICATION	3
2.1 Laminae Property Specimens	3
2.2 Test Coupon Design	3
2.3 Material Selection	10
2.4 Quality Assurance	11
III LAMINA-LAMINATE MATERIAL PROPERTIES	12
3.1 Lamina Material Properties	12
3.2 Laminate Material Properties	15
IV CHARACTERIZATION OF FAILURE MODES AND MECHANISMS	21
4.1 Nondestructive Test Techniques	21
4.2 Test Procedures	24
4.2.1 Quasi-Static Tension and Compression	24
4.2.2 Fatigue testing	25
4.3 Experimental Results	25
4.3.1 Failure Modes and Mechanisms in Type A Coupons	26
4.3.2 Failure Modes and Mechanisms in Type B Coupons	37
4.3.3 Failure Modes and Mechanisms in Type C Coupons	49

TABLE OF CONTENTS (Continued)

<u>Section</u>	<u>Page</u>
4.3.4 Failure Modes and Mechanisms in Type D Coupons	63
4.3.5 Summary of Test Results	74
V ENVIRONMENTAL FACTORS AND EFFECTS	80
5.1 Elevated Temperature Testing	80
5.2 Elevated Temperature Results	81
VI MODEL DEVELOPMENT	85
6.1 Modeling Approach	91
6.2 Models for Tensile Loading	97
6.2.1 Cumulative Damage Model	111
6.2.2 Illustrative Example	126
6.3 Models for Compressive Loading	148
REFERENCES	162
APPENDIX	166

LIST OF ILLUSTRATIONS

<u>Number</u>	<u>Title</u>	<u>Page</u>
1.	Lamina Tensile Specimen Geometry	4
2.	Test Coupon Geometry	5
3.	Interlaminar Normal Stress Distribution for 25/50/25 Laminates	8
4.	Definition of Buckling Stress and Strain	14
5.	DIB Enhanced X-Ray Radiographs - Type A, Quasi-Static Tension	27
6.	Edge Replica of Transverse Crack in 90° Laminae - Type A, Quasi-Static Tension	30
7.	Edge Replica of Transverse Crack in -45° Laminae - Type A, Quasi-Static Tension.	31
8.	Edge Replica of Longitudinal Cracking - Type A, Quasi-Static Tension	32
9.	Damage Modes and Chronology - Type A, Quasi-Static Tension	33
10.	Stiffness Change - Type A, Quasi-Static Tension	34
11.	Damage Modes and Chronology - Type A, Tension-Tension Fatigue	35
12.	Damage Modes and Chronology - Type A, Tension-Compression Fatigue	35
13.	Damage Modes and Chronology - Type B, Quasi-Static Tension	38
14.	Stiffness Change - Type B, Quasi-Static Tension	39
15.	Damage Modes and Chronology - Type B, Tension-Tension Fatigue	40
16.	Stiffness Change - Type B, Tension-Tension Fatigue	41

LIST OF ILLUSTRATIONS (Cont.)

<u>Number</u>	<u>Title</u>	<u>Page</u>
17.	Residual Strength Curve for Type B Coupons Under Tension-Tension Fatigue	42
18.	Edge Replica of Delamination in a Type B Coupon Under Compression-Compression Fatigue	43
19.	X-Ray Radiograph of a Delamination in Type B Coupon Under Compression-Compression Fatigue	44
20.	S-N Curve for Type B. Coupons Under Compression-Compression Fatigue	45
21.	Longitudinal Stiffness Change - Type B, Compression-Compression Fatigue	46
22.	Poisson Stiffness Change - Type B, Compression-Compression Fatigue	47
23.	Damage Modes and Chronology - Type B, Tension-Compression	48
24.	Damage Modes and Chronology - Type C, Quasi-Static Tension	50
25.	Stiffness Change - Type C, Quasi-Static Tension	51
26.	Damage Modes and Chronology - Type C, Tension-Tension Fatigue	52
27.	Edge Replicas Depicting Damage Modes in Type C Coupons Under Tension-Tension Fatigue	54
28.	Stiffness Change - Type C, Tension-Tension Fatigue	55
29.	Residual Strength Curve for Type C Coupons Under Tension-Tension Fatigue	56
30.	Stiffness Change - Type C, Compression-Compression Fatigue	57
31.	S-N Curve for Type C Coupons Under Tension-Compression Fatigue	58

LIST OF ILLUSTRATIONS (Cont.)

<u>Number</u>	<u>Title</u>	<u>Page</u>
32.	Damage Modes and Chronology - Type C. Tension-Compression Fatigue	59
33.	Edge Replica Demonstrating Successively Inward Interfacial Cracking in a Type C Coupon Under Tension-Compression	60
34.	Longitudinal Stiffness Change - Type C, Tension-Compression Fatigue	61
35.	Poisson Stiffness Change - Type C, Tension-Compression Fatigue	62
36.	Damage Modes and Chronology - Type D, Quasi-Static Tension	64
37.	Stiffness Change - Type D, Quasi-Static Tension	65
38.	Damage Modes and Chronology - Type D, Tension-Tension Fatigue	66
39.	Stiffness Change - Type D, Tension-Tension Fatigue	67
40.	Residual Strength Curve for Type D Coupons Under Tension-Tension Fatigue	68
41.	S-N Curve for Type D Coupons Under Tension-Compression Fatigue	69
42.	Edge Replicas of the Progression of Damage in Type D Coupons Under Tension-Compression Loading	70
43.	Damage Modes and Chronology - Type D, Tension-Compression Fatigue	71
44.	Longitudinal Stiffness Change - Type D, Tension-Compression Fatigue	72
45.	Poisson Stiffness Change - Type D, Tension-Compression Fatigue	73
46.	Summary of Quasi-Isotropic Quasi-Static Tension Results	76
47.	Summary of Quasi-Isotropic Tension-Tension Fatigue Results	77

LIST OF ILLUSTRATIONS (Cont.)

<u>Number</u>	<u>Title</u>	<u>Page</u>
48.	Quasi Isotropic Life and Residual Strength Data	78
49.	Stiffness Change - Type A, 250°F, Quasi-Static Tension	82
50.	Stiffness Change - Type A, 250°F, Quasi-Static Compression	83
51.	Schematic of the Long-Term Fatigue Behavior of Composite Laminates	93
52.	Stiffness Reduction for a Fatigue Specimen Loaded at an Amplitude of 70% of the Ultimate Strength	95
53.	Longitudinal Young's Modulus Reduction for a [0/±45/0] _s Graphite Epoxy Laminate Cycled at 0.85 of the Static Ultimate Strength, and a [0/90] ₂ Glass Epoxy Specimen Cycled at 0.6 of the Static Ultimate Strength	96
54.	Crack Spacing in -45 ply of [0/90/±45] _s Graphite Epoxy Laminates Under Cyclic and Quasi-Static Loading	98
55.	Moire Fringe Pattern of a [0/90] ₃ Laminate Between Cracked Sections in the 90° Plies.	103
56.	Predicted and Observed Strain Distributions in the 0° Plies of a [0/90] ₃ Laminate Between Cracked Sections of the 90° Plies.	104
57.	General Schematic Representation of Local Net-Section Stress Situation Near a Matrix Crack	105
58.	Interlaminar Stresses Near the Tip of a Matrix Crack in a 90° Ply of a [0/±45/90] _s Graphite Epoxy Laminate	107
59.	Local Crack Coupling and Delamination Near Matrix Cracks	108

LIST OF ILLUSTRATIONS (Cont.)

<u>Figure</u>	<u>Title</u>	<u>Page</u>
60.	Schematic of Interior Delamination and Crack Growth	109
61.	Damage Modes During Fatigue Loading of Composite Laminates	112
62.	Approach to Cumulative Damage Model Development Contrasted with Fracture Mechanics Concepts	115
63.	Proposed Degradation Equation	116
64.	Role of Mechanics Analysis in Cumulative Damage Model	117
65.	Phenomenological Inputs to the Cumulative Damage Model	119
66.	Experimental Inputs to Degradation Model	120
67.	Scenario for Tension-Tension Cyclic Loading of a Laminate which has No Major Delamination Mode	122
68.	Scenario for Tension-Compression Cyclic Loading of a Laminate for which Edge Delamination Controls Behavior	123
69.	Flow Diagram of Model Use Procedure	125
70.	Linear Approximations of the Reduction of Normalized Residual Strength as a Function of Fraction of Fatigue Life	127
71.	Nonlinear Approximations of the Reduction of Normalized Residual Strength	132
72.	Residual Strength Observations and Calculated Values for Two-Step Spectrum Loading	133
73.	Linear Approximation of Residual Life for Spectrum Loading	135
74.	Predicted Residual Lives for High-Low and Low-High Spectral Fatigue Loading	136

LIST OF ILLUSTRATIONS (Cont.)

<u>Figure</u>	<u>Title</u>	<u>Page</u>
75.	Damage Rate Modifier Schematic Representation	138
76.	Modeling Concepts for Residual Life Determinations	140
77.	Computational Sequence for Tension-Tension Fatigue	142
78.	Computational Relationships in Sequence for Residual Property Determination in Tension-Tension Fatigue	143
79.	Damage Rate Function as a Function of Cycles	146
80.	Residual Strength Curve and Life Calculation for T300-5208 [0/90/+45] _s Laminate Under Tension-Tension Fatigue Loading at a Constant Amplitude of 347.6 MPa	149
81.	Edge View of Laminate Loaded in Cyclic Compression Showing Delamination Near the Specimen Surfaces	151
82.	Idealized Longitudinal Delamination Schematic	152
83.	Dependence of Longitudinal Delamination on Ligament Length	154
84.	Dependence of Longitudinal Delamination Growth on Ligament Thickness	155
85.	Schematic of Predicted Longitudinal Delamination Growth Pattern	157
86.	Delamination Growth Across Specimen Width and the Attendant Stiffness Change as Described by O'Brien	158
87.	Proportionality Between Total Strain Energy Release Rate and Across-the-Width Delamination Growth Rate as Described by O'Brien	159

LIST OF TABLES

<u>Number</u>	<u>Title</u>	<u>Page</u>
1	Summary of Laminate Configurations	7
2	Lamina Tensile Properties	16
3	Lamina Compressive Properties	17
4	Summary of Lamina Engineering Properties	18
5	Laminate Tensile and Compressive Properties	20
6	Test Matrix for the Characterization of Damage Development/Stiffness Change	22
7	Example: $[0/90/\pm 45]_S$, T300-5208	101
8	Residual Strength Predictions	130

SECTION I

INTRODUCTION

The use of advanced composite materials for aerospace structural applications has evolved as a result of the advantages they offer in such areas as strength-to-weight ratio and ease of manufacture. As the use of advanced composites as primary load carrying structural elements becomes more attractive and realistic, so the need to analytically predict the composites performance, particularly, service life increases. A life prediction methodology can also be used in the optimization of designs and materials.

The overall objective of this program is to develop a cumulative damage model for advanced composite materials. This involves the development of analytical models and experimental procedures for accurately predicting and characterizing the mechanical response of advanced composites which have been subjected to conditions representative of those seen in service.

This report reviews the achievements of the first of three phases into which the program has been divided. The objective of this initial model development phase was to determine and model the effects of basic parameters on the damage accumulation process. In the second phase, the model will be refined on the basis the results of this first phase and further experimentation. The model is to be verified in the third phase.

The objective of the first phase of the investigation was the development of an initial modeling concept and the identification of key parameters. The technical components of the investigation that were required to fulfill these objectives were conducted in five interrelated experimental and analytical tasks that may be briefly described as follows:

- o Specimen Fabrication Design - Fabrication and quality assurance of coupons to be used in lamina property determination and the characterization failure modes and mechanisms.
- o Lamina and Laminate Material Properties - Tensile and compressive testing to determine the moduli, Poisson's ratios, strength and ultimate strain of the 45° laminae and the laminates fabricated above.

- o Failure Mode and Mechanisms Characterization - Monitoring of damage development during quasi-static tension and compression and tension-tension, compression-compression and tension-compression fatigue testing using stiffness measurements, edge replication and enhanced X-ray radiography techniques.
- o Environmental Factors and Effects - Monitoring of damage development during quasi-static tension and compression and tension-compression fatigue tests at the environmental condition of 250°F, dry using stiffness measurements.
- o Model Development - The conception and development of an analytical cumulative damage model using a property degradation approach. The model development reflects the observations made during experimental investigations in an iterative process of observation and refinement.

The procedures and results of the components of the investigation, briefly outlined above, are now discussed in the following sections.

SECTION II

SPECIMEN FABRICATION

Details regarding the design, material choice and quality assurance of the specimens used in material property determination and in mechanical testing for the characterization of damage modes are provided in the following sections. The 0° , 90° and $\pm 45^\circ$ laminae were used to determine lamina mechanical properties. Test coupons made up of four different stacking sequences were tested to characterize the damage accumulation process.

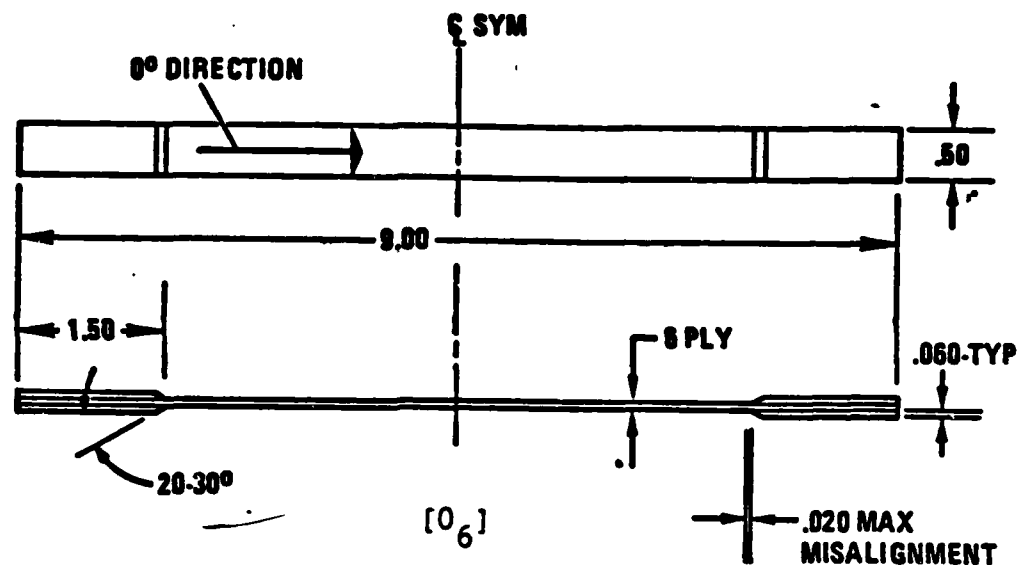
2.1 Laminae Property Specimens

Since the cumulative damage models developed in this program are based on a property degradation approach, it is important to obtain the mechanical properties of 0° , 90° and $\pm 45^\circ$ laminae. The mechanical properties of longitudinal elastic modulus, Poisson's ratio, strength and ultimate strain were determined from standard tensile and compressive testing. The actual properties of the different laminae and limitations of the testing machines led to the use of three different specimen geometries.

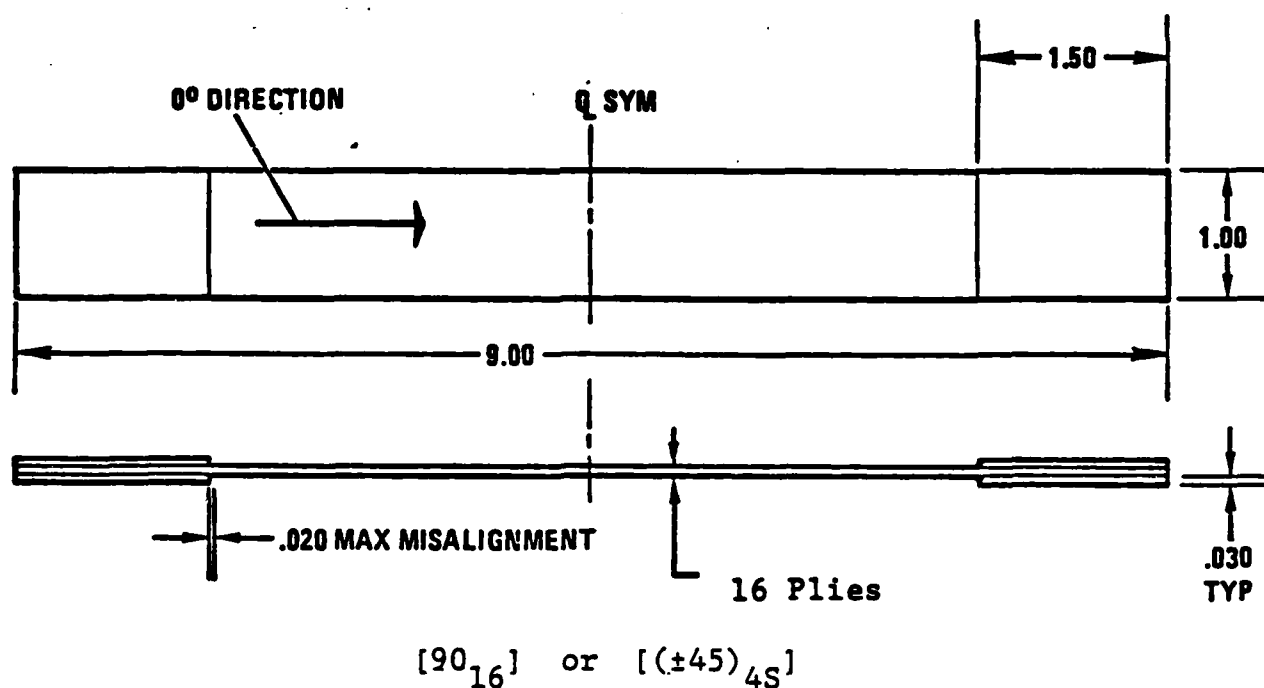
Two specimen geometries were used in the tensile tests. The first, for 0° laminae, is shown in Figure 1a. It was 6 plies thick and had a 7" x 0.5" gage length. The coupons used for the 90° and $\pm 45^\circ$ laminae tensile testing were thicker and wider at 16 plies and 1 inch, respectively (Figure 1b). The geometry of the specimens used in the compression testing of 0° , 90° and $\pm 45^\circ$ laminae was based on that of the test coupons, whose design will be discussed in the next section. The dimensions are the same as those shown in Figure 2 (test coupon geometry) except that the thickness of the 0° compression specimens was 24 plies instead of 48.

2.2 Test Coupon Design

The methodology developed during this program should define the generic response of graphite epoxy laminates. It is therefore important that the selected specimen geometry should not unduly bias the experimental results on which the modeling is to be based. The specimens were to be subjected to loading conditions of quasi-static tension and



(a) 0° Lamina Tensile Specimen Configuration



(b) 90°, ±45° Lamina Tensile Specimen Configuration

Figure 1 Lamina Tensile Specimen Geometry

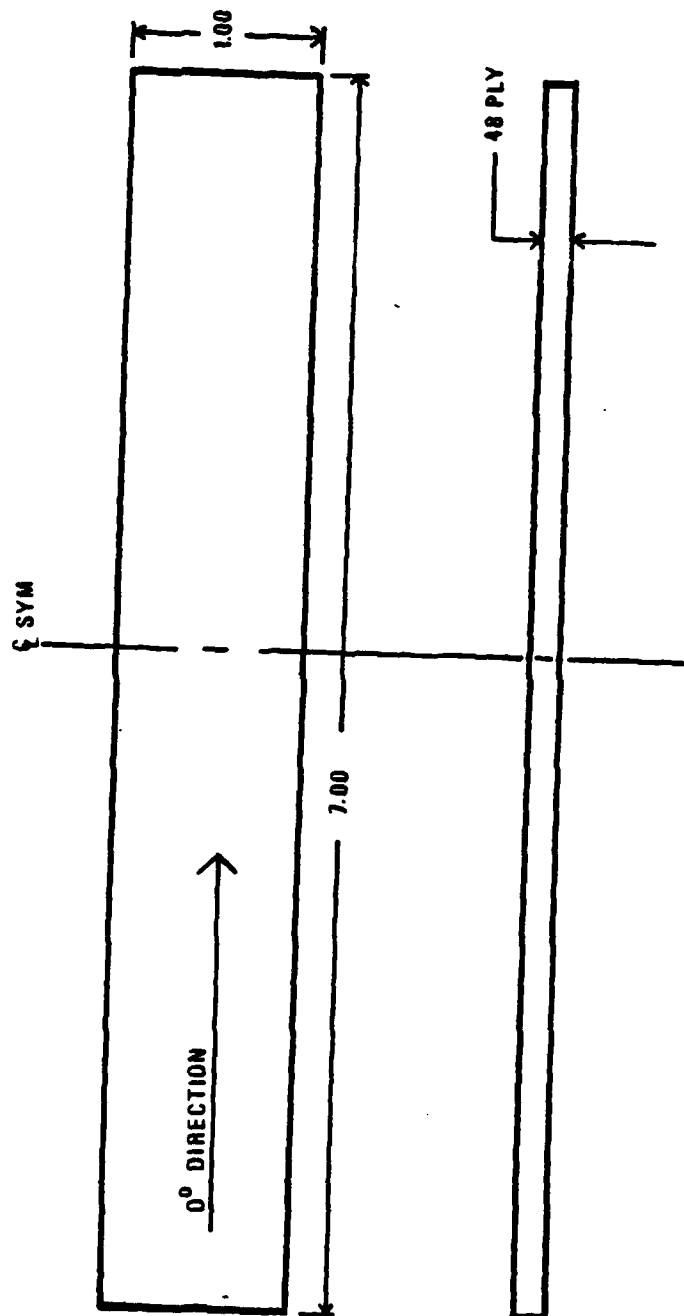


Figure 2 Laminate Specimen Configuration

compression and tension-tension, compression-compression and tension-compression cyclic testing. At the same time, NDE and stiffness measurements were to be conducted in order to monitor damage development. These considerations led to the following desirable features in the coupon design.

In order to avoid potential scaling problems which could occur if different geometries were used for different loading cases (e.g., thin tensile coupons and thick compression coupons), it was desirable that only one geometry be required for testing under all loading conditions. It was also felt that the specimens should exhibit measurable changes in properties (stiffness, strength) with damage development and that they should be easily investigated nondestructively. Edge effects were to be minimized within the constraints of reasonable cost of fabrication and testing.

Thick, non-supported coupons (Figure 2) were chosen in preference to honeycomb core sandwich beams and thinner coupons with anti-buckling supports for their relative cost advantages, ease of access for NDE investigation, and well-defined stress distribution. They were designed such that they resisted buckling under compressive loads yet were not so strong that excessively large loads were required to induce damage. The four-inch unsupported length that remained after allowance for 1-1/2 inch gripping length at each end resulted in a central, two-inch axial gage length that contained uniform stresses. The specimen width (one inch) provided for a test section that was not influenced by edge stresses and would stabilize Poisson stiffness (axial stress divided by transverse strain) readings.

Four laminates were investigated during this first phase. Three of the laminates were in the same laminate family represented by 25/50/25, which represents percentages of 0°, $\pm 45^\circ$ and 90° laminae, respectively. They were stacked in different orders so as to determine the effect of stacking sequence on damage development through variations in constraining plies and in interlaminar stresses. The fourth laminate belonged to the 10/45/45 family and defines a low stiffness extreme of laminate families. The stacking sequences and designations (for easier reference) of the four laminates are listed in Table 1.

As mentioned previously in the general design goal discussion, the effects of the specimen geometry on the laminate response must be minimized and clearly defined so that they may be accounted for in the cumulative damage model. Specimen buckling has been of prime concern in the

Table 1 Summary of Laminate Configurations

<u>Laminate Family</u>	<u>Stacking Sequence</u>	<u>Designation</u>
25/50/25	$[0/\pm 45/90/90/\mp 45/0]_{3S}$	A
25/50/25	$[0/90/\pm 45/\mp 45/90/0]_{3S}$	B
25/50/25	$[0/\pm 45/90/-45/-45/90/+45/0]_{3S}$	C
10/45/45	$[0[+45/90/90/\mp 45/90/90/\pm 45/90]_S 0]_S$	D

discussion of specimen design thus far. However, the presence of interlaminar stresses due to the edge singularity in coupon specimens is also an important factor in specimen design. Since coupon specimens have traction free edges, these stresses can never be eliminated. To define the specimen response to these stresses, three 25/50/25 laminate stacking sequences have been proposed. This will provide data representative of both tensile and compressive interlaminar normal stress conditions.

Figure 3 displays the total through-the-thickness stress distribution (interlaminar normal stress, σ_z , plus residual thermal stresses) developed in the three 25/50/25 laminates at 0.3% uniaxial strain. These stress values were determined by applying basic laminated plate theory to determine the in-plane stresses for each lamina and by then applying the Pipes-Pagano approximation. The figure shows that under applied axial tensile loading, the Type A laminate develops tensile stresses while the Type B laminate develops compressive stresses of approximately the same

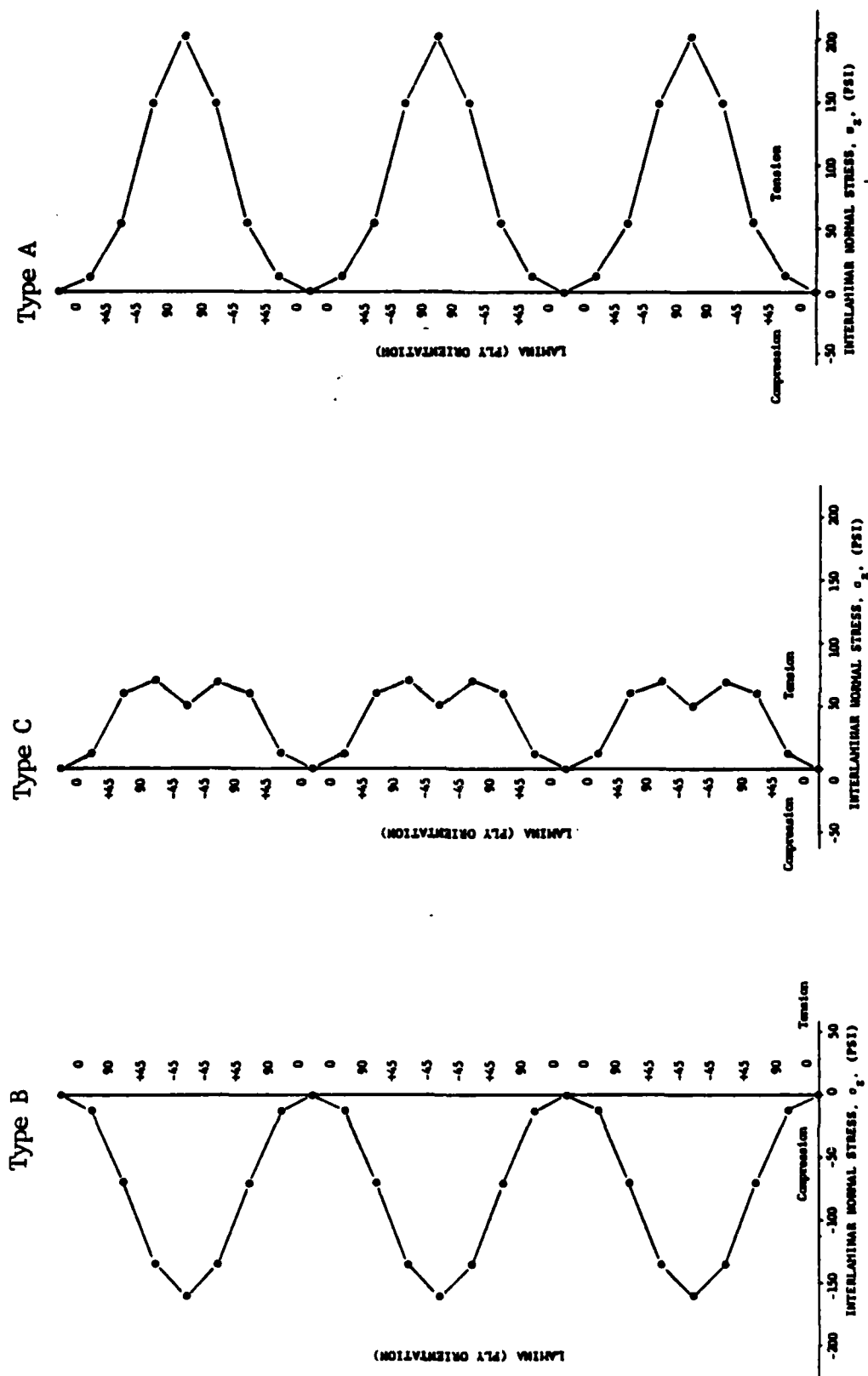


Figure 3 Interlaminar Normal Stress Distribution For 25/50/25 Laminates

magnitude. The third 25/50/25 laminate, Type C, develops relatively small tensile interlaminar normal stresses.

Three 25/50/25 laminates were proposed to examine three separate conditions: Tensile under tensile load; tensile under compressive load and minimum stresses under both load conditions. The objective here was to separate all those possible interactions of interlaminar stress and load. The laminates were also chosen because their profiles contained solely tensile or solely compressive stresses (no mixed tensile/compressive profiles). This was done to simplify the study of the damage development mechanisms active within the specimen. Since fully reversed tension-compression fatigue will be one of the load conditions, a laminate with a mixed tension/compression profile could tend to delaminate at one location under tensile load and at another location under compressive load. Addressing this interaction seemed to be beyond the scope of the Phase I effort. The fact that the laminates develop tensile and compressive profiles with approximately equal peak magnitudes will facilitate comparison of their effect on damage development.

The applied analysis predicts that these laminates will demonstrate several interesting features. As the figures show, sandwiching characteristic groups of eight lamina to produce the required 48 ply thick laminate in this manner results in a distribution which consists of a series of repeated characteristic profile steps. For purposes of data presentation, the six characteristic groups will be referred to as ply-groups 1 through 6. Applying laminate analysis to determine the stresses in each lamina and the Pipes-Pagano approximation uses these values to predict the interlaminar normal stresses, the predicted amplitudes of the individual ply group profiles are equal.

Another by-product of that approximate analysis, namely, the assumption that the stresses are active over a region which extends inward from the specimen edge a distance equal to the specimen thickness, indicates that the magnitude of these stresses rapidly decreases with increased thickness. For example, applying the approximation to an eight ply thick $[0/\pm 45/90]_S$ laminate subjected to an axial strain of 0.3% indicates that a tensile stress of 7500 psi will exist at the $90^\circ/90^\circ$ midplane. However, applying the analysis to a 48 ply thick $[0/\pm 45/90/90/\pm 45/0]_{3S}$ laminate under an equal strain indicates that the magnitude of σ_z at the $90^\circ/90^\circ$ interface (now one of six peaks) is reduced to 208 psi. In short, since the stresses are now postulated to act over a larger area, their magnitude is decreased. This decrease is equal to the ratio of the squares of the laminate

thicknesses, i.e., $t_{8\text{ply}}^2/t_{48\text{ply}}^2$ or $1/36$ in this case. The validity of this predicted reduction in σ_z is verified qualitatively by experimental observation. Edge replication of $[0/\pm 45/90]_s$ laminates loaded in axial tension reveals that at an applied stress of 71.6 ksi (0.9% strain) delamination extends along the entire specimen length. However, similar examination of a $[0/\pm 45/90]_{6s}$ laminate load to tensile failure at 20 KIP (75.7 ksi or 1.01% strain) revealed no indications of longitudinal cracking.

If the predicted interlaminar normal stress values are accurate, edge delamination does not appear to be a factor in the damage development of the laminates under quasi-static loading even at loads near failure. This will satisfy one of the design goals stated earlier: to minimize the effect of specimen geometry on the material response.

Although delamination does lead to reduced laminate stiffness and strength, the growth of delamination has not been the focus of this program. It has been modeled by a number of investigators and is included as a special case of the model developed here. Minimizing the singularity at the edge of the specimen allows matrix cracks to develop which can, as will be shown later, be initiation sites for delamination growth, particularly in larger structural elements where ply terminations, holes, etc., may not exist.

2.3 Material Selection

Material selection was based on the following criteria: (1) application of the material to aerospace structures; (2) availability of well-defined material properties (i.e., lamina mechanical property values required for basic analysis); (3) ability to conduct an effective quality assurance program; and (4) ability to fabricate laminates.

When the program began, two graphite/epoxy systems were used by GD/FWD in the production of horizontal and vertical tail skins for its F-16 aircraft. These systems are Varmco's T300/5208 and Hercules' AS/3502. Both material systems satisfy the criteria listed above and were considered viable candidates for use in this investigation. T300/5208 was the first material to meet aerospace industry glass transition temperature requirements and is perhaps more widely used. However, AS/3502 was developed and qualified as an alternate material and is being considered for use by many other aerospace manufacturers. AS/3502 was selected due to its availability at the time the program was initiated.

2.4 Quality Assurance

All specimens that were used in this program were accepted, processed and inspected in accordance with standard GD/FWD material and processing specifications. In addition, NDE techniques were used to screen the coupons following machining and edge polishing. Only defect-free coupons were tested. Records of ultrasonic, X-ray radiography and edge replica inspections of the initial state were made for later comparison with similar characterizations that were made during the testing. The details of the Quality Assurance Plan appear in Appendix A.

SECTION III

LAMINA-LAMINATE MATERIAL PROPERTIES

The cumulative damage models developed in this program require the basic mechanical properties of the lamina (i.e., tensile and compressive strengths, moduli, Poisson's Ratio, etc.) as input parameters. An accurate and complete set of these values is therefore most important. A series of tests were performed to experimentally determine these values for 0°, 90° and $\pm 45^\circ$ lamina fabricated from the same batch of material that was used to fabricate the laminates studied in the program. These data were statistically compared to the large data base gathered by General Dynamics in conjunction with material qualification for design of the F-16. This provided sufficient data on the material properties to determine the parameters of the properties statistical distribution.

The material properties of all laminates examined in Phase I of this program were also determined. The mechanical tests were used to guide the test effort in the failure modes and mechanism task as well as provide data on the initial conditions prior to any testing.

3.1 Lamina Material Properties

A series of monotonic tension and compression tests was conducted in order to determine the mechanical properties of 0°, 90° and $\pm 45^\circ$ laminae in the environmental conditions of room temperature, dry and 250°F, dry. The geometries of the specimens that were used were described in Section 2.1 and appear in Figures 1 and 2.

Three strain gages were mounted on each specimen. Two gages were used to monitor axial or longitudinal strain while the third gage measured the transverse or Poisson strain. The longitudinal gages were mounted on opposite faces of the specimen and were monitored separately to evaluate any specimen bending or buckling. Each strain gage output was plotted versus applied load. Experimental results included: ultimate stress and strain, Poisson's Ratio, and modulus of elasticity. These values were determined for both tensile and compressive loading. The axial stress at 3000 and 4500 microstrain was identified as a key value and was also recorded.

These tests determined all the mechanical properties needed to totally populate the reduced lamina compliance matrix. E_{11} and ν_{12} have been determined from the 0° lamina tests. E_{22} was calculated as the initial slope of the stress-strain curve during the 90° lamina tests. ν_{21} was also calculated from the 90° tests and can be verified²¹ using the relation

$$\nu_{21} = \nu_{12} \frac{E_{22}}{E_{11}}$$

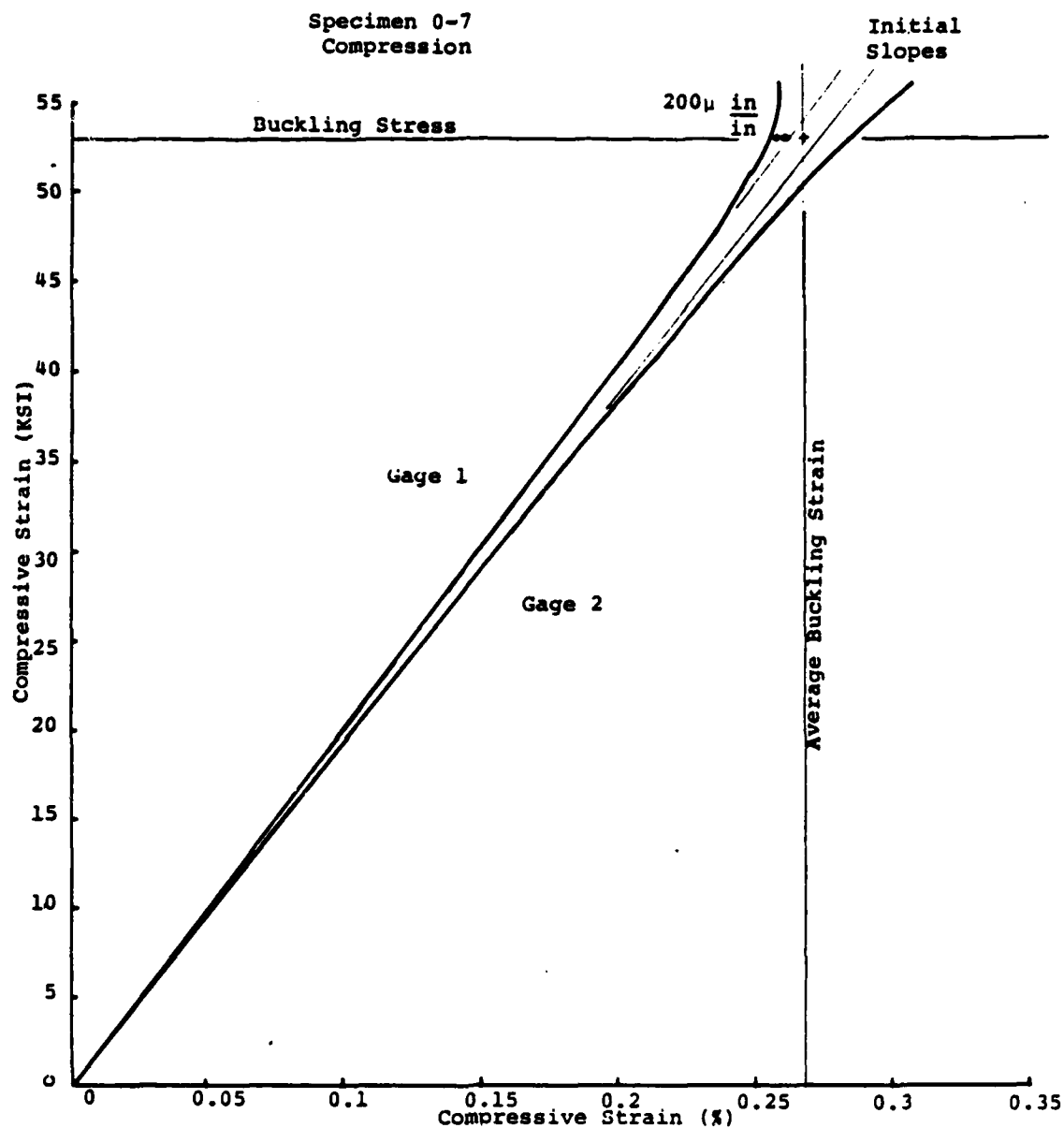
The shear modulus G_{12} was determined by using the relationship

$$G_{12} = \frac{E_x}{2(1+\nu_{xy})}$$

where E_x and ν_{xy} are respectively the modulus of elasticity and Poisson's Ratio of the $\pm 45^\circ$ specimen.

The experimentally-determined values of E_{11} , E_{22} , ν_{12} and G_{12} can be used in laminate analysis to compute the stresses and strains in each ply if the applied loads are known. Laminate analysis is an integral part of the proposed model. It will be used to determine the initial stress distribution and to redistribute the internal stresses after damage has occurred. Ultimate values of tensile and compressive stress and strain are also required in the determination of damage initiation. It should be noted that failure in the $\pm 45^\circ$ lamina tests is not related to the ultimate values of lamina shear stress or lamina shear strain.

The tensile tests were conducted at a constant displacement rate of 0.05 inches per minute until the specimen failed. The stress and strain at failure were defined as the ultimate stress and strain. The compression tests were conducted at the same displacement rate until the onset of buckling occurred. The point of buckling instability was defined as the stress at which one of the stress-strain curves indicated a nonlinear deviation from the initial tangent line of 200 microstrain in a direction of increasing stiffness (Fig. 4). The buckling strain was taken to be the average strain measured by the two strain gages at the buckling stress. The severely nonlinear behavior exhibited by the $\pm 45^\circ$ coupons under compression



Stress-Strain Plot for 0° Compression Test

Figure 4 Definition of Buckling Stress and Strain

meant that no measurements of buckling stress and strain were made.

The room temperature, dry environmental condition was provided by the ambient laboratory conditions with no enclosure surrounding the specimen. In the elevated temperature tests, the specimens were heated by wrapping aluminum foil around the specimen and then winding electrical resistance heating tape on top of the aluminum. A VARIAC transformer was used to regulate the heat provided to the specimen, the specimen temperature being measured by a centrally mounted thermocouple. The uniformity of the temperature field across the test section had been previously ascertained by the use of three thermocouples. Manual control provided a temperature of 250°F, $\pm 1^\circ\text{F}$.

The results of the lamina testing under tensile and compressive loading are shown in Tables 2 and 3, respectively, for the room and elevated temperature conditions. The corresponding engineering mechanical properties, again for tension and compression, are summarized in Table 4. As can be seen from Table 4, the higher temperature resulted in lower moduli, the larger decreases being seen in the matrix-dominated properties.

3.2 Laminate Material Properties

The same material properties of modulus, Poisson's ratio, stress at 3000 and 4500 microstrain, and ultimate stress and strain that were measured for laminae were also measured for the four laminates investigated in the characterization of failure modes and mechanisms.

The tests also provided information pertinent to the various damage monitoring tests performed in Phase I. For example, the load-strain curves developed during these mechanical property characterization tests were used to identify structurally significant points of investigation (in terms of load levels) in the damage monitoring tests. The ultimate stress and strain values determined in these tests helped to define the fatigue load levels investigated in those failure mode/mechanism characterization tests. Finally, the stiffness and strength data gathered in these tests were compared to values recorded during the damage monitoring tests.

The specimens were monotonically loaded at a load rate of 4,000 lbs/min. Two longitudinal and one transverse strain gage were used to measure the strains. The same

Table 2 Lamina Tensile Properties

Property	0° Lamina		90° Lamina		45° Lamina	
	Room Temp	250°F	Room Temp	250°F	Room Temp	250°F
Modulus (ksi)	20.5	19.70	1.47	1.27	2.96	2.44
Poisson's Ratio	0.31	0.295	0.027		0.78	0.63
Stress at 3000 $\mu\epsilon$ (ksi)	62.0	59.1	4.48	3.91	8.77	6.88
Stress at 4500 $\mu\epsilon$ (ksi)	93.9	88.8	6.64	5.61	12.40	9.62
Ultimate Stress (ksi)	246.0	222.0	7.31	6.57	26.9	22.0
Ultimate Strain (%)	1.12	1.08	0.50	0.54	1.55	4.55

Table 3 Lamina Compressive Properties

Property	0° Lamina		90° Lamina		±45° Lamina	
	Room Temp	250°F	Room Temp	250°F	Room Temp	250°F
Modulus (MSI)	20.1	19.22	1.48	1.47	2.90	2.62
Poisson's Ratio	0.33	0.311	0.025	0.021	0.70	0.74
Stress at 3000 $\mu\epsilon$ (KSI)	(1)	(1)	4.47	4.36	8.5	7.6
Stress at 4500 $\mu\epsilon$ (KSI)	(1)	(1)	6.72	6.49	12.2	10.6
Buckling Stress (KSI)	50.1	39.0	12.18	8.67	(2)	(2)
Buckling Strain (KSI)	0.257	0.204	0.826	0.611	(2)	(2)

(1) did not obtain this strain level before buckling occurred

(2) due to an extensive non-linear stress-strain relationship the buckling point was undistinguishable

Table 4 Summary of Lamina Engineering Properties

Property	Tension		Compression	
	Room Temp	250°F	Room Temp	250°F
E_{11} (MSI)	20.5	19.70	20.1	19.22
E_{22} (MSI)	1.47	1.27	1.48	1.47
G_{12} (MSI)	0.83	0.75	0.85	0.75
ν_{12}	0.31	0.30	0.33	0.31
ν_{21}	0.022	0.019	0.024	0.024

definition of buckling (200 microstrain offset) as was used in the laminae tests was incorporated in the laminate compression tests. The results of the tension and compression tests are summarized in Table 5.

Coupon types A, B and C have the same percentage of 0° , $\pm 45^\circ$ and 90° laminae but vary in stacking sequence. The stacking sequences in Types A and C are such that tensile interlaminar normal stresses are produced under a tensile load whereas the stacking sequence comprising the type B coupon produces a compressive interlaminar normal stress under a tensile load. As a result, the ultimate tensile stress in the Type B coupons is somewhat greater (Table 5). Table 5 shows that the buckling stress under a compressive load is also greatest in the Type B coupons. The Type D coupons, which have less 0° plies than the Type A, B and C coupons therefore have a lower modulus (Table 5). Type D laminates have a higher percentage of 90° lamina which results in a lower Poisson's ratio. The ultimate and buckling strains in the Type D coupon are greater than those of the 25/50/25 family.

Table 5 Laminate Tensile and Compressive Properties

Property	Type A		Type B		Type C		Type D	
	Tension	Compression	Tension	Compression	Tension	Compression	Tension	Compression
Modulus (MSI)	7.61	7.47	7.48	7.39	7.31	7.16	4.45	4.42
Poisson's Ratio	0.31	0.30	0.31	0.30	0.29	0.28	0.22	0.22
Stress at 3000 $\mu\epsilon$ (KSI)	23.0	22.0	23.0	21.7	22.4	21.3	13.6	13.2
Stress at 4500 $\mu\epsilon$ (KSI)	34.6	32.5	34.6	32.3	33.6	31.6	20.3	19.7
Ultimate Stress (KSI)	72.9	40.4	77.9	51.6	72.3	43.0	49.0	37.0
Ultimate Strain (%)	0.99	0.53	1.02	0.74	1.01	0.63	1.26	0.89

SECTION IV

CHARACTERIZATION OF FAILURE MODES AND MECHANISMS

The overall objective of this task is to quantify total material response through careful experimentation. Damage induced in selected laminates under the fundamental loading conditions of monotonic tension and compression, tension-tension, compression-compression and tension-compression fatigue were thoroughly catalogued. Damage defined, for the purposes of this program, as lateral and transverse cracking and delamination growth. In addition to establishing the chronology and location of damage development, changes in specimen stiffness and reductions and strength were also established. These material responses were related to the damage states existing in the specimens at that time. Both destructive and nondestructive test techniques were employed to monitor the damage development. The techniques applied included surface replication, enhanced X-ray radiography and stiffness measurements. This data was input to the cumulative damage model developed in this program.

Table 6 contains the test matrix for the tests which were performed to support the initial model development. The general philosophy of Phase I is reflected in the test matrix. In this phase, the model was formulated. To establish a broad base of applicability, material parameters (e.g., stacking sequence and percentage of 0° lamina) were varied while loading parameters (i.e., fatigue frequency, R values, amplitude, etc.) were held constant. Making the model sensitive to the response of such a wide variety of structurally-pertinent laminates eliminated the possibility of producing an analysis whose accuracy is restricted to one particular combination of lamina.

4.1 Nondestructive Test Techniques

Surface replication is a well-established metallographic procedure adapted to optical and electron microscopy. This technique has recently been adapted to composite materials. The basic procedure is quite straightforward. A thin strip of 0.005"-thick cellulose acetate tape is anchored to the polished surface of the specimen by any simple adhesive tape. A small amount of acetone is then injected between the specimen and the replicating tape. The acetone locally dissolves the replicating tape which flows into cracks in the composite laminate. The cellulose acetate hardens,

TABLE 6 TEST MATRIX FOR THE CHARACTERIZATION OF DAMAGE DEVELOPMENT/STIFFNESS CHANGE

LAMINATE	QUASI-STATIC		FATIGUE		
	TENSION (T)	COMPRESSION (C)	TENSION- TENSION (T-T)	COMPRESSION- COMPRESSION (C-C)	TENSION- COMPRESSION (T-C)
A [0/+45/90/90/+45/0] _{3S}	5	5	6	6	10
B [0/90/+45/+45/90/0] _{3S}	3	2	3	4	3
C [0/+45/90/-45/-45/90/ +45/0] _{3S}	3	3	3	3	3
D [0/[+45/90/90/+45/90/ 90/+45/90] _S /0] _S	3	2	3	4	3
A, 250°F	3	3	0	0	3

bearing an imprint of the specimen edge, and in a few minutes is peeled from the specimen.

Surface replicas provide a permanent record of the damage state over the entire length of the specimen at the instant that a certain load level is reached. This technique can be applied while the specimen is in the test machine under load so that recordings will capture the damage state in its most enlarged or open state. If the inspection is made after the load is removed from the specimen, many smaller cracks may close and may not be detected. The replicas are easily stored for re-examination and future reference. Furthermore, it is a simple technique that does not require complicated or extensive equipment.

Surface preparation is an important step in applying this technique. The entire specimen edge is metallurgically polished on a polishing wheel using a 3 micron aluminum oxide/water suspension system on a felt polishing cloth.

A low voltage (25 kv and 20 Ma) X-ray NDE technique modified for composite material application was used to monitor damage development through the specimen width. An opaque additive, diiodobutane (DIB), is introduced to the composite through the specimen edge. The DIB enters the cracks and delaminations which develop in the specimens by capillary action. The images of the voids and delaminations are greatly enhanced by the highly attenuating characteristics of the opaque additive.

Radiographs of the damage growth in the composite specimens were enlarged when prints were made from the exposed film. The darkened areas on the prints represented flawed areas where the opaque additive had penetrated. The actual length and area of the damage zones were from the prints using the appropriate scaling factor.

A 110 kv Picker portable X-ray unit was used in this study. It has a 2.25mm beryllium window and a focal spot of 0.5mm. Kodak Type M industrial X-ray film was employed. A 66-sec. exposure time at a source to specimen distance of 2 feet was used for each exposure.

Changes in specimen stiffness were also monitored during the mechanical testing. An extensometer was employed in the measurement of the axial strain. It has a two-inch gage length and was seated in aluminum V-blocks which were bonded to the specimens prior to testing. The two-inch gage length provided for an averaging of the damage so as to eliminate the effects of any local material variances. The V-blocks

provided for reproducible seating of the extensometer which was removed during fatigue testing and mounted at discrete inspection times. The half-inch transverse gage length was also originally spanned by an extensometer. However, the mounting of the transverse extensometer was not as simple as the longitudinal one and the repeatability difficult and time consuming. Consequently, a strain gage with a half-inch gage was found to have sufficient resolution and provide repeatable results, and was used at General Dynamics. VPI continued to use the transverse extensometer.

4.2 Test Procedures

4.2.1 Quasi-static Tension and Compression

The experimental procedure employed in both the quasi-static tension and compression tests was quite straightforward. The specimen was installed in the MTS hydraulic grips, a nominal initial tensile load was applied and initial NDE evaluations were made. This small initial load was applied to open any initial cracks which may have resulted from curing or handling. Experience has indicated that these cracks may go undetected if a slight load is not applied. Once this initial examination has been made, the tensile load was removed, extensometers were mounted, and the initial modulus of the specimen was recorded on a subsequent loading to the NDE load level. Quasi-static (tension or compression) ramp loading was then initiated. This loading was periodically halted for further NDE measurements. During these subsequent investigations, the specimen was returned to zero load and its modulus was measured (in both tension and compression). The extensometers were removed and the specimens were reloaded to a level which opened existing cracks but did not precipitate further damage development. It was necessary to remove the load on the specimen because the duration of the hold-at-load was so long that maintaining the applied load could adversely affect the test results. This is especially true near the end of the test where higher loads were applied to the specimen.

After the NDE inspection was completed, the extensometers were remounted and ramp loading was continued until the next load level was reached and the NDE process was repeated. Loading continued in this manner until specimen failure occurred.

4.2.2 Fatigue Testing

Three types of fatigue tests were conducted in Phase III of this program: tension-tension, compression-compression and tension-compression at stress ratios equal to 0.1, 10, and -1, respectively. All fatigue tests featured constant amplitude sinusoidal waveform loading. Tests were run in load control at a frequency of 10 Hz.

The experimental procedure employed was similar to that described for quasi-static tests. The specimen was mounted in MTS hydraulic grips and a nominal initial load applied to open any existing cracks. While holding at this load, an initial NDE reading was taken to record any initial damage within the specimen. The load was then removed. An extensometer was mounted on the specimen. The specimen was loaded to the mean load, and the engineering modulus of the specimen was measured. Fatigue cycling then began. Loading was halted periodically to measure stiffness change and damage development. The procedure employed during these inspections was: return specimen to zero load, then reload to mean load to measure the modulus; remove the extensometer, and perform NDE evaluation (replication, X-ray radiography, ultrasonics, etc.); again remove load and remount the extensometer, reload to mean load, measure the modulus and begin cycling again.

Specimens were loaded in this manner until one million cycles had been applied. Fatigue loading was then halted and the specimens were quasi-statically loaded to failure to determine their residual strength. A number of specimens (included in the total number of fatigue specimens shown in Table VI) were cycled as described above but were halted before one million cycles had been applied. The specimens were then quasi-statically loaded to failure to determine residual strength. The purpose of these tests was to determine intermediate residual strength values. The determination of when to halt fatigue loading will be made after the first few full fatigue tests. These points were linked to milestone damage development/stiffness change features (e.g., when saturation spacing was first attained, or when laminate stiffness had been reduced a certain percentage).

4.3 Experimental Results

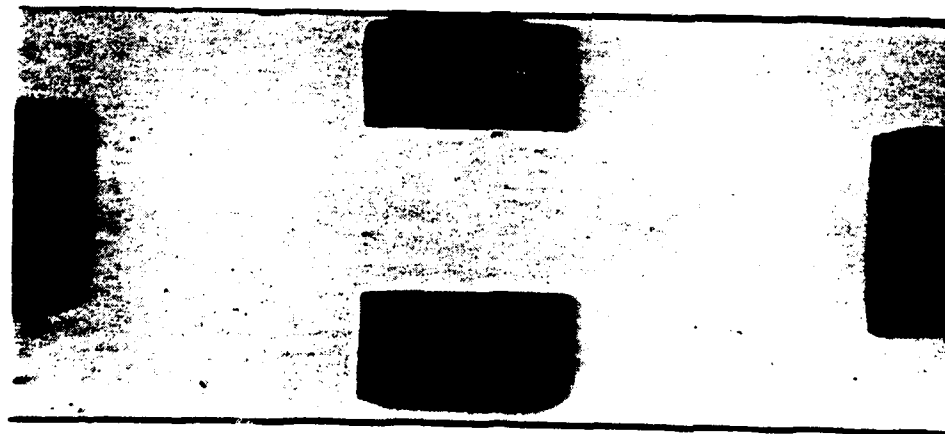
The results now to be presented document the modes and chronology of damage that were observed during the quasi-static and fatigue testing. The damage modes were chiefly

identified using the edge replica techniques with the X-ray radiographs being used for verification.

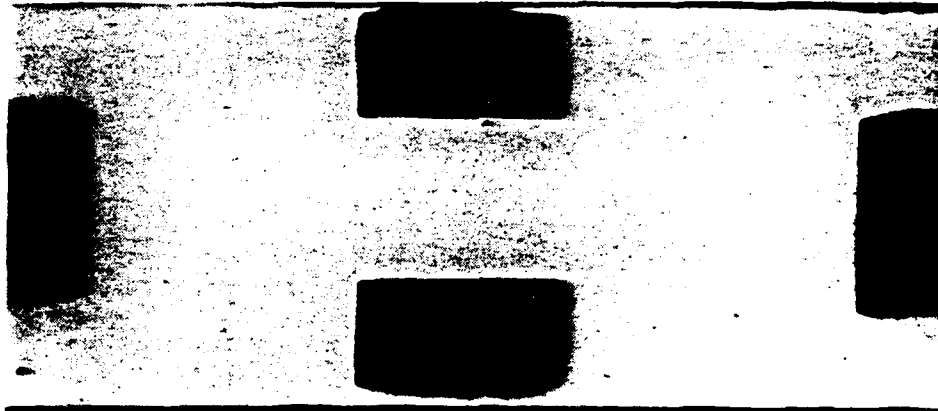
4.3.1 Failure Modes and Mechanisms in Type A Coupons Stacking Sequence: $[0/\pm 45/90/90/\mp 45/0]_{3S}$

Quasi-static loading with damage monitoring of Type A laminates at successively higher loads to a maximum applied strain of 1% produced transverse cracks in the double 90° laminae which in turn resulted in transverse cracks in the adjacent -45° laminae. Longitudinal cracks along the $90^\circ/90^\circ$, $\pm 45^\circ$ and $90^\circ/-45^\circ$ interfaces were then seen to appear. A sequence of X-ray radiographs shown in Figure 5 exemplify typical X-ray data. The initiation of 90° transverse cracks can be seen to have occurred by the time a load level corresponding to 0.6% strain had been reached. No cracks are visible in the radiograph taken at the 4500 microstrain level. Edge replicas identified the onset of transverse cracking in -45° laminae at the 0.7% strain level. A saturation spacing of 0.038 inches in both sets of the transverse cracks had occurred by the time a 1% strain was achieved. One percent strain also marked the initiation of the three modes of interfacial cracking in the outermost eight-ply groups of $[0/\pm 45/90]_S$. Examples of edge replicas of the transverse cracks in the 90° and -45° laminae and longitudinal cracking are shown in Figures 6, 7, and 8, respectively. The sequence of events is summarized in the bar chart of Figure 9. Longitudinal stiffness change (Figure 10) occurred after the 0.6% applied strain level which corresponds to the onset of transverse cracking. Stiffness continued to degrade until failure, where a retention of 95.5% at the 1% strain level was measured. The Poisson stiffness retention at 1% strain was 97%. Quasi-static compression tests of Type A coupons produced no observable damage, nor could any stiffness change be measured.

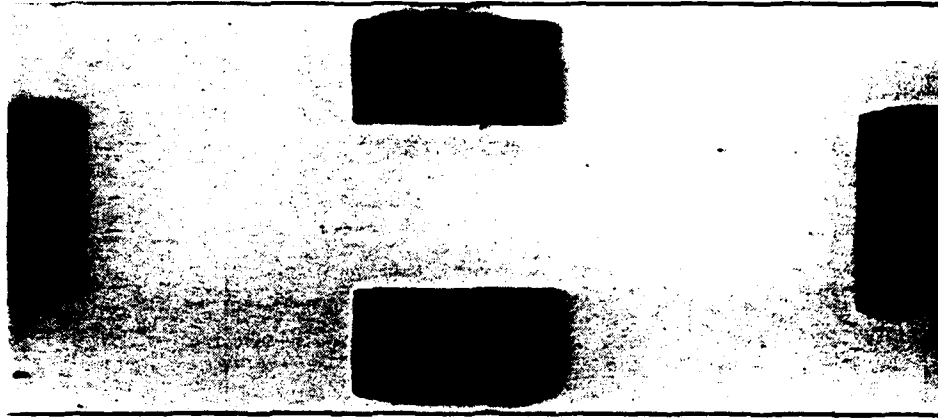
Tension-tension fatigue testing of Type A specimens was conducted in load control at strain levels that were initially 4500 and 6000 microstrain. Figure 11 summarizes the damage accumulation processes. At the 4500 microstrain level, cracks initiated in the 90° plies and extended through the $90^\circ/-45^\circ$ interfaces and into the -45° plies during the first cycle. The number of cracks in the 90° and -45° plies increased as additional cycles were applied, though no cracks appeared in the $+45^\circ$ plies. By 5×10^4 cycles, the cracks in the -45° degree plies had extended into the $+45^\circ/-45^\circ$ interfaces in the outermost ply groups to form a number of local, short length cracks along these interfaces.



Initial



3000 $\mu\text{in/in}$



4500 $\mu\text{in/in}$

Figure 5 DiB Enhanced X-Ray Radiographs - Type A, Quasi-Static Tension

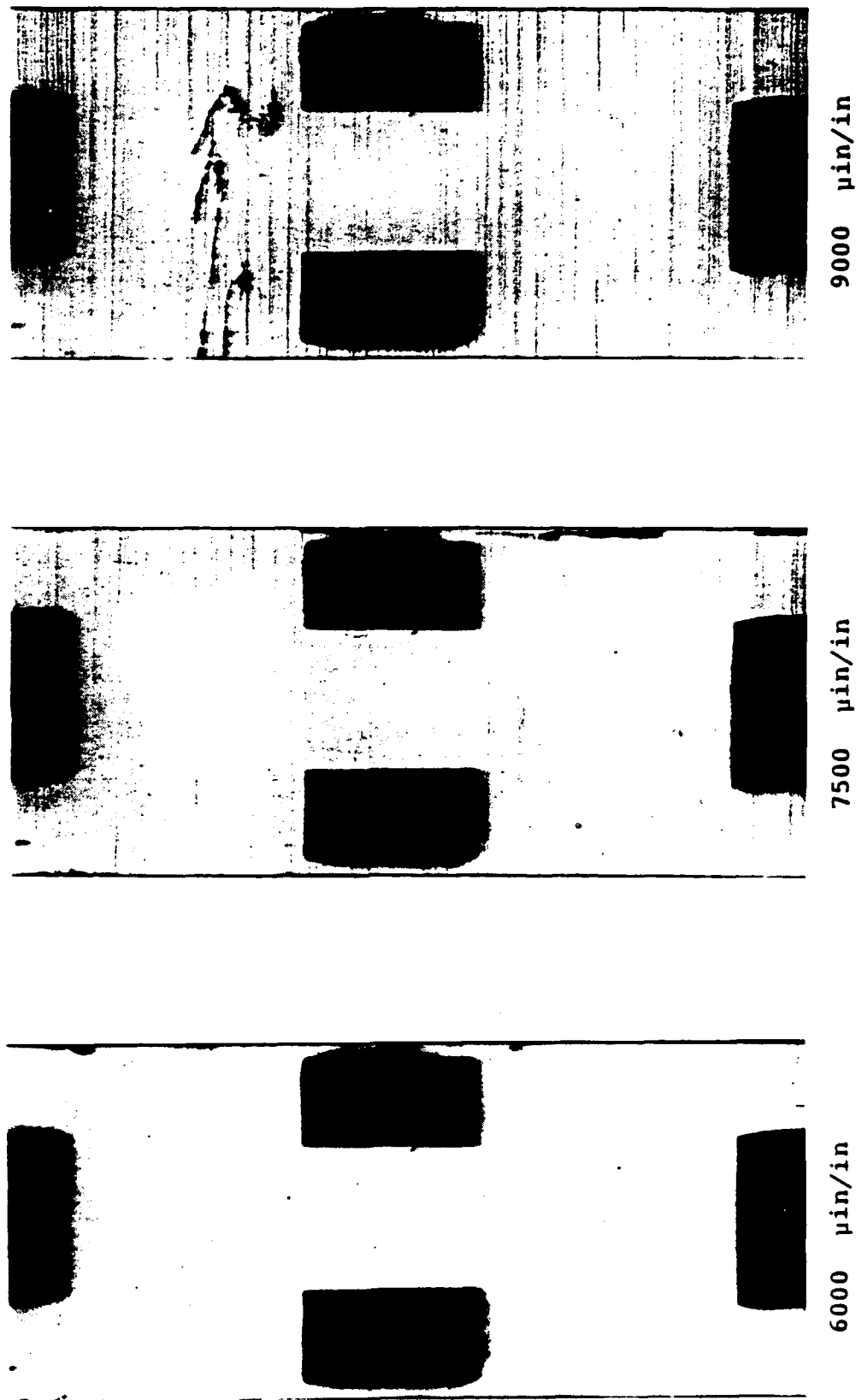


Figure 5 (Continued) DIB Enhanced X-Ray Radiographs - Type A, Quasi-Static Tension

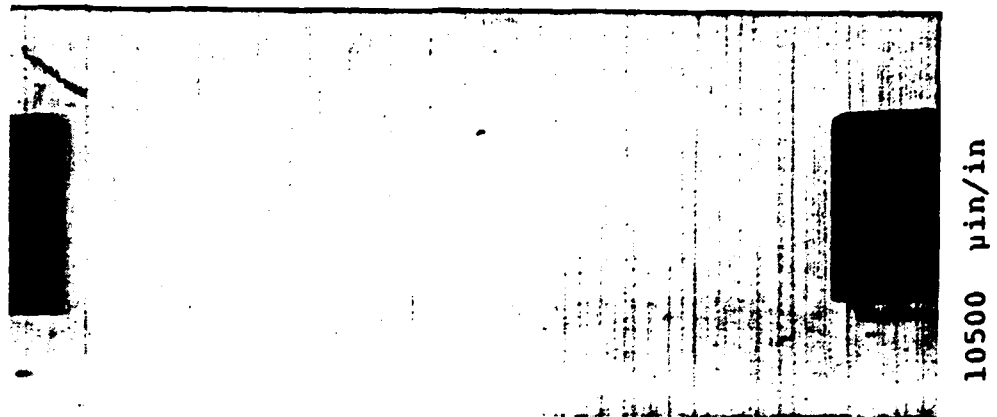
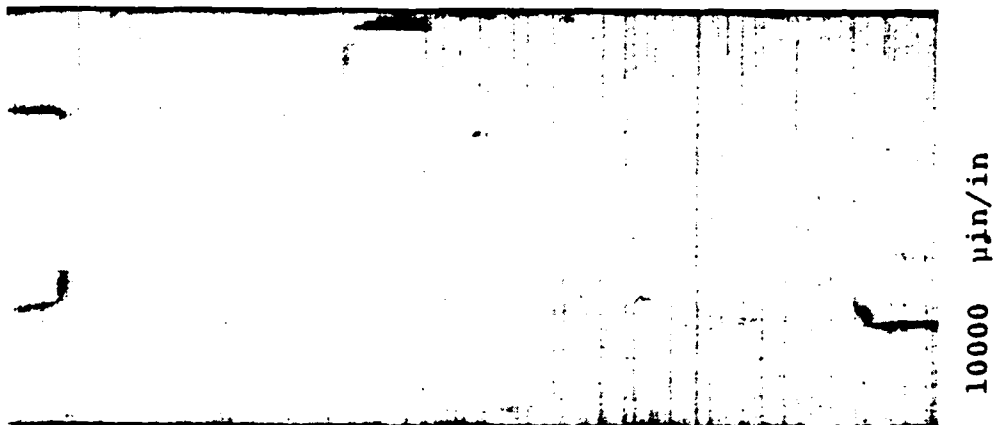
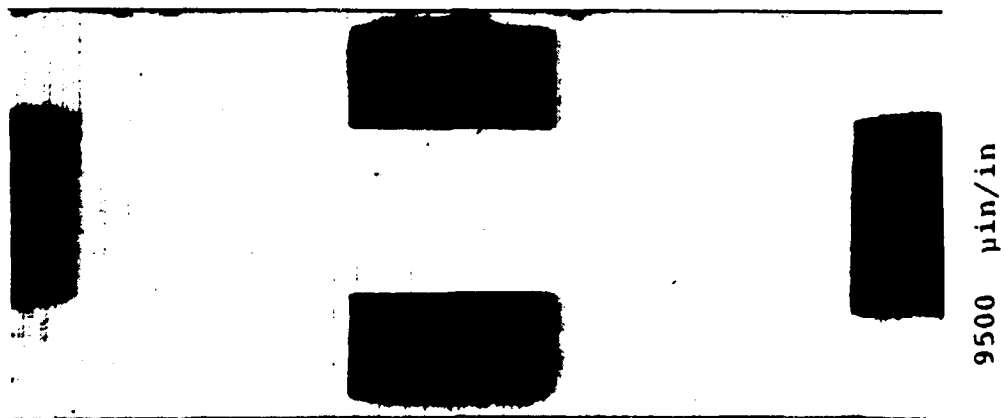


Figure 5 (Continued) DIB Enhanced X-Ray Radiographs - Type A, Quasi-Static Tension

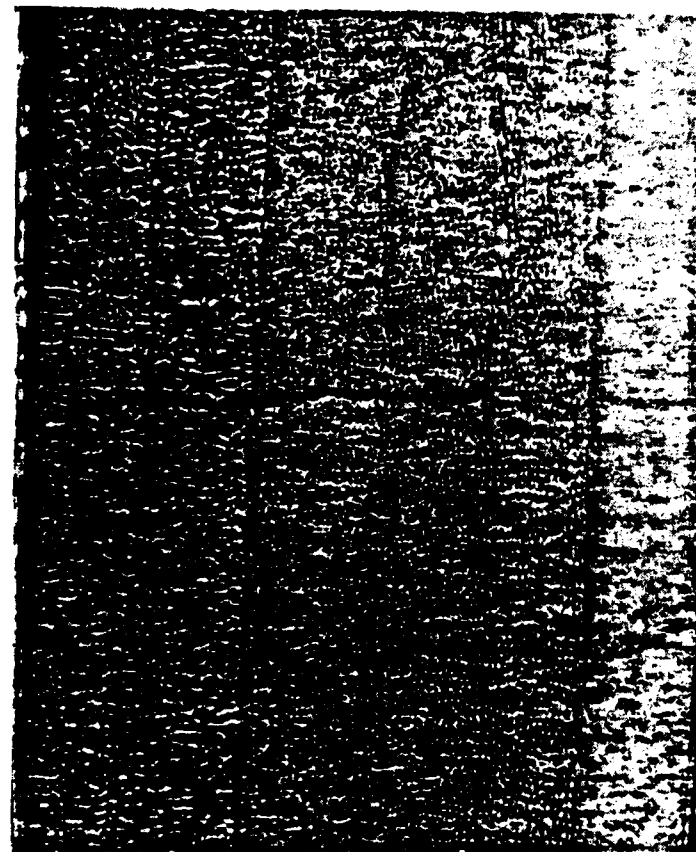


Figure 6. Photomicrograph of Transverse Crack in 90° Laminae
- Type A, Quasi-Static Tension

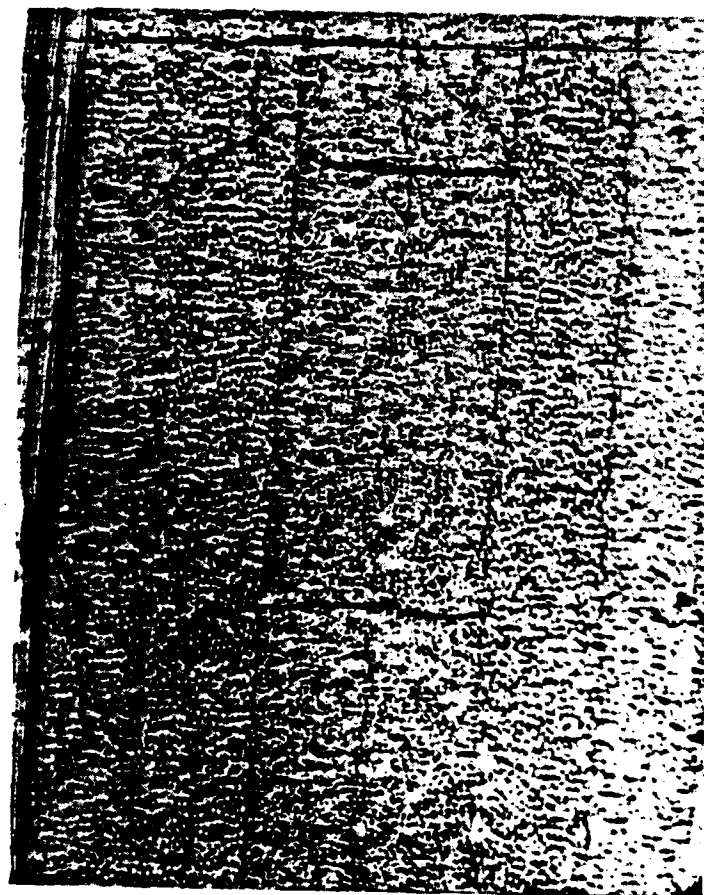


Figure 7 Photomicrograph of Transverse Crack in -45° Lamina
Type A, Quasi-Static Tension

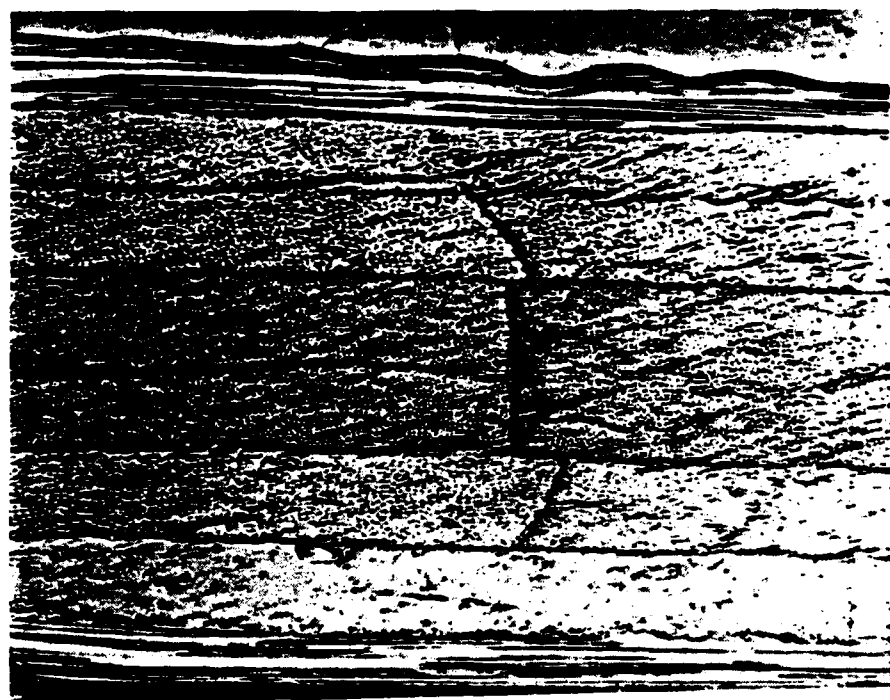
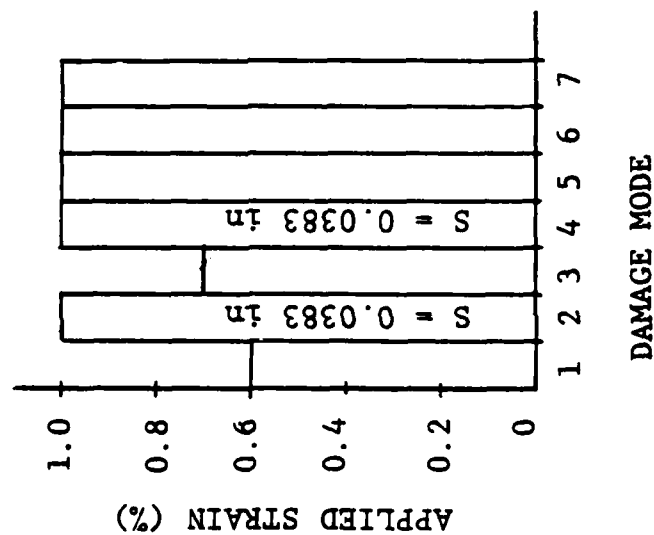


Figure 8 Edge Replica of Longitudinal Cracking
Type A, Quasi-Static Tension

QUASI-STATIC TENSION

TYPE A



DAMAGE MODE

1. Initiation 90° Transverse
2. Saturation 90° Transverse
3. Initiation -45° Coupling
4. Saturation -45° Coupling
5. Initiation 90/90° Interface
6. Initiation +45 Interface
7. Initiation 90/-45° Interface

S = Saturation Spacing

Figure 9 Damage Modes And Chronology - Type A, Quasi-Static Tension

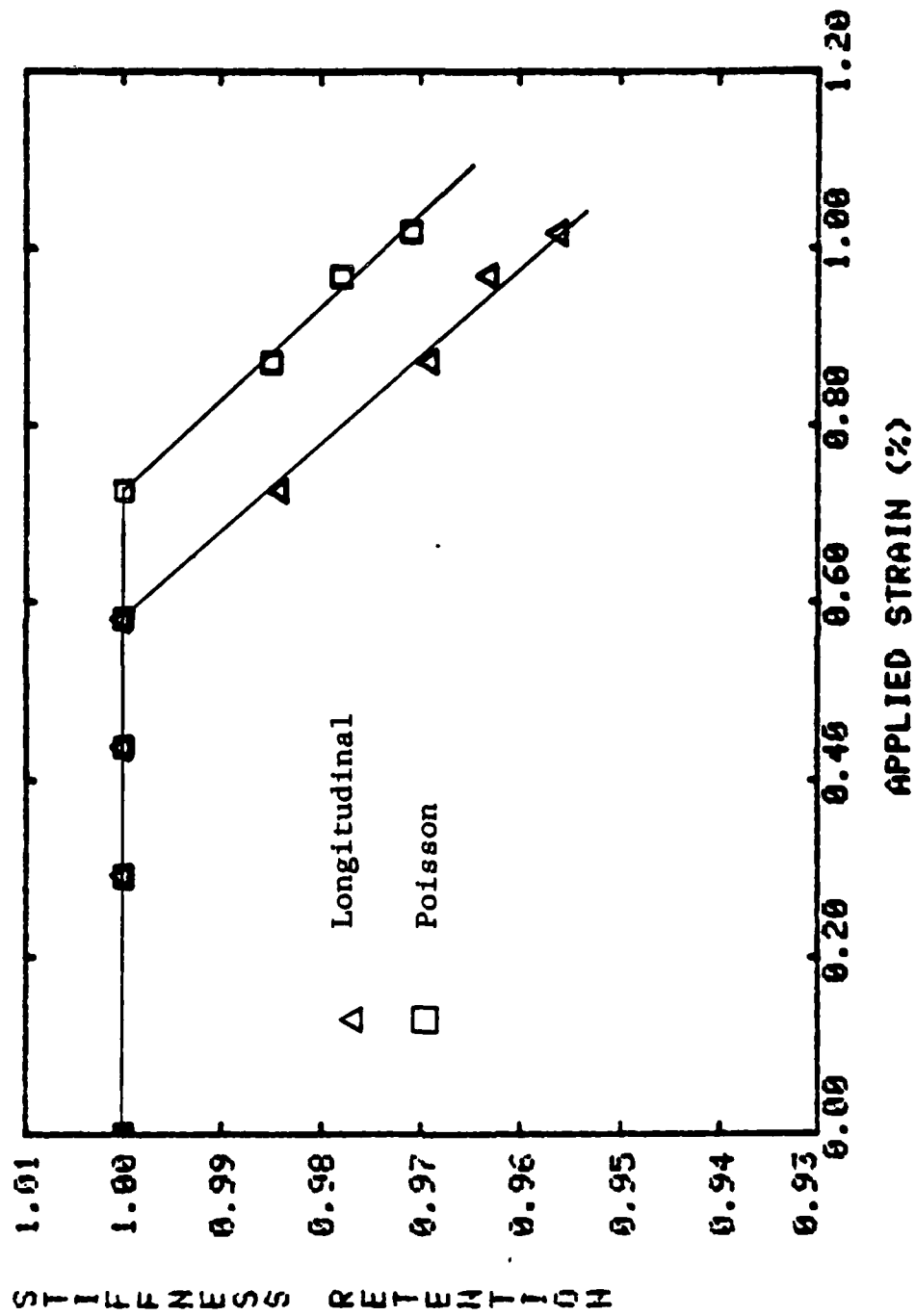


Figure 10 Stiffness Change - Type A, Quasi-Static Tension

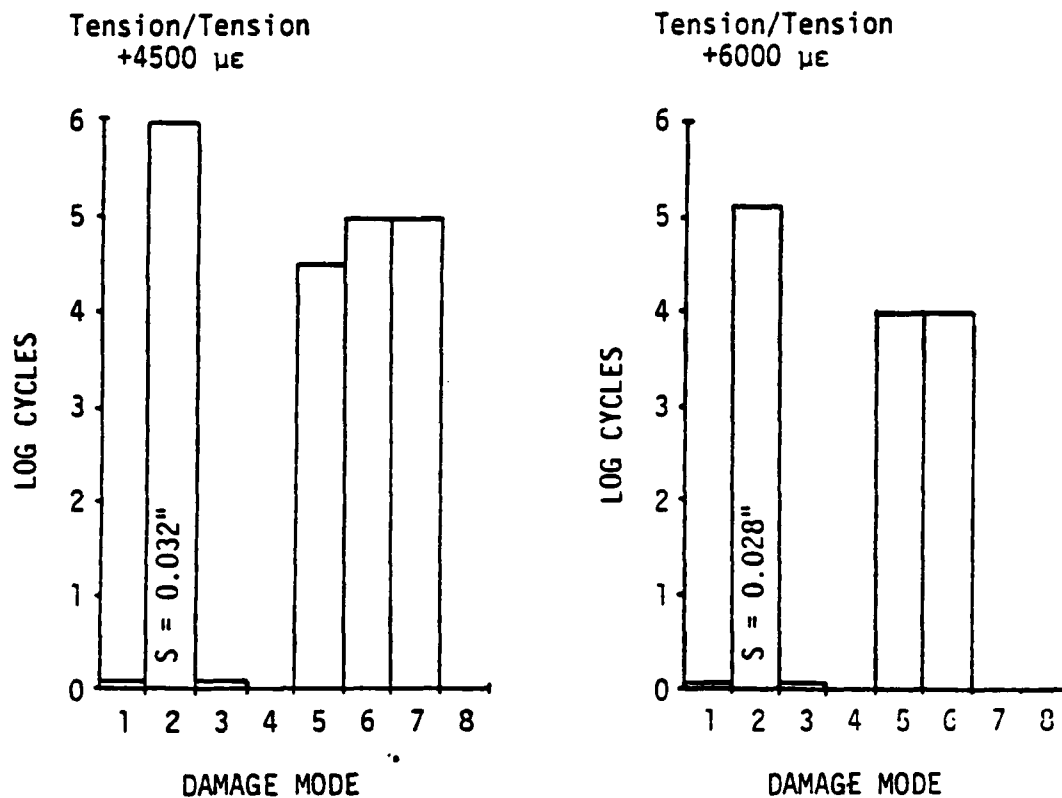


Figure 11 Damage Modes and Chronology -- Type A , Tension-Tension

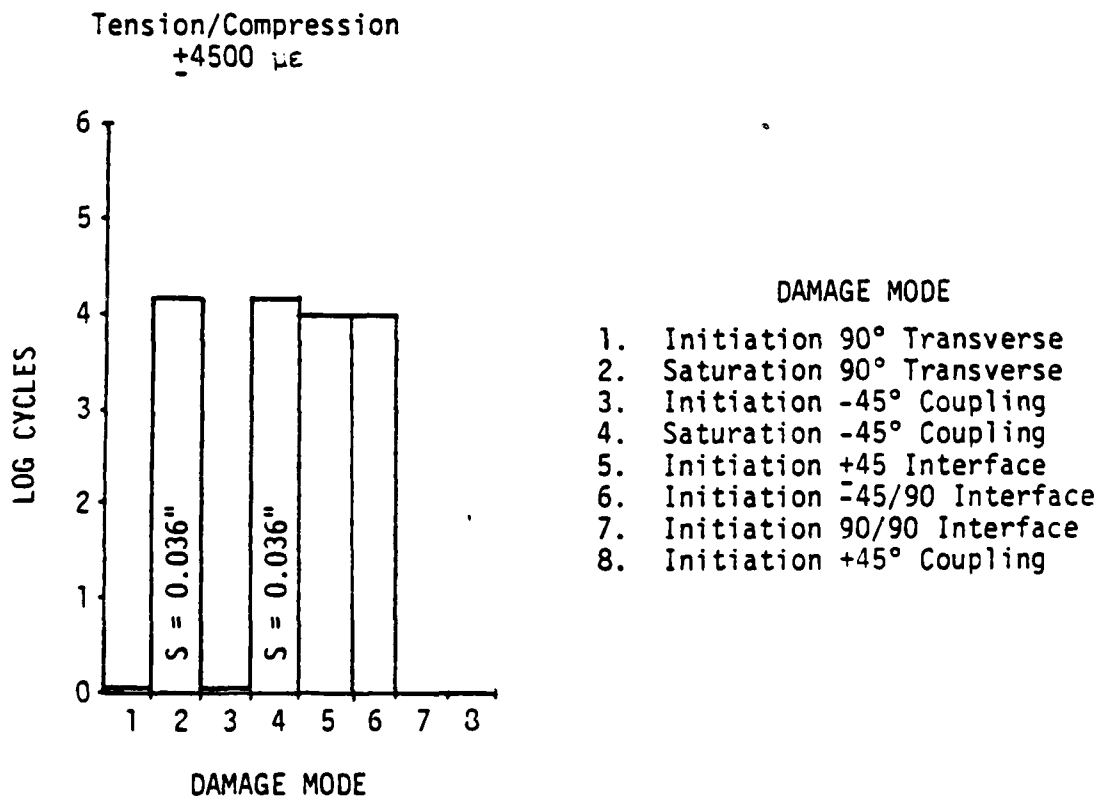


Figure 12 Damage Modes and Chronology --Type A , Tension Compression

After one million cycles, the average spacing of cracks in the 90° plies was 0.032 inches, which was approximately the same as that observed in the quasi-static tension tests. The local cracks in the +45/-45 interfaces had propagated along the length of the specimen with similar cracks appearing at the -45/90 and 90/90 interfaces. Again all interfacial cracks were in the outermost ply groups and no cracks were visible in the +45° plies.

At 6500 microstrain, tension-tension, the same sequence of events that was observed at 4500 microstrain occurred during the first cycle. However, -45/90 and +45/-45 interfacial cracking occurred after only 10K cycles. By 170K cycles, all six ply groups contained cracks in the -45/90 and +45/-45 interfaces. The spacing of the cracks in the 90° plies was 0.028 inches.

Compression-compression fatigue testing of Type A coupons was conducted at initial strain levels of 4500 and 6000 microstrain. In both cases no off-axis plies had cracked after one million cycles. After one million cycles, a 10mm crack had appeared in the outermost +45/-45 interface in the 4500 microstrain test; also a crack appeared in the second +45/-45 interface of the outermost ply group in the 6000 microstrain test. The crack crossed the +45° ply and ended in the 0/+45 interface. After one million cycles of compression-compression fatigue, a specimen was then subjected to 1K cycles of tension-tension fatigue to introduce cracks in the 90° and -45° plies. Between eight and ten cracks were observed in each group of plies. The compression-compression loading sequence was resumed for 30K cycles and cracks along the first +45/-45 interface of ply groups one and six were noted. These interfacial cracks were associated with the cracks in the -45° plies introduced during the tensile cyclic loading.

Tension-compression testing was conducted at 4500 microstrain. The results are summarized in Figure 12. Cracks initiated in the 90° plies and extended through the 90/-45 interfaces and the -45° plies during the first cycle. The number of cracks in the 90 and -45° plies increased as additional cycles were applied. By 10K cycles, the +45/-45 and -45/90 interfaces in ply groups one and six had local, short length cracks. By 40K cycles, the +45/-45 and -45/90 interfaces in ply groups one, two, five and six contained cracks. The average spacing of cracks in 90° and -45° plies was 0.036 inches. However, the number of cracks in ply groups three and four, where no interfacial damage had developed, was greater than in those groups having interfacial damage.

4.3.2 Failure Modes and Mechanisms in Type B Coupons Stacking Sequence $[0/90/+45/-45/90/0]_{3S}$

Tensile testing of the Type B coupons at successively higher loads to a maximum applied strain at approximately 1% produced only transverse cracking in the 90° and +45° laminae. The 90° cracking started by about 0.87% applied strain (Fig. 13) and did not reach a verifiable saturation spacing before failure. Cracks in the +45° laminae were always associated with cracks in the adjacent 90° lamina, but not every transverse crack in the 90° resulted in a crack in the 45° lamina. There were approximately three 90° cracks to every 45° crack just prior to failure. The stiffness changes that resulted are shown in Figure 14. The longitudinal and Poisson stiffness retentions dropped to 93.9% and 96.7%, respectively, prior to failure. Compressive testing of Type B coupons produced no observable damage, nor could any stiffness change be measured.

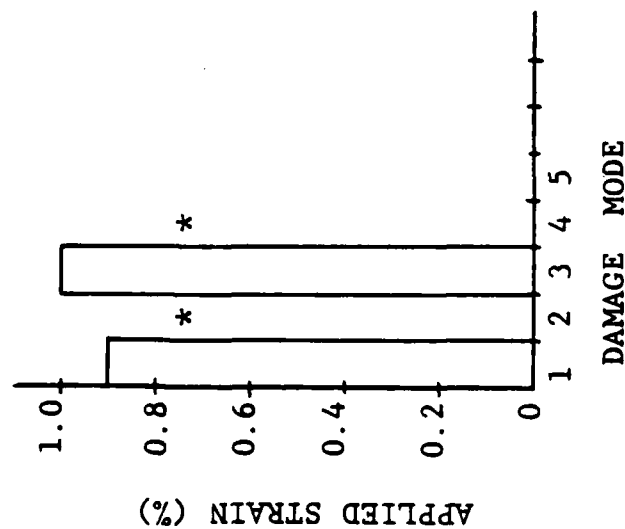
Tension-tension fatigue testing was conducted at maximum applied strain levels of 4500 and 6000 microstrain. Figure 15 indicates that transverse cracking in the 90° laminae was the only damage that had occurred by 687K cycles at the 4500 microstrain level. At 6000 microstrain, the 90° transverse cracking resulted in cracks in the +45° laminae which in turn produced transverse cracks in the double -45 laminae. Interfacial cracking along the +45° lamina interfaces was the last damage mode to occur. The saturation spacings indicate that there were approximately twice as many 90° cracks as +45° cracks and three times as many +45° cracks as double -45° cracks. Initiation of the four types of cracking had occurred by 10K, 50K, 300K and 1000K cycles, respectively. After 687K cycles, at 4500 microstrain, there was a 96% longitudinal stiffness retention and no Poisson stiffness change. At 6000 microstrain, Figure 16 indicates that there was a 97% Poisson stiffness retention after 400K cycles and a 96% longitudinal stiffness retention after one million cycles. Residual strength measurements were made of the coupons following testing. Three specimens had been tested at 6000 microstrain and one at 4500 microstrain. The latter had suffered no loss in strength by 687K cycles (Figure 17), whereas 6000 microstrain resulted in loss in strength of 15% by 1 million cycles.

Compression-compression fatigue testing of the Type B coupons was conducted at four maximum strain levels of 4500, 5000, 5500, and 6000 microstrain. Specimen failure occurred at the latter three strain levels by delamination of the interface of the +45° laminae closest to the exterior (Figure 18). The corresponding X-ray radiograph of a

QUASI-STATIC TENSION

TYPE B

- DAMAGE MODE
1. Initiation 90° Transverse
 2. Saturation 90° Transverse
 3. Initiation +45° Coupling
 4. Saturation +45° Coupling



*. Saturation Not Observed

Figure 13 Damage Modes And Chronology - Type B - Quasi-Static Tension

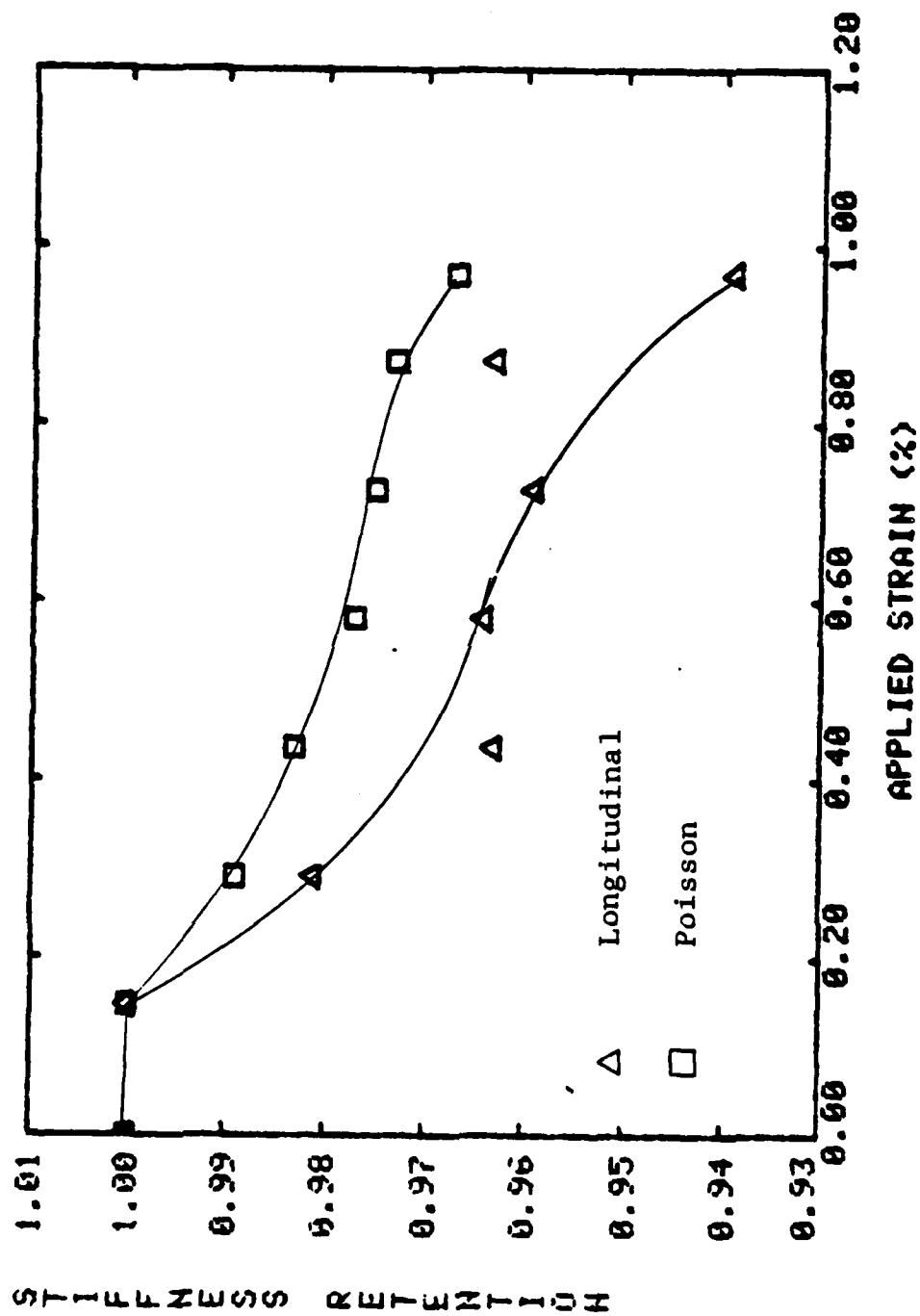


Figure 14 Stiffness Change - Type B, Quasi-Static Tension

DAMAGE MODE

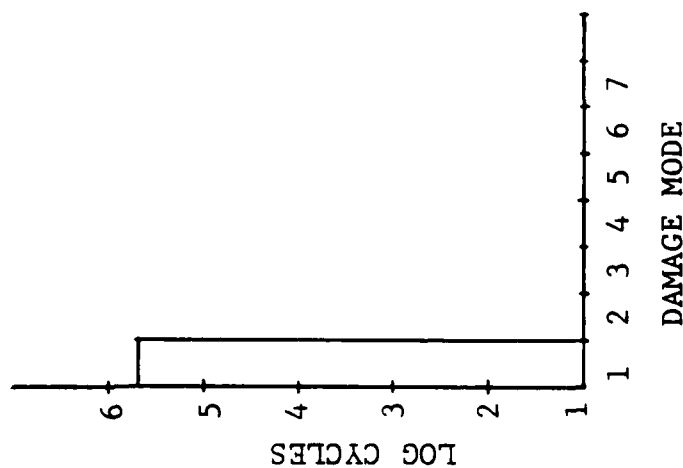
1. Initiation 90° Transverse
2. Saturation 90° Transverse
3. Initiation +45° Coupling
4. Saturation +45° Coupling
5. Initiation -45° Coupling
6. Saturation -45° Coupling
7. Initiation +45 Interface

TENSION-TENSION FATIGUE

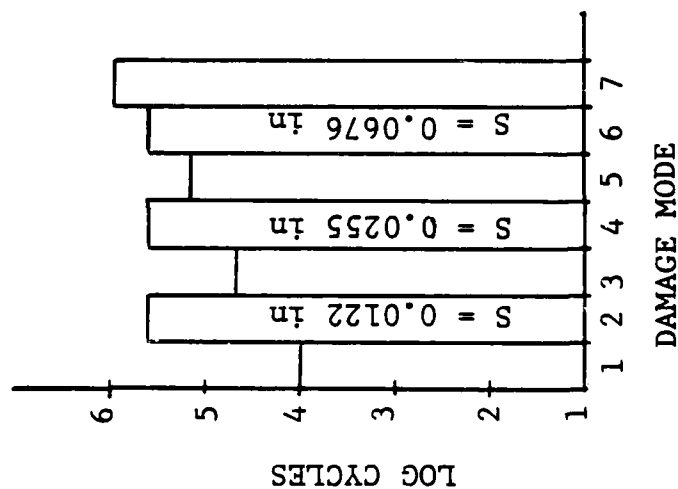
TYPE B

S = Saturation spacing

B1-5, 4500 $\mu\epsilon$



B2-8, 6000 $\mu\epsilon$



B2-6, 6000 $\mu\epsilon$

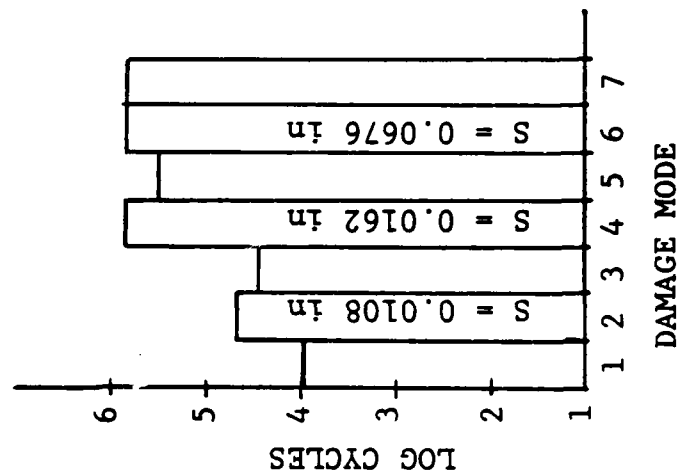


Figure 15 Damage Modes And Chronology - Type B - Tension-Tension Fatigue

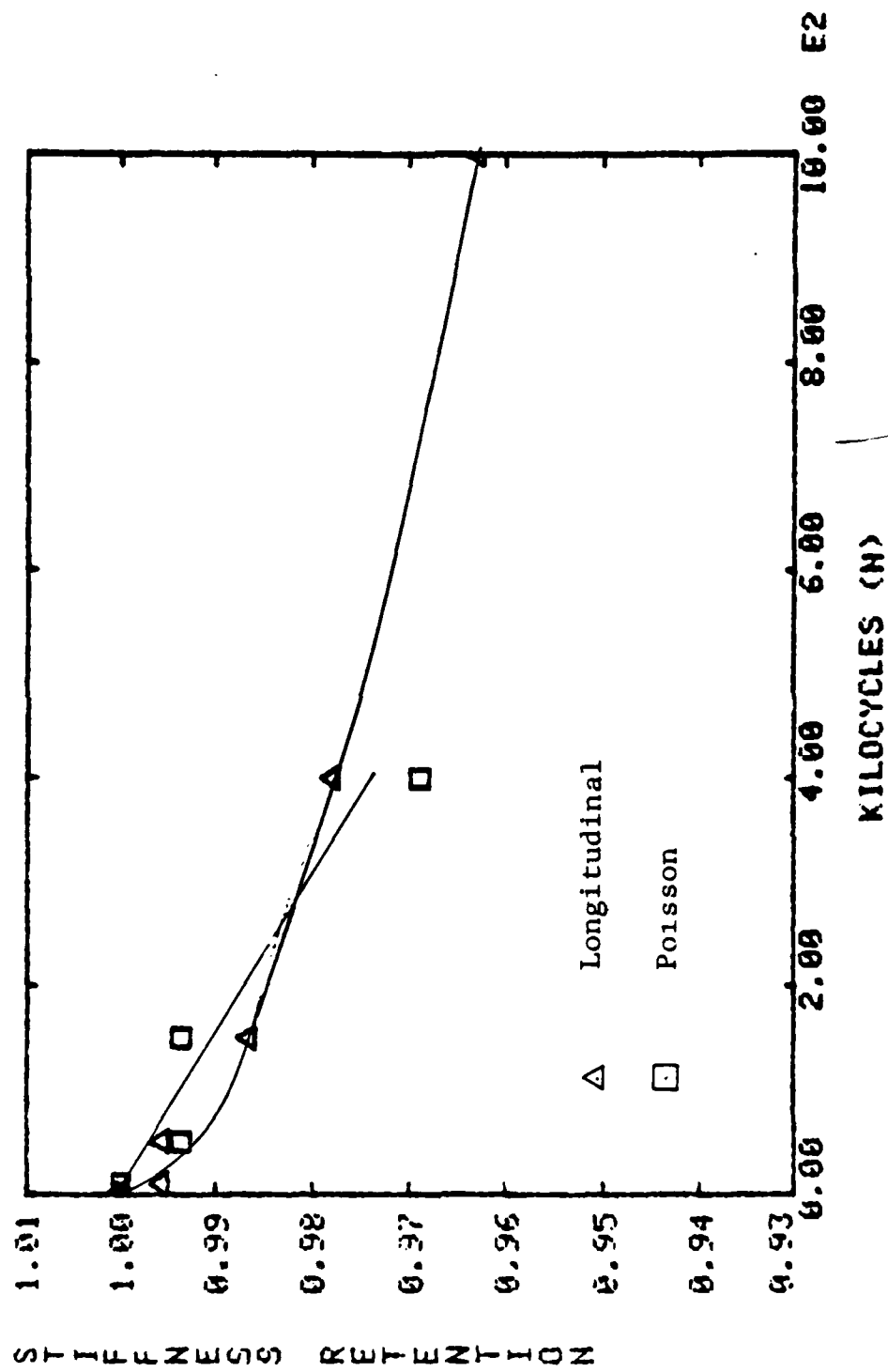


Figure 16 Stiffness Change - Type B, Tension-Tension Fatigue

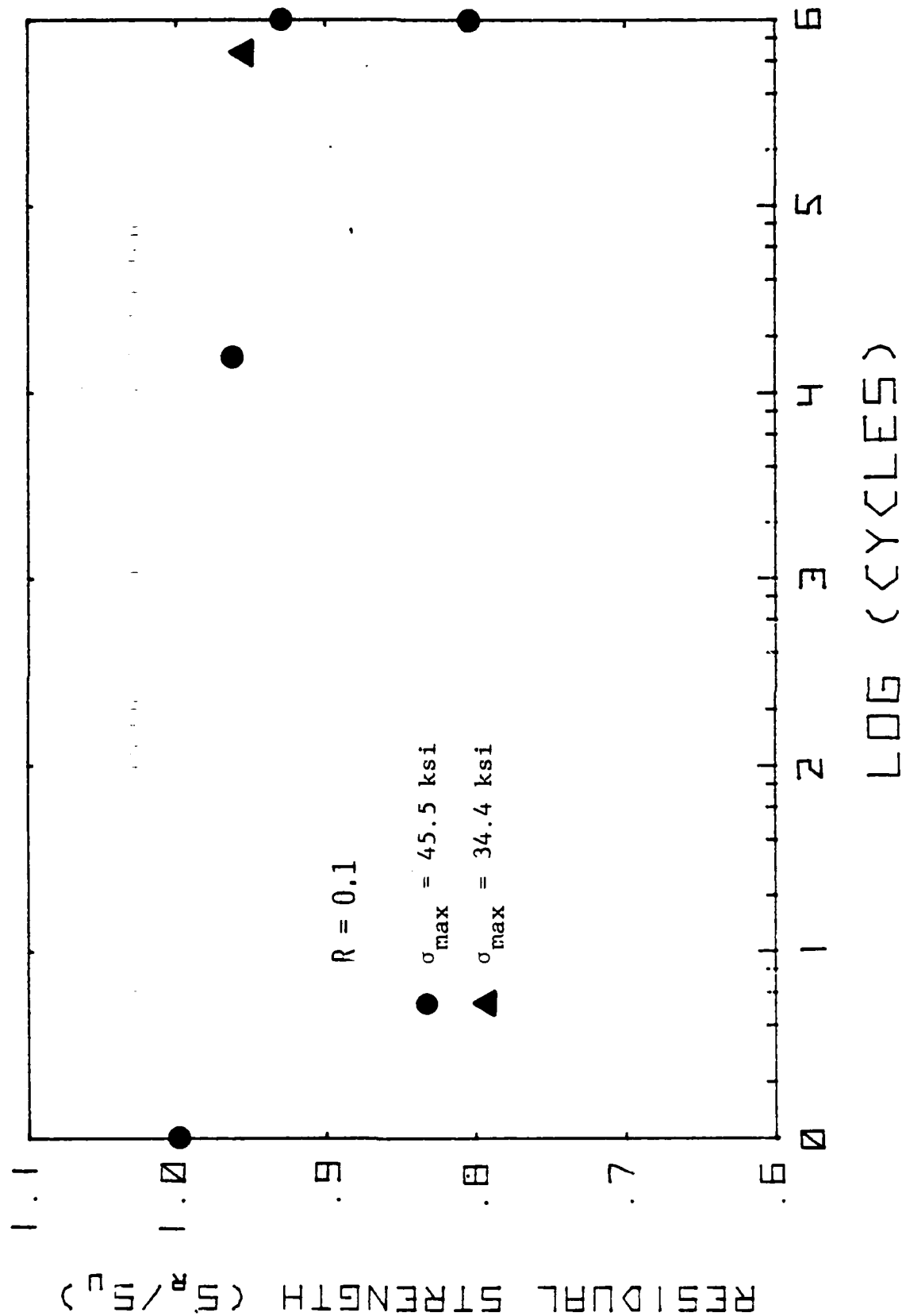


Figure 17 Residual Strength Curve for Type B Coupons Under Tension-Tension Fatigue



Figure 18. Edge Replica of + 45 Interface Delamination in a Type B Coupon Under Compression-Compression Fatigue



(a) Type B
Compression-Compression



(b) Type D
Tension-Compression



(c) Type C
Tension-Compression



Figure 19 X-Ray Radiographs of Delaminations in Test Coupons

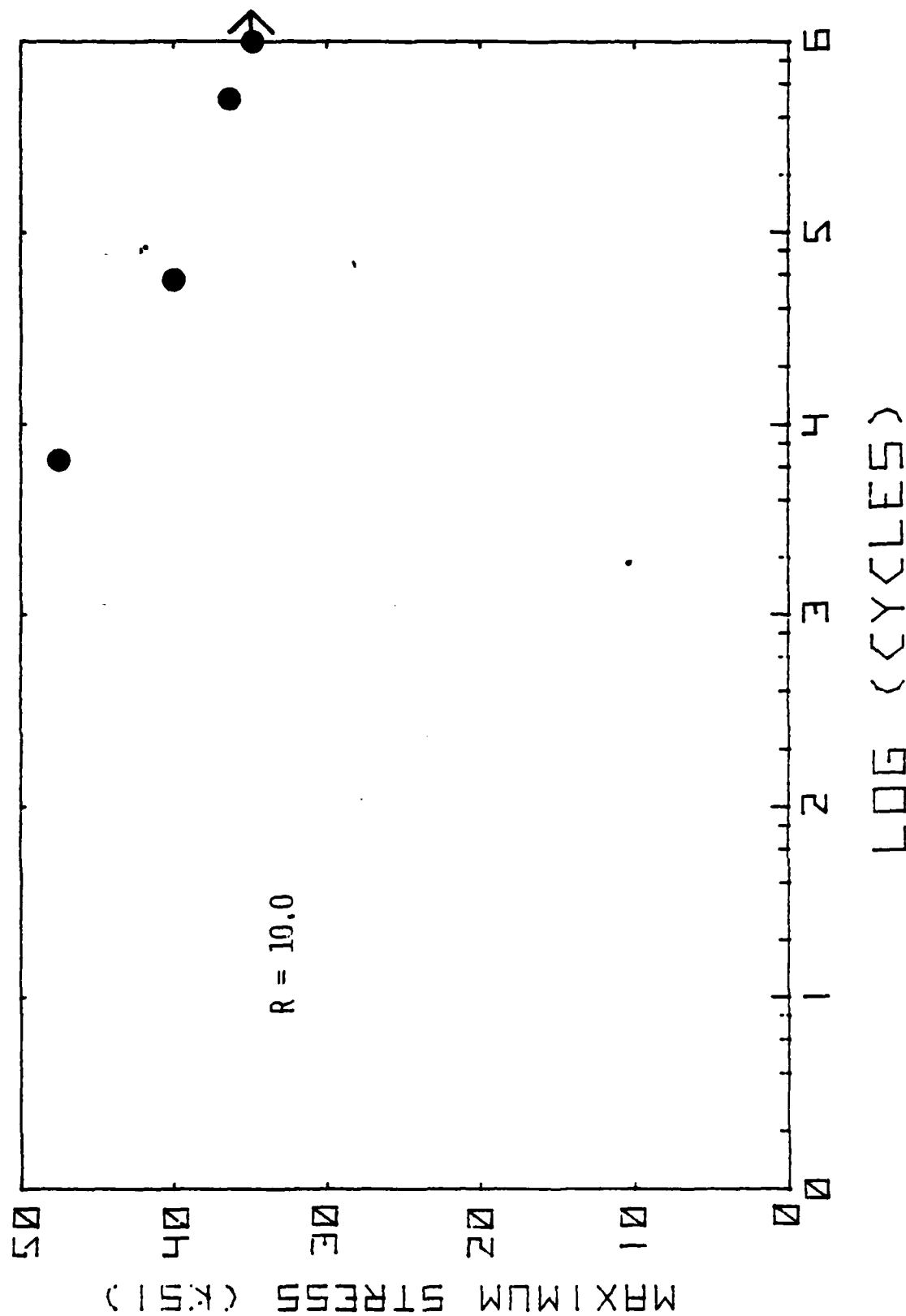


Figure 20 S-N Curve for Type B Coupons Under Compression-Compression Fatigue

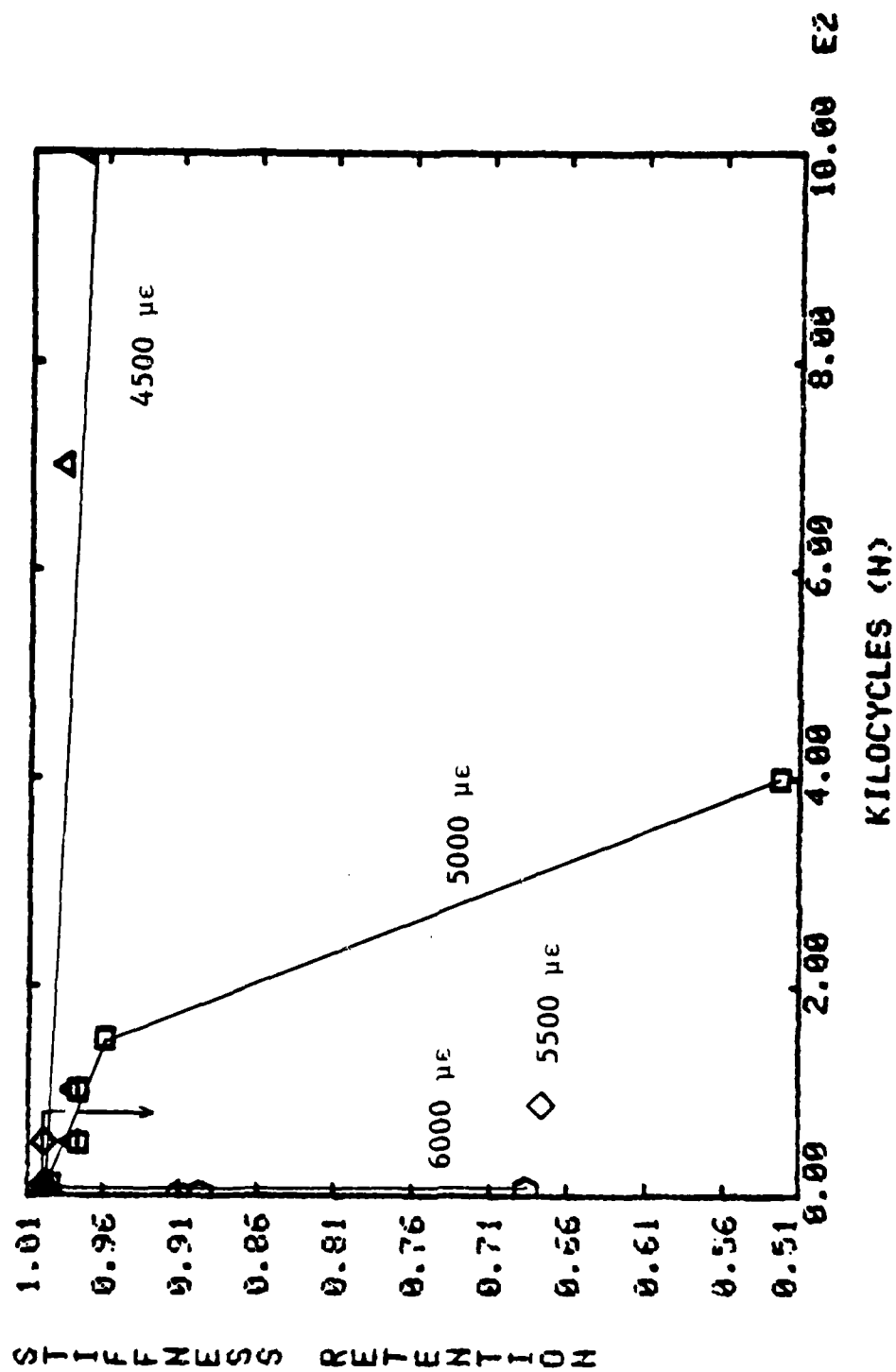


Figure 21 Longitudinal Stiffness Change - Type B, Compression-Compression Fatigue

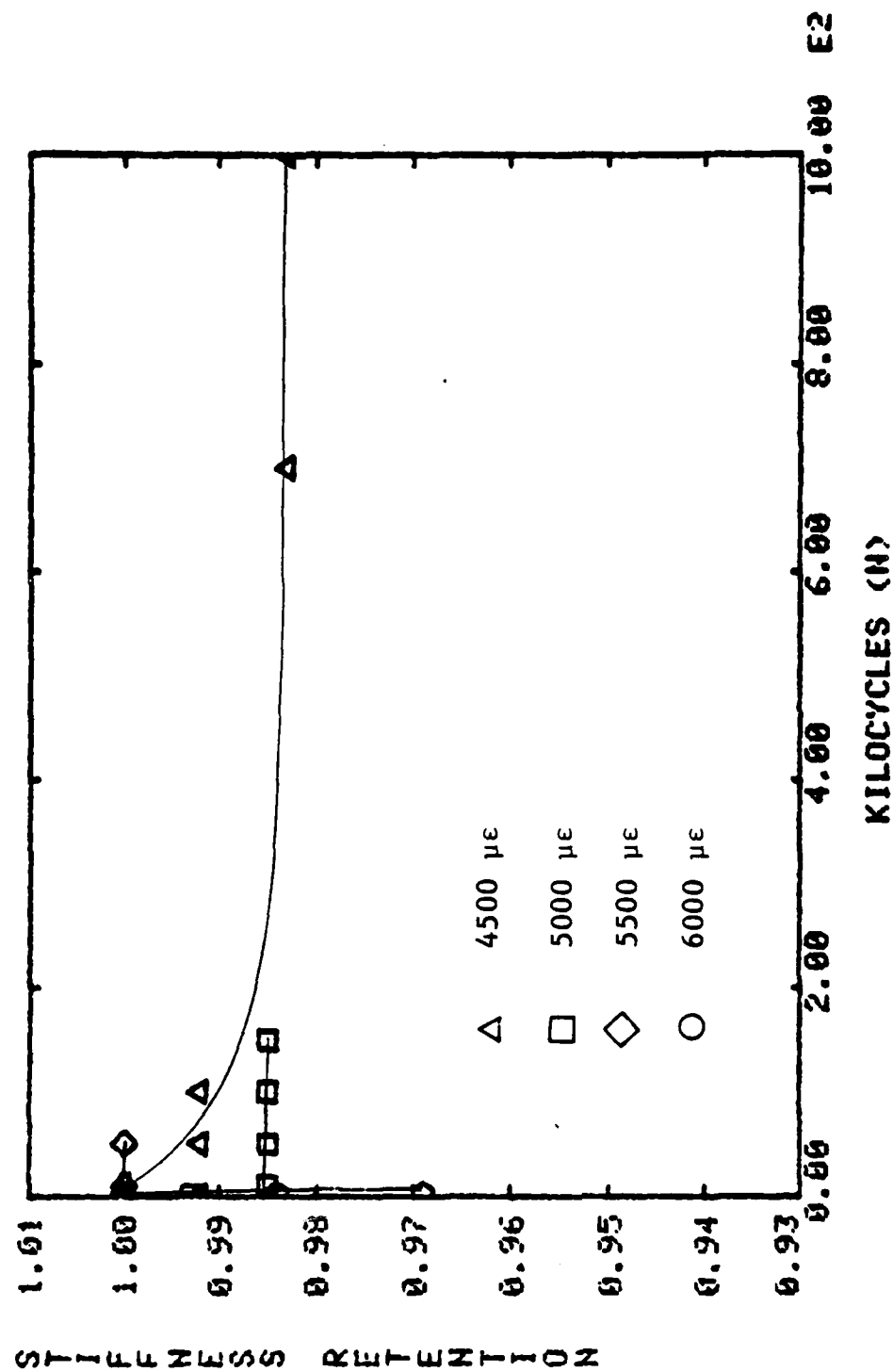


Figure 22 Poisson Stiffness Change - Type B, Compression-Compression Fatigue

TENSION-COMPRESSION FATIGUE

TYPE B

DAMAGE MODE

1. Initiation 90° Transverse
2. Saturation 90° Transverse
3. Initiation +45° Coupling
4. Saturation +45° Coupling
5. Initiation -45° Coupling
6. Saturation -45° Coupling
7. Initiation ±45 Interface

±4500 $\mu\epsilon$

±6000 $\mu\epsilon$

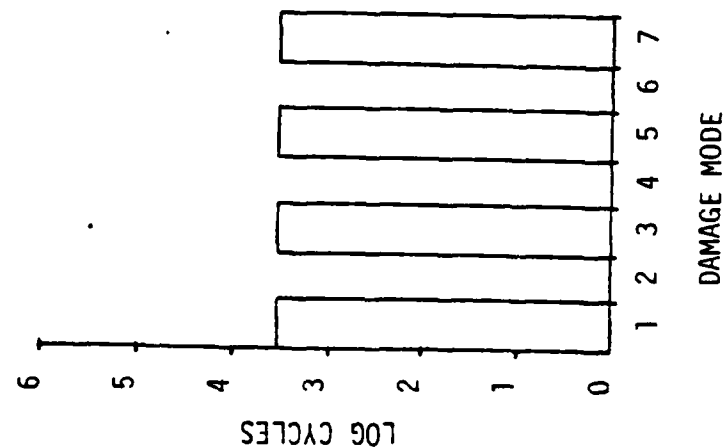
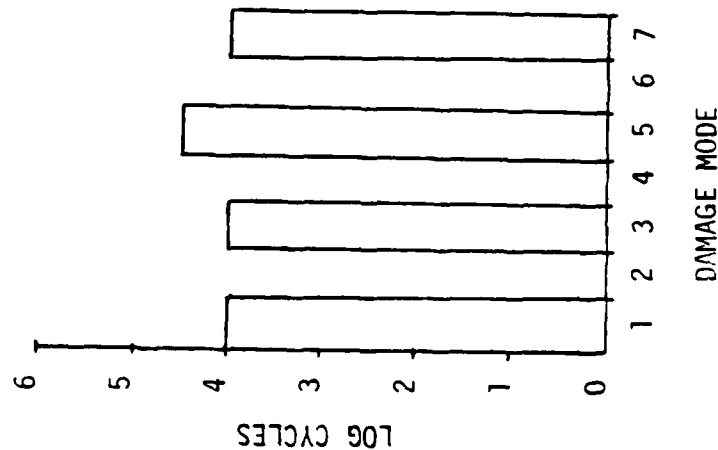


Figure 23 Damage Modes and Chronology - Type B, Tension-Compression

delamination is shown in Figure 19a. The S-N curve is depicted in Figure 20. The edge replicas indicated that no transverse cracking took place prior to the delamination. The delamination initiated between 1K and 10K cycles in the 5000 microstrain, 50K cycles in the 5500 microstrain, 4K cycles in the 6000 microstrain and was not observed in the 4500 microstrain tests. The longitudinal and Poisson stiffness changes are shown in Figures 21 and 22, respectively. The change in longitudinal stiffness just prior to failure was well recorded in the 5000 and 6000 microstrain tests because of massive delamination along the length.

Tension-compression fatigue of Type B coupons was conducted at maximum applied strain levels of 4500 and 6000 microstrain. Figure 23 summarizes the features of the damage development. At 4500 microstrain, transverse cracking in the 90° and +45° plies and longitudinal cracking along the ±45 interface had occurred by 10K cycles. Initiation of transverse cracking in the -45° plies occurred by 50K cycles. Saturation of transverse cracking was not observed by the end of the testing at one million cycles. The same damage modes occurred sooner (Fig. 23) when the Type B coupons were tested at 6000 microstrain; saturation was not observed.

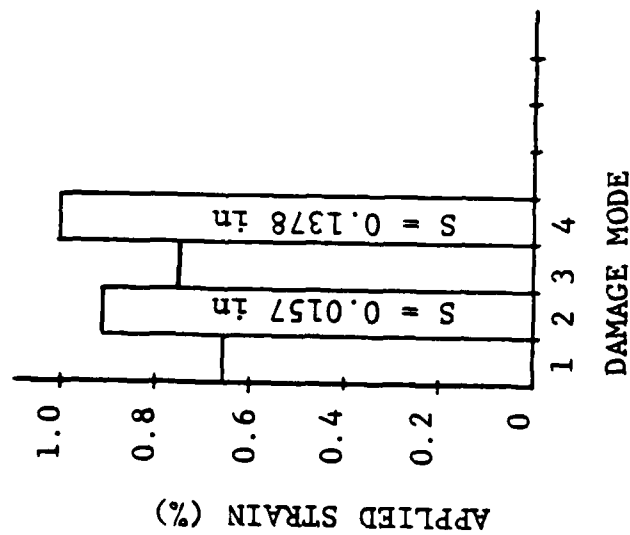
4.3.3 Failure Modes and Mechanisms in Type C Coupons Stacking Sequence: [0/+45/90/-45/-45/90/+45/0]_{3S}

Tensile testing of the Type C coupons at successively higher loads to a maximum applied strain of approximately 1% resulted in transverse cracking in the 90° and the double -45° laminae. The 90° transverse cracks started by 0.65% applied strain (Figure 24) and reached a saturation spacing of 0.0157 in. at an applied strain of 0.9%. Initiation and saturation of the cracking in the double -45° laminae occurred at strain levels of 0.75% and 1%, respectively, with a saturation spacing of 0.1378 in. These damage modes resulted in longitudinal and Poisson stiffness retentions of 94% (Figure 25). No damage or stiffness changes were observed when Type C coupons were loaded in quasi-static compression.

In addition to the two damage modes observed earlier under quasi-static tensile loading, tension-tension fatigue also produced transverse cracks in the +45° laminae and longitudinal cracks along the -45°/-45° interface. The transverse cracks in the +45 laminae were always coupled to transverse cracks in the 90° laminae. The tension-tension

QUASI-STATIC TENSION

TYPE C



DAMAGE MODE

1. Initiation 90° Transverse
2. Saturation 90° Transverse
3. Initiation -45° Coupling
4. Saturation -45° Coupling

S = Saturation Spacing

Figure 24 Damage Modes And Chronology - Type C - Quasi-Static Tension

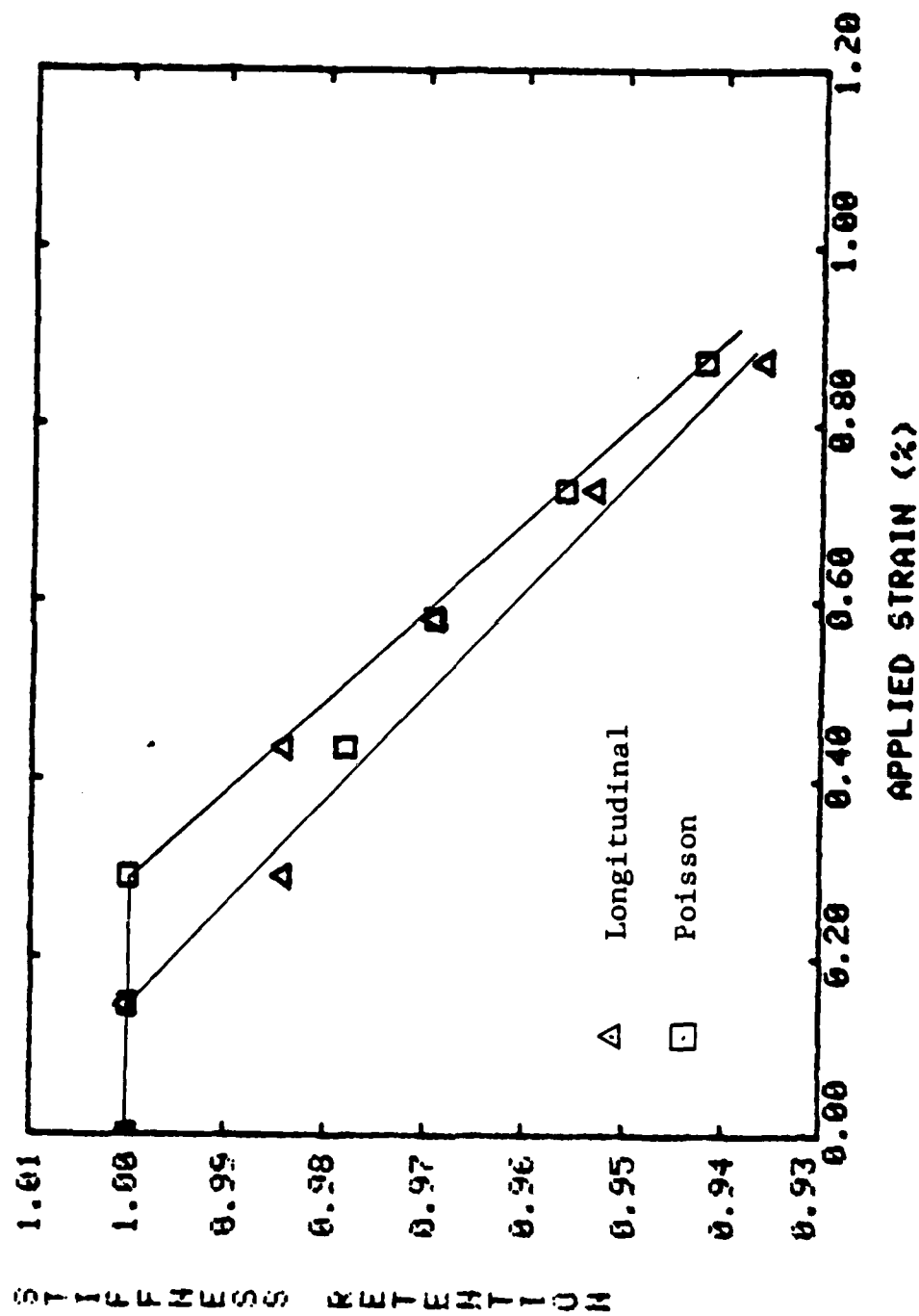


Figure 25 Stiffness Change - Type C, Quasi-Static Tension

DAMAGE MODE

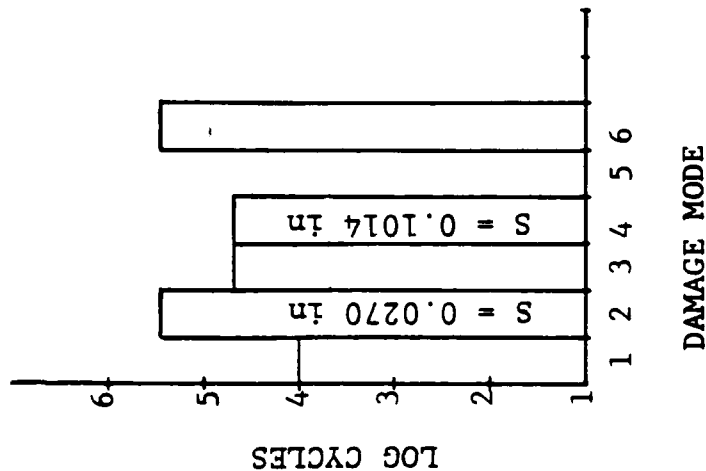
1. Initiation 90° Transverse
2. Saturation 90° Transverse
3. Initiation -45° Coupling
4. Saturation -45° Coupling
5. Initiation +45° Coupling
6. Initiation -45/-45 Interface

TENSION-TENSION FATIGUE

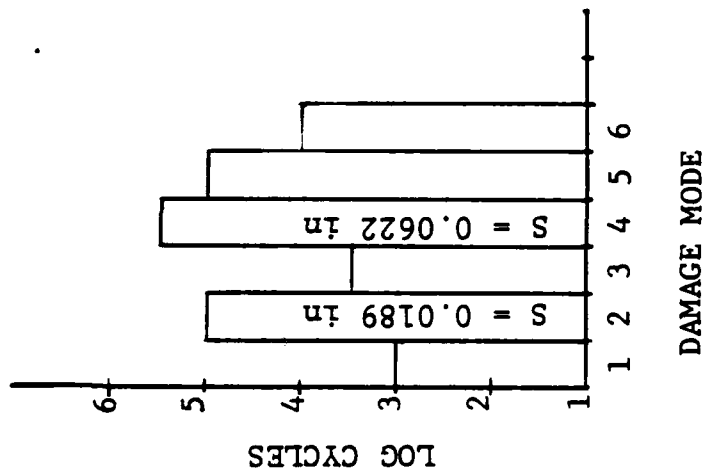
TYPE C

S = Saturation Spacing

C4-3 4500 $\mu\epsilon$



C2-1, 6000 $\mu\epsilon$



C4-2, 6000 $\mu\epsilon$

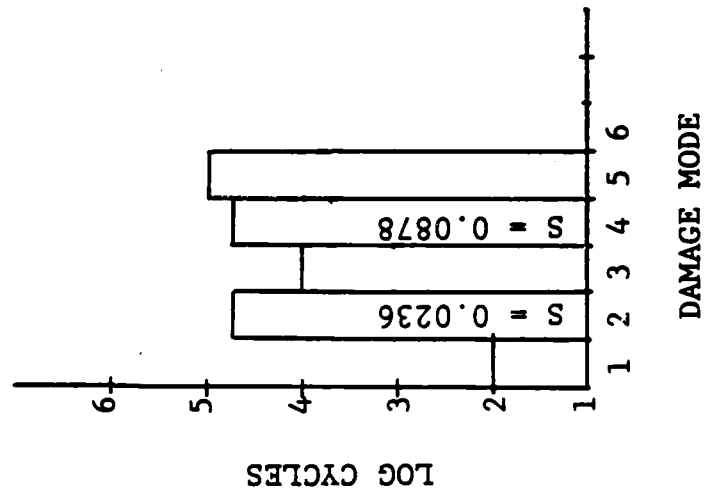
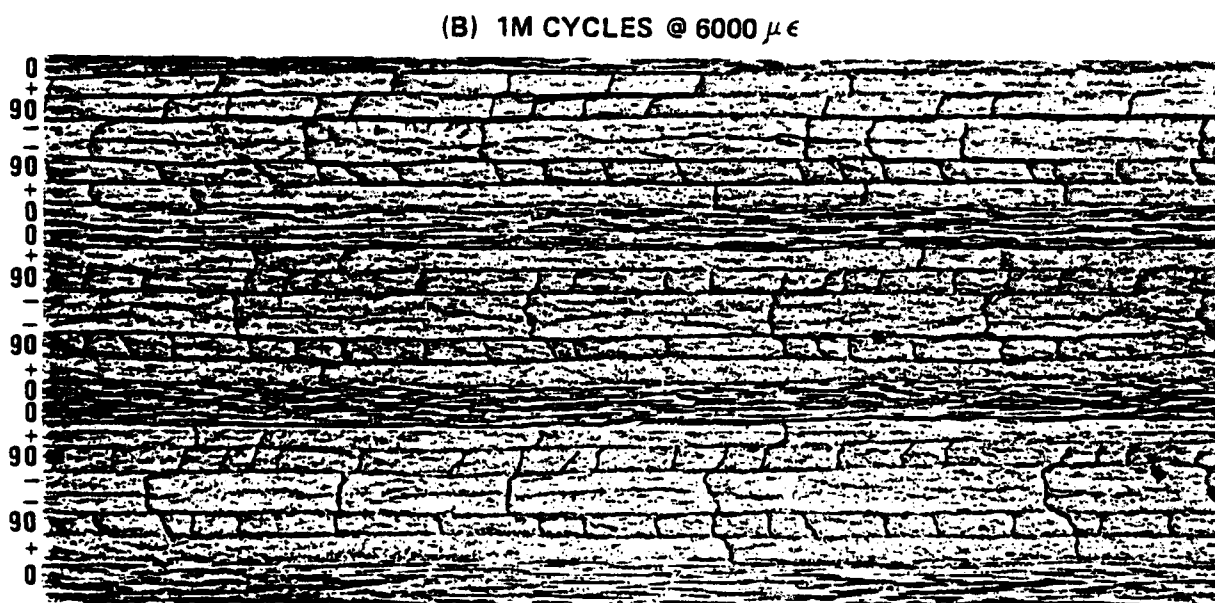
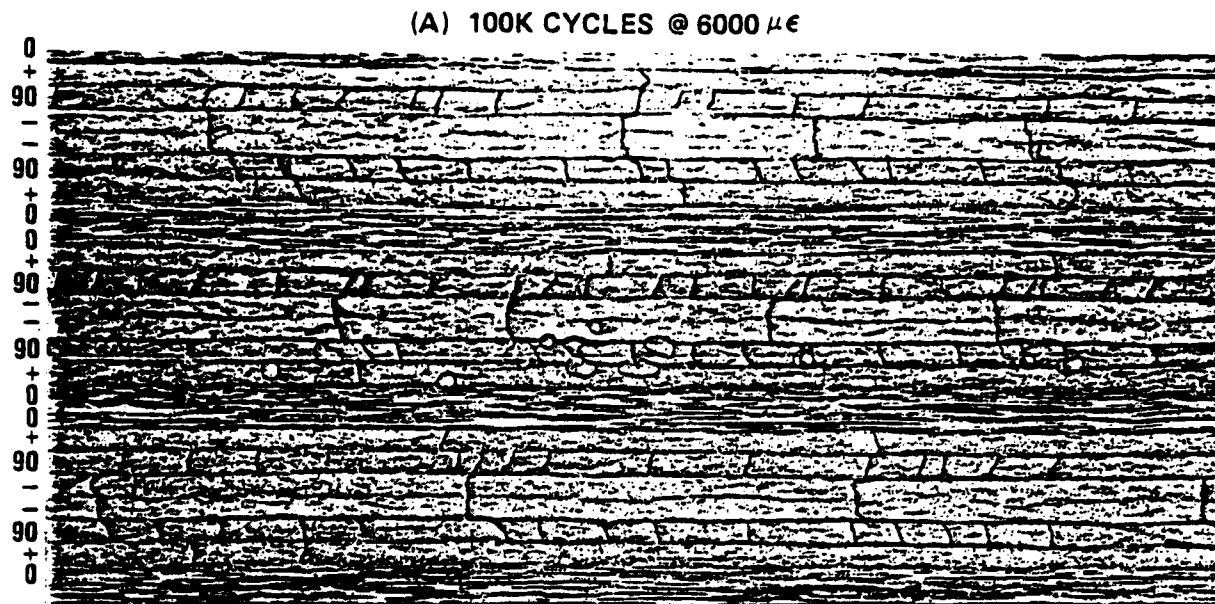


Figure 26 Damage Modes And Chronology - Type C - Tension-Tension Fatigue

fatigue tests were conducted at strain levels of 4500 and 6000 microstrain. At 4500 microstrain, the transverse cracks in the 90° and double -45° laminae and longitudinal -45°/-45° interface cracks had initiated by 10K, 50K and 300K cycles, respectively, (Figure 26). No coupling to the +45° laminae was observed. The specimen had not failed by the time the test was terminated at 1 million cycles. Two specimens were tested at 6000 microstrain. Specimen C2-1 was tested to one million cycles and all four damage modes were observed. Initiation occurred earlier by 1K, 5K, and 100K cycles for cracks in the 90°, -45°, and +45° laminae, respectively. Interfacial damage along edge replicas, taken at 100K cycles and 1 million cycles depict (Fig. 27) the transverse cracking and the development of longitudinal cracking at the interfaces. Testing of specimen C4-2 was terminated at 186K cycles, before transverse and interfacial cracking was observed. The saturation spacing at 4500 microstrain was greater than that at 6000 microstrain with about 5 times as many cracks in the 90° laminae as cracks in the -45° laminae in both cases (Figure 26). The stiffness changes at 6000 microstrain are shown in Figure 28. By 300K cycles the Poisson stiffness retention was 94% and at 1 million cycles the longitudinal stiffness retention had dropped to 86%. No measurable stiffness degradation was observed after one million cycles at 4500 microstrain. Figure 29 depicts the residual strength curve at the two strain levels. In spite of the observed damage and stiffness change at 6000 microstrain, there was no loss in residual strength for this specimen.

Compression-compression fatigue testing of Type C coupons was conducted at 6000, 7000, and 8000 microstrain. The 6000 and 7000 microstrain tests resulted in no visible damage or stiffness change by one million cycles. However, failure occurred at 364K cycles in the 8000 microstrain test. Because of the catastrophic failure, no damage was recorded by edge replication before fracture occurred, but Figure 30 indicates changes in longitudinal and Poisson stiffnesses of 13% and 6%, respectively.

Tension-compression fatigue testing at strain levels of 4000 and 4500 microstrain was conducted. The S-N curve (Figure 31) shows that failure occurred by 85K cycles (4500 microstrain) and 675K cycles (4000 microstrain). This is in sharp contrast to the results of the purely tensile or compressive fatigue loadings reported above where no failure occurred at even higher strain levels. In addition to the transverse cracking in the 90°, -45° and +45° laminae seen earlier, interface cracks were seen at the 0°/+45°, -45°/90° interfaces (Figure 32). Interfacial cracking did not occur



MIDPLANE

Figure 27 Damage Growth in a Type C Specimen under T/T Fatigue Test

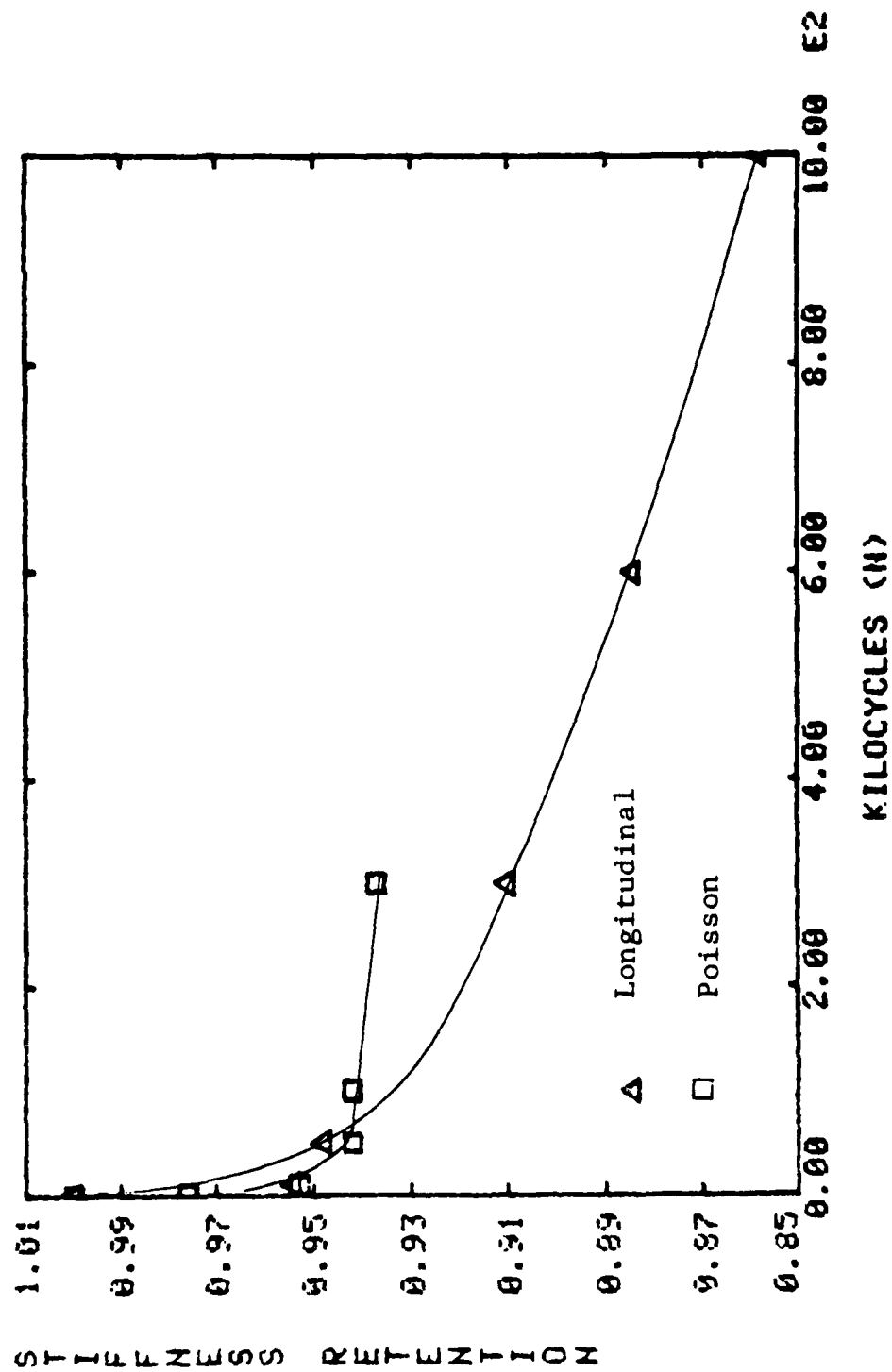


Figure 28 Stiffness Change, Type C, Tension-Tension Fatigue

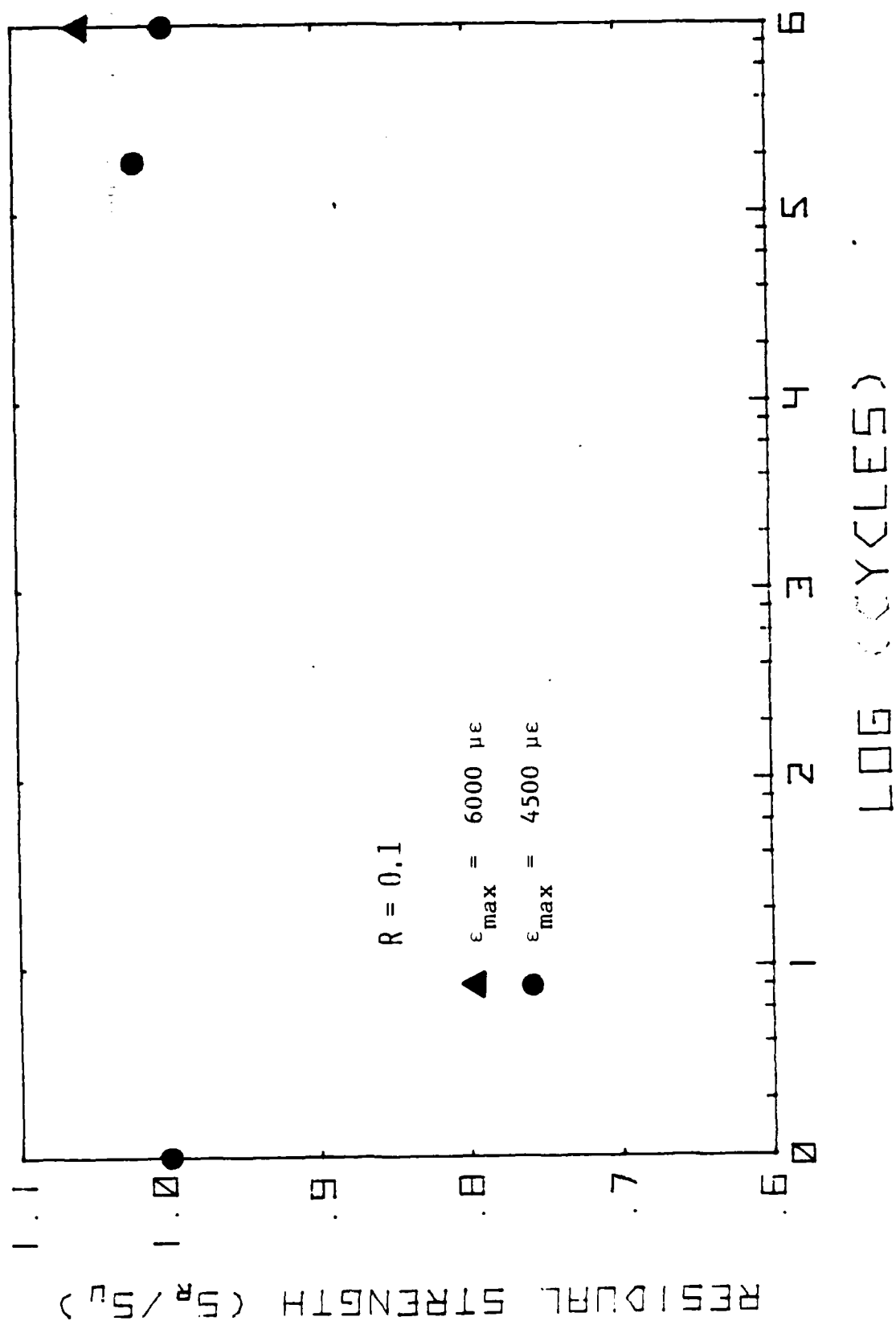


Figure 29 Residual Strength Curve for Type C Coupons Under Tension-Tension Fatigue

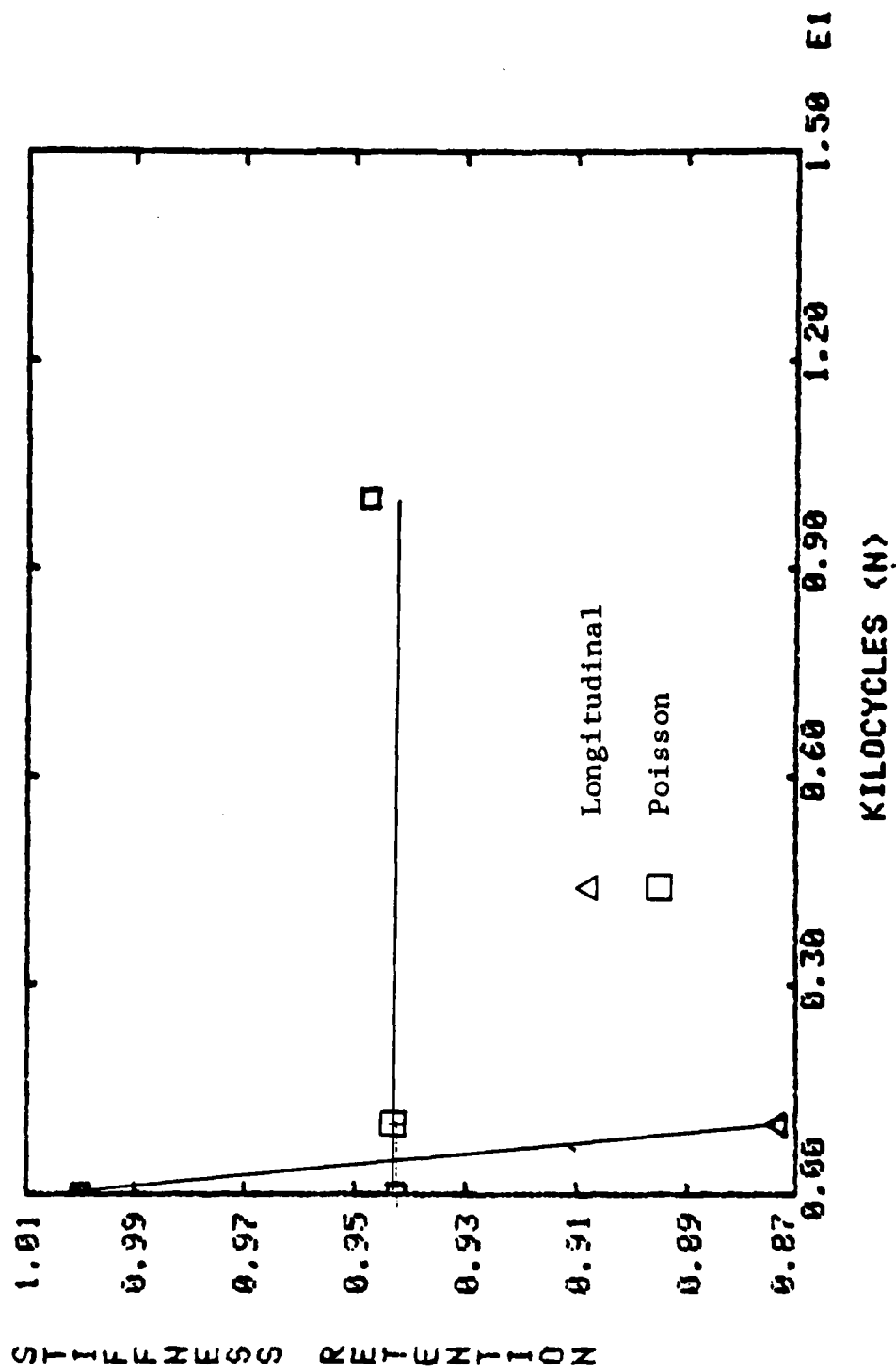


Figure 30 Stiffness Change - Type C, Compression-Compression Fatigue

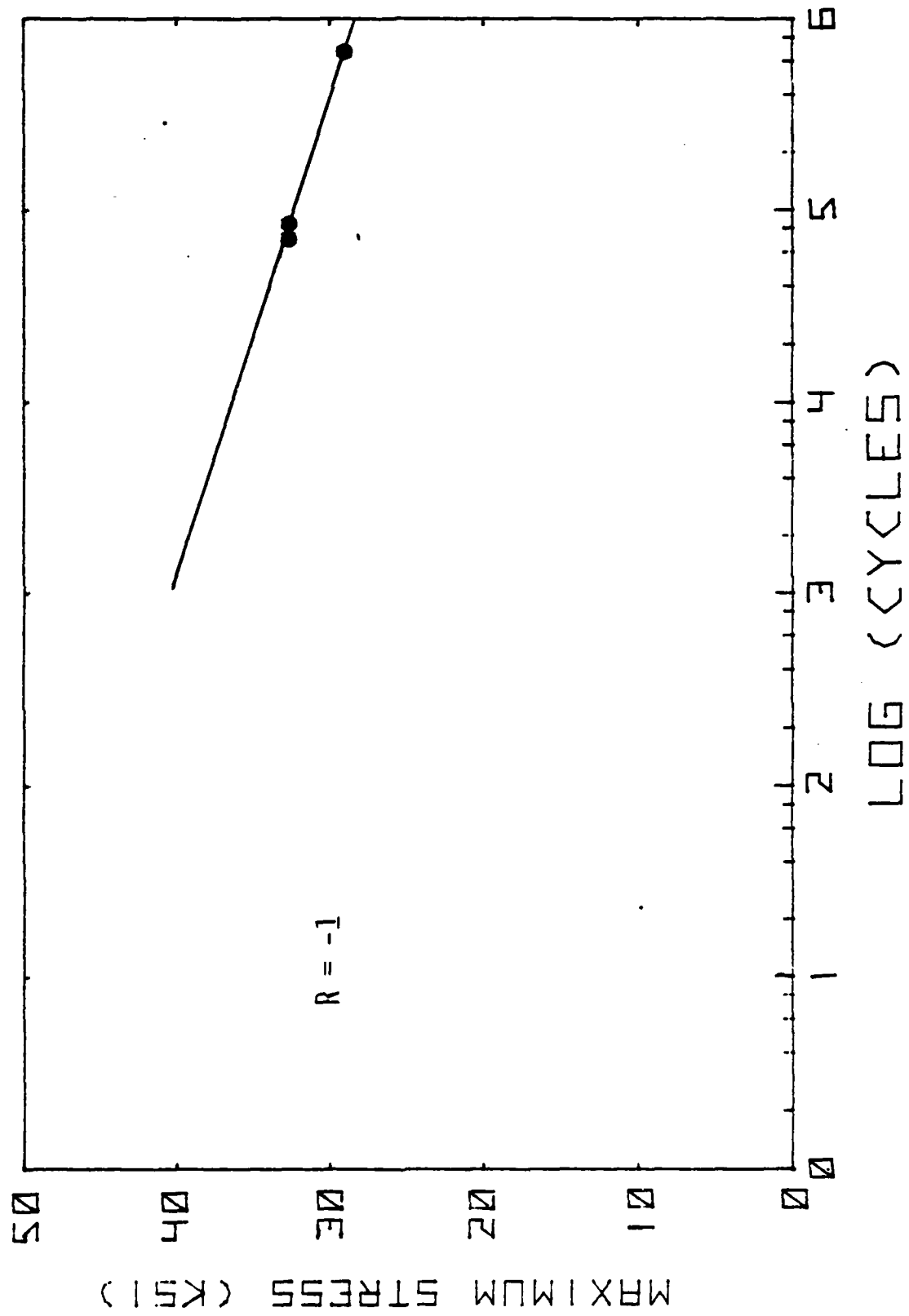


Figure 31 S-N Curve For Type C Coupons Under Tension-Compression Fatigue

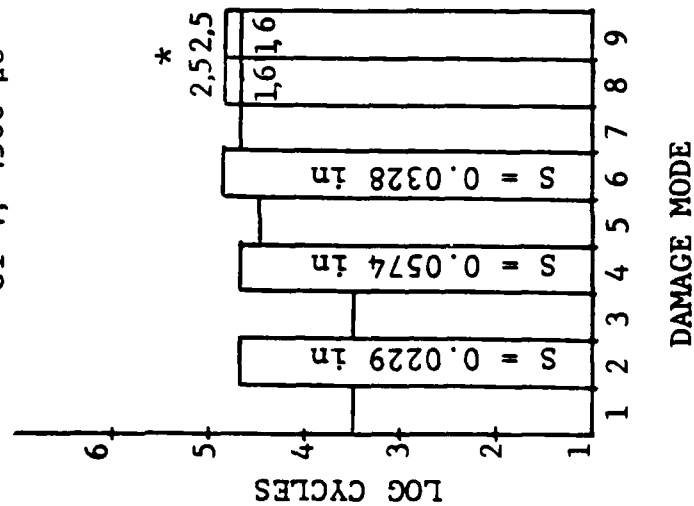
TENSION-COMPRESSION FATIGUE

TYPE C

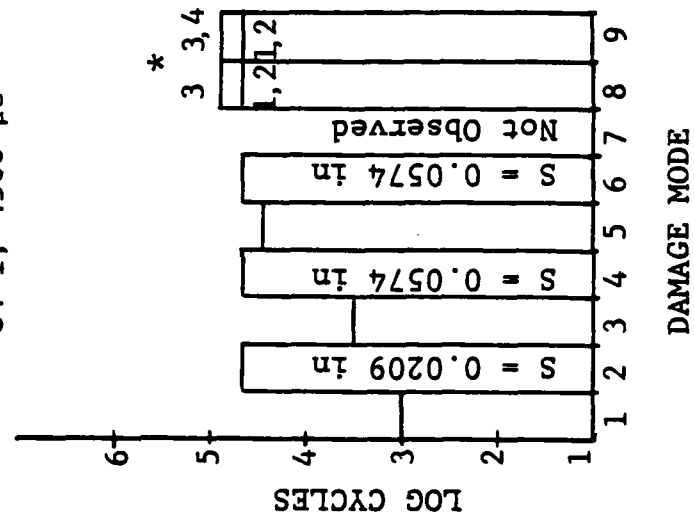
DAMAGE MODE

1. Initiation 90° Transverse
2. Saturation 90° Transverse
3. Initiation -45° Coupling
4. Saturation -45° Coupling
5. Initiation +45° Coupling
6. Saturation -45° Coupling
7. Initiation 0/+45 Interface
8. Initiation -45/90 Interface
9. Initiation +45/90 Interface

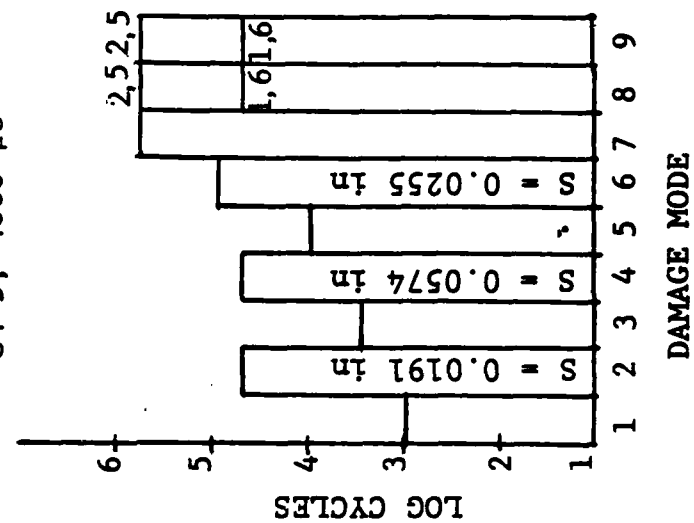
C1-4, 4500 $\mu\epsilon$



C4-1, 4500 $\mu\epsilon$



C4-5, 4000 $\mu\epsilon$

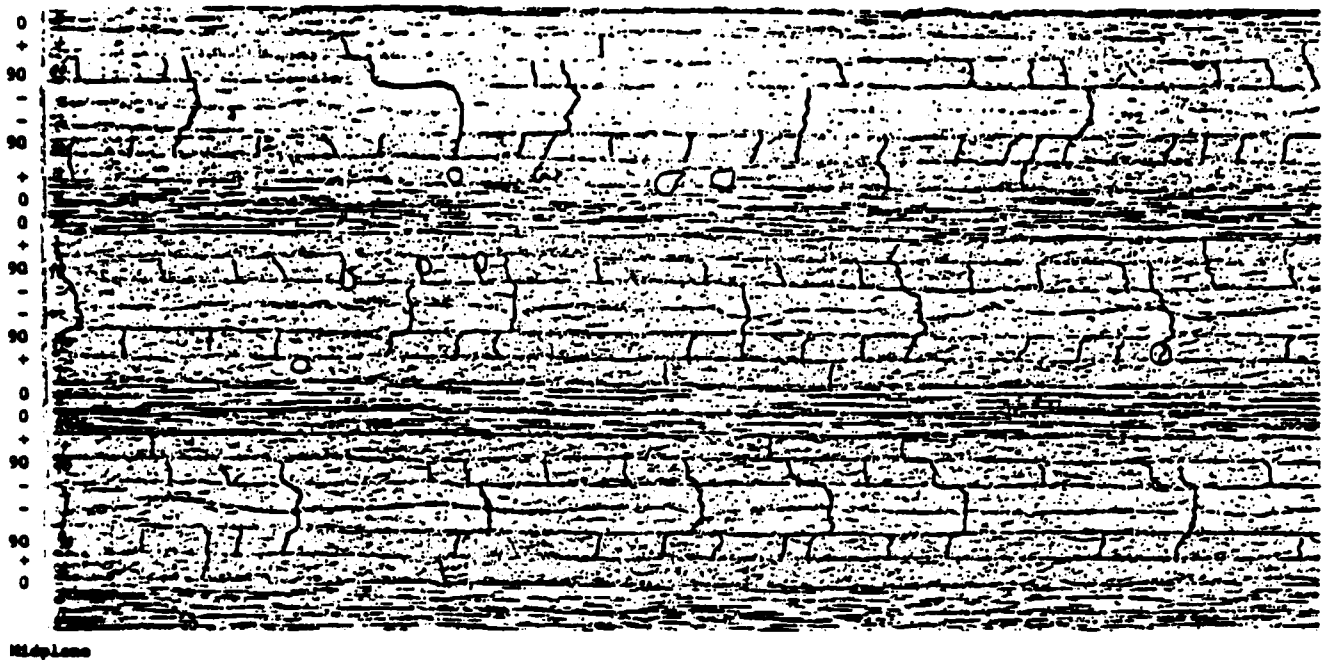


* Integers 1-6 refer to the 1st through 6th ply-groups, groups 1 & 6 being on the coupon surface.

Figure 32 Damage Modes And Chronology - Type C - Tension-Compression Fatigue

TYPE C (T-C)

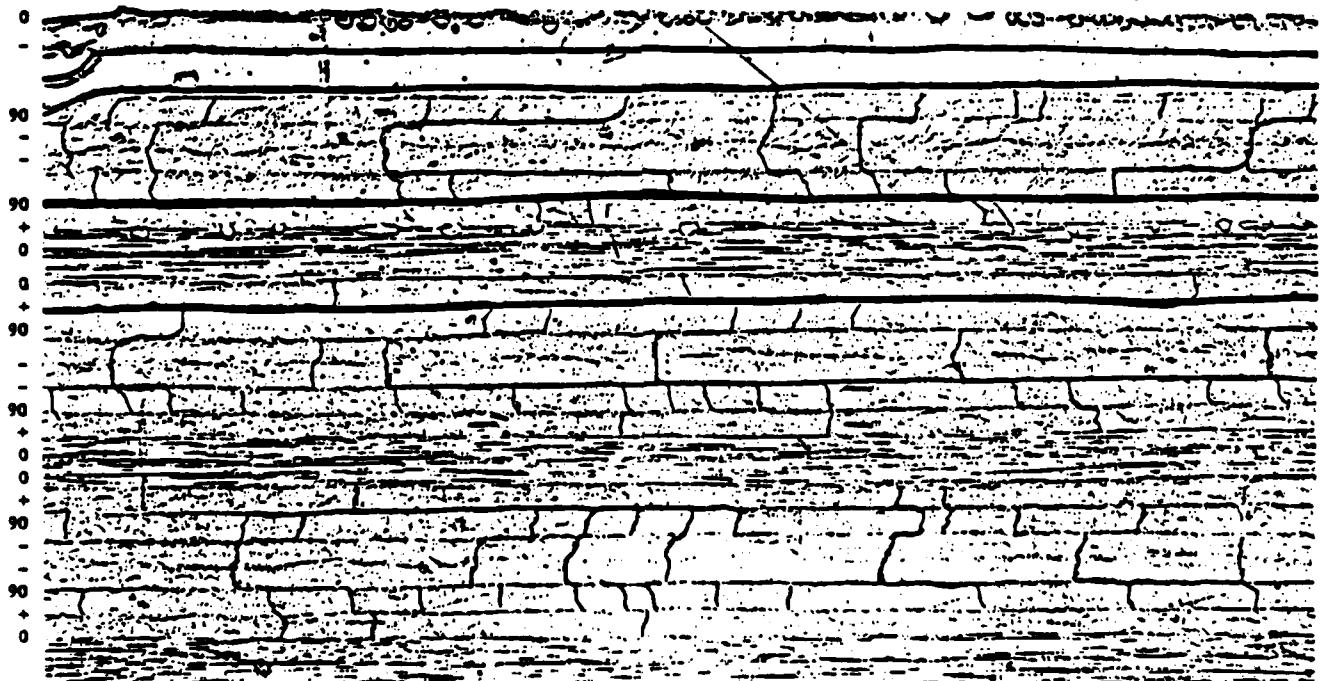
50K @ 4000 μ e



Midplane

TYPE C (T-C)

650K @ 4000 μ e



Midplane

Figure 33 Edge Replicas Demonstrating Successively Inward Interfacial Cracking in a Type C Coupon Under Tension-Compression

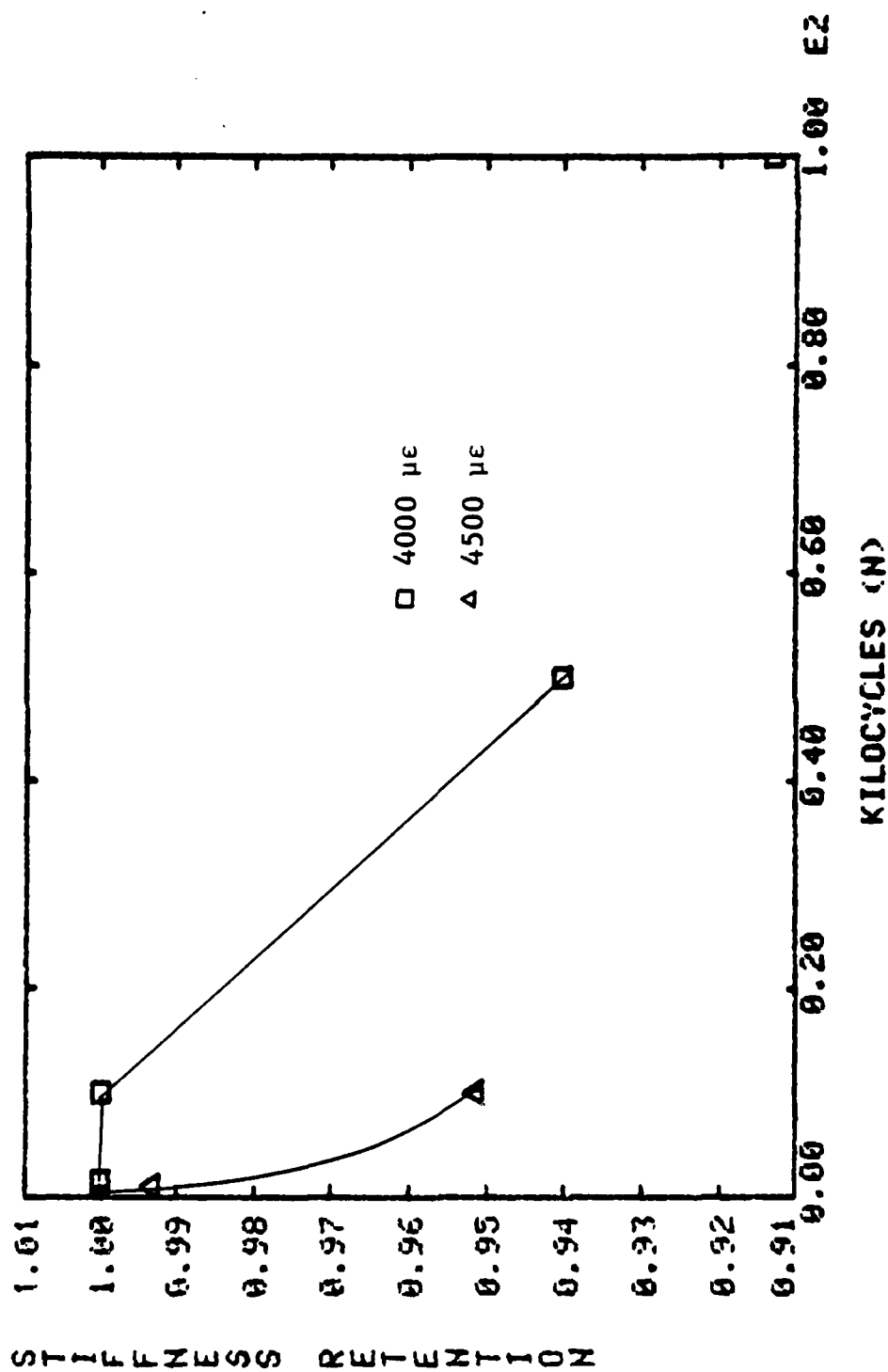


Figure 34 Longitudinal Stiffness Change - Type C, Tension-Compression Fatigue

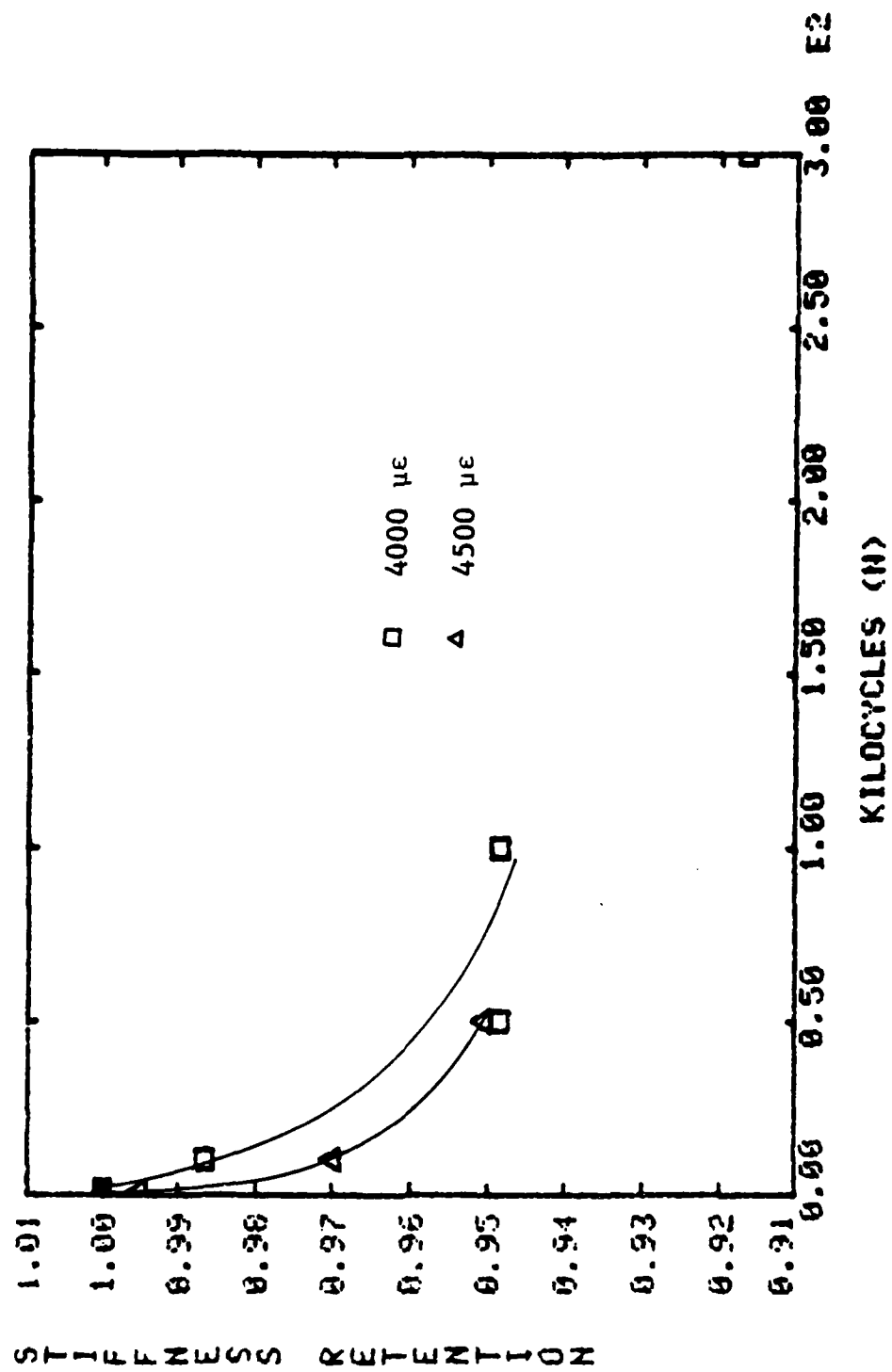


Figure 35 Poisson Stiffness Change - Type C, Tension-Compression Fatigue

simultaneously in all ply groups, forming first in the outer ply groups (Figure 33). The saturation spacing of the cracks in the 90° , -45° and $+45^\circ$ laminae was 0.0209, 0.0574 and 0.0328 inches, respectively. Cycles to initiation of damage seemed to be fairly insensitive to strain level although the cyclic interval between the occurrence of interface cracks in the first ply-group and second ply-group was greater at the lower strain level. The longitudinal and Poisson stiffness changes (Figures 34 and 35) at the 4000 microstrain level are consistent with the same stiffness change occurring sooner at the 4500 microstrain level.

4.3.4 Failure Modes and Mechanisms in Type D Coupons Stacking Sequence: $[0/[\pm 45/90/90/\pm 45/90/90/\pm 45/90]_s 0]_s$

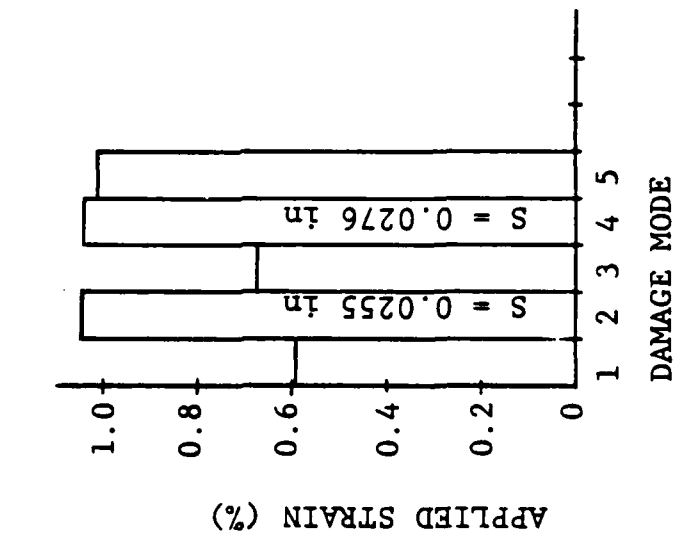
Quasi-static tensile testing of Type D coupons to successively greater loads resulted in transverse cracks in the 90° and the -45° laminae followed by delamination along the $\pm 45^\circ$ interface. Transverse cracking in the 90° and -45° laminae initiated by 0.6% and 0.7% strain, respectively (Figure 36). Saturation spacings of 0.0255 and 0.0276 inches occurred at a strain level of approximately 1% which was also the strain level at which $\pm 45^\circ$ interfacial cracking occurred. The damage resulted in longitudinal and Poisson stiffness changes on the order of 10% (Figure 37). Quasi-static compressive loading again resulted in no observable damage or stiffness change.

Tension-tension fatigue testing of Type D coupons was conducted at a strain level of 5000 microstrain. The same damage modes that were apparent in the quasi-static testing were observed during the fatigue testing. Figure 38 indicates that transverse cracking had initiated by 1K and 5K cycles in the 90° and -45° laminae and that saturation had occurred by 700K cycles with an average saturation spacing of 0.0308 inches in both cases. Initiation of $\pm 45^\circ$ interface cracks were observed by 700K cycles. None of the three specimens failed before one million cycles but all showed longitudinal and Poisson stiffness changes of about 8% (Figure 39). Residual strength measurements were made of two of the specimens which had been further cycles to 1.5 and 2.0 million cycles. The residual strengths are shown in Figure 40 as a variation with number of cycles.

Compression-compression fatigue testing of Type D coupons was conducted at strain levels of 5000, 5500, 6000 and 6500 microstrain. After one million cycles, no damage was observed at the first three strain levels. Delamination

QUASI-STATIC TENSION

TYPE D



DAMAGE MODE

1. Initiation 90° Transverse
2. Saturation 90° Transverse
3. Initiation -45° Coupling
4. Saturation -45° Coupling
5. Initiation +45 Interface

S = Saturation Spacing

Figure 36 Damage Modes And Chronology - Type D - Quasi-Static Tension

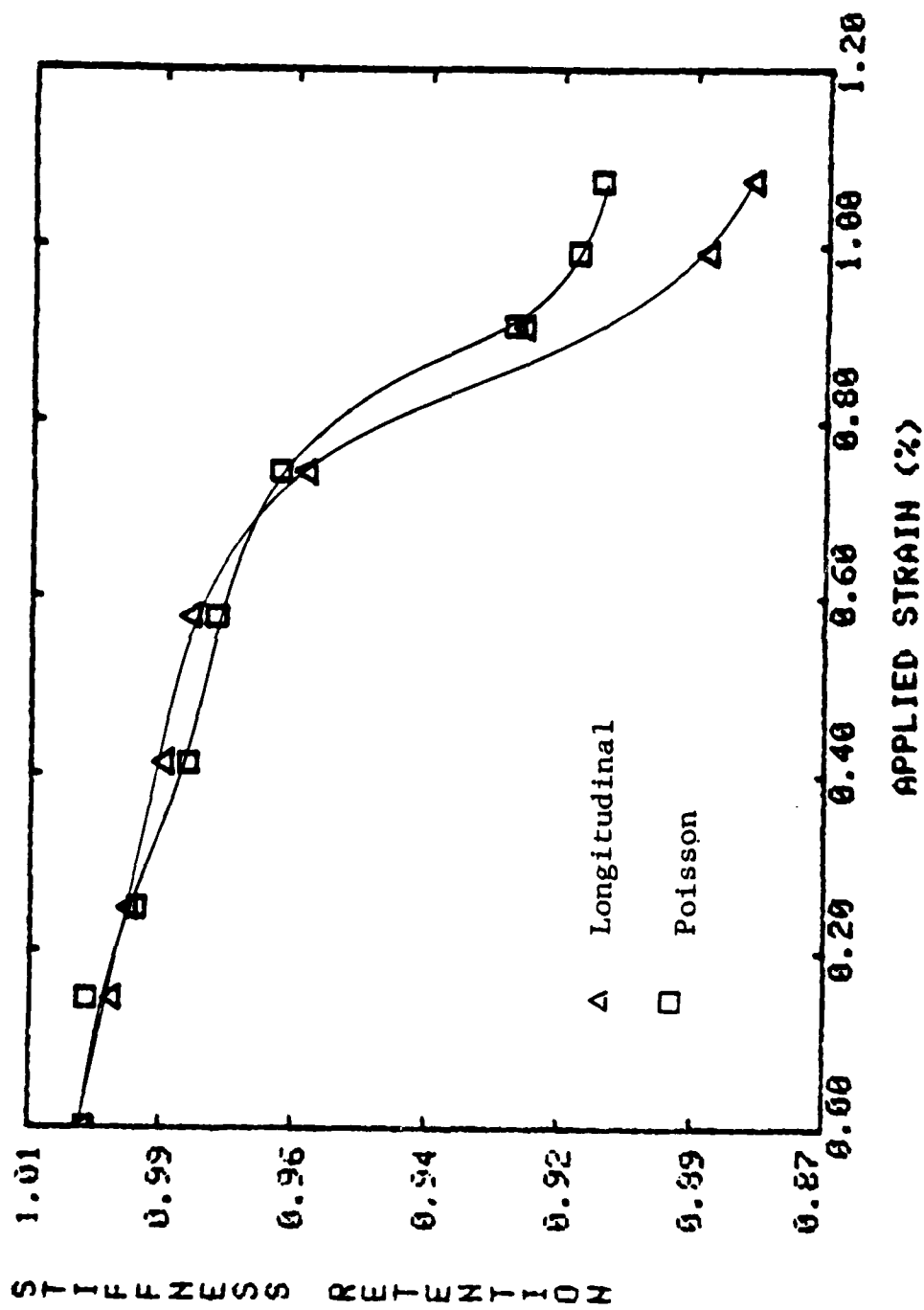


Figure 37 Stiffness Change - Type D, Quasi-Static Tension

TENSION-TENSION FATIGUE

TYPE D

S = Saturation Spacing

DAMAGE MODE

1. Initiation 90° Transverse
2. Saturation 90° Transverse
3. Initiation -45° Coupling
4. Saturation -45° Coupling
5. Initiation #1 ±45 Interface
6. Initiation #2 ±45 Interface

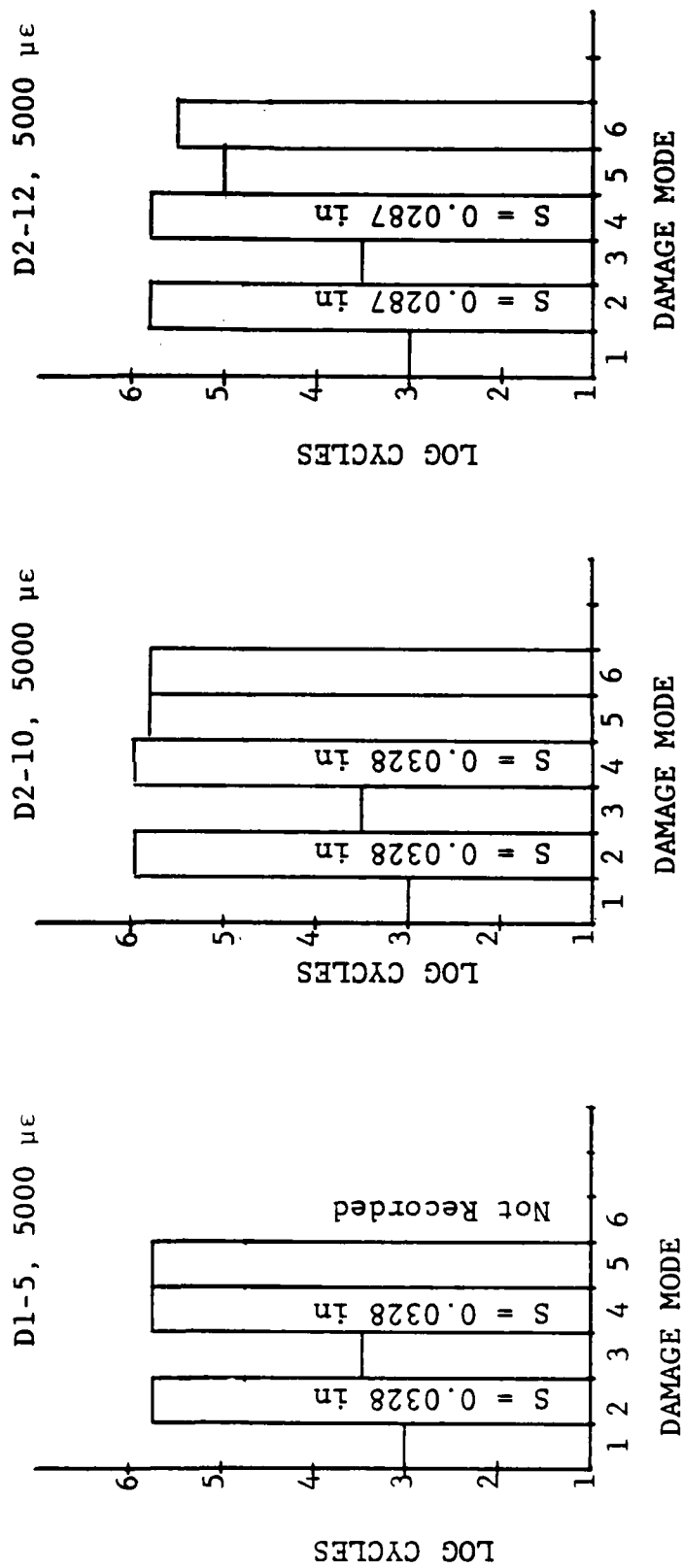


Figure 38 Damage Modes And Chronology - Type D - Tension-Tension Fatigue

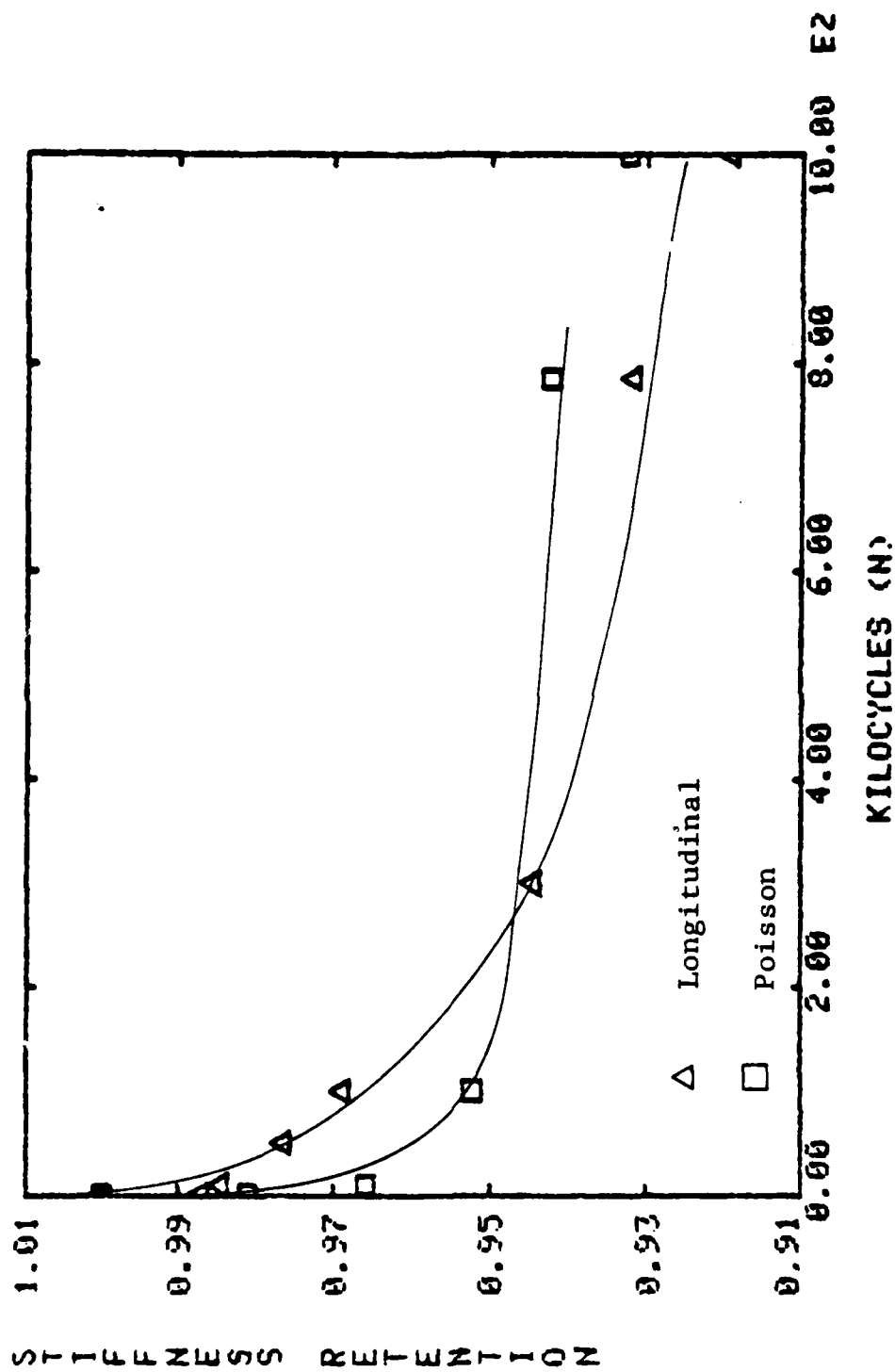


Figure 39 Stiffness Change - Type D, Tension-Tension Fatigue

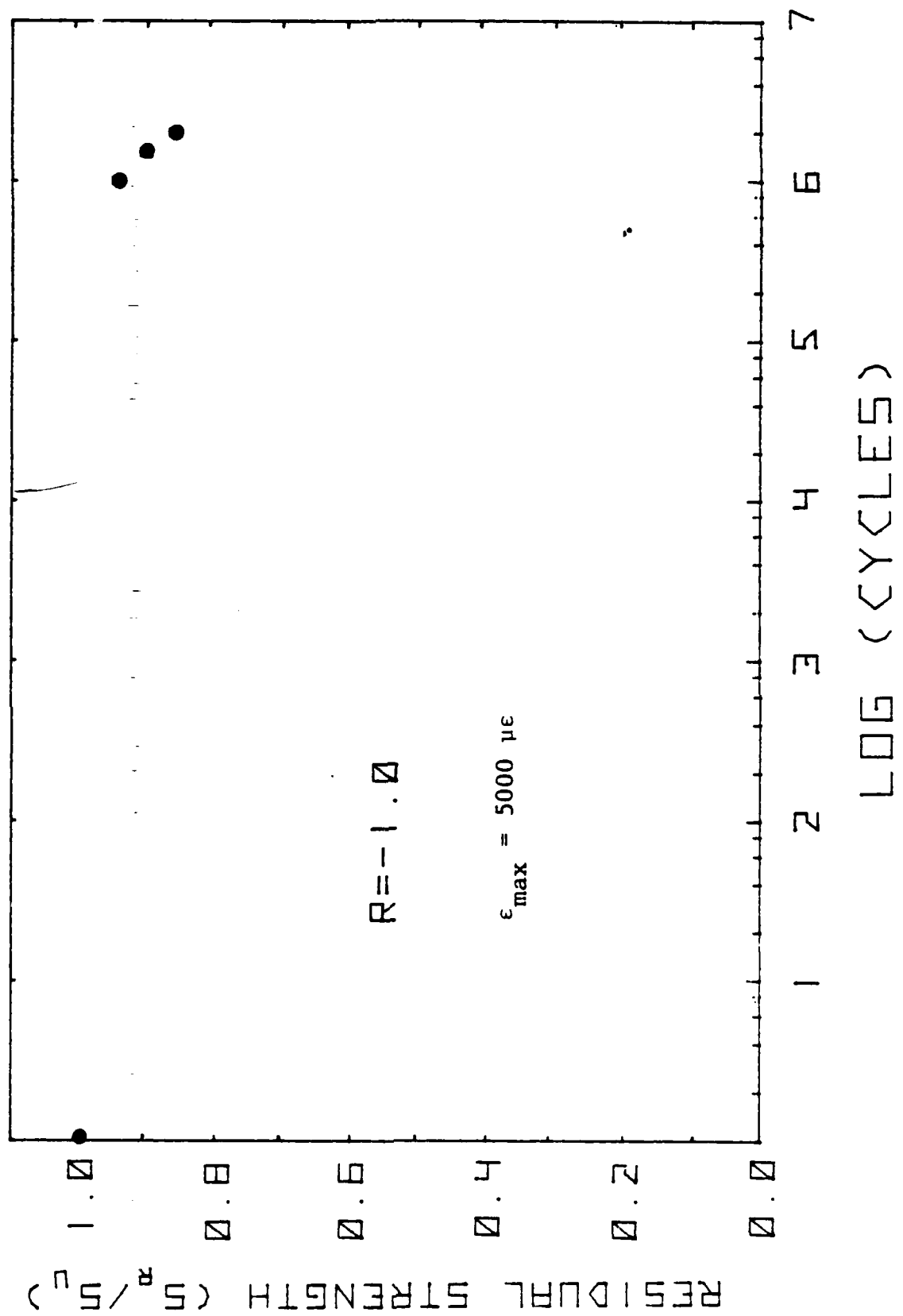


Figure 40 Residual Strength Curve for Type D Coupons Under Tension-Tension Fatigue

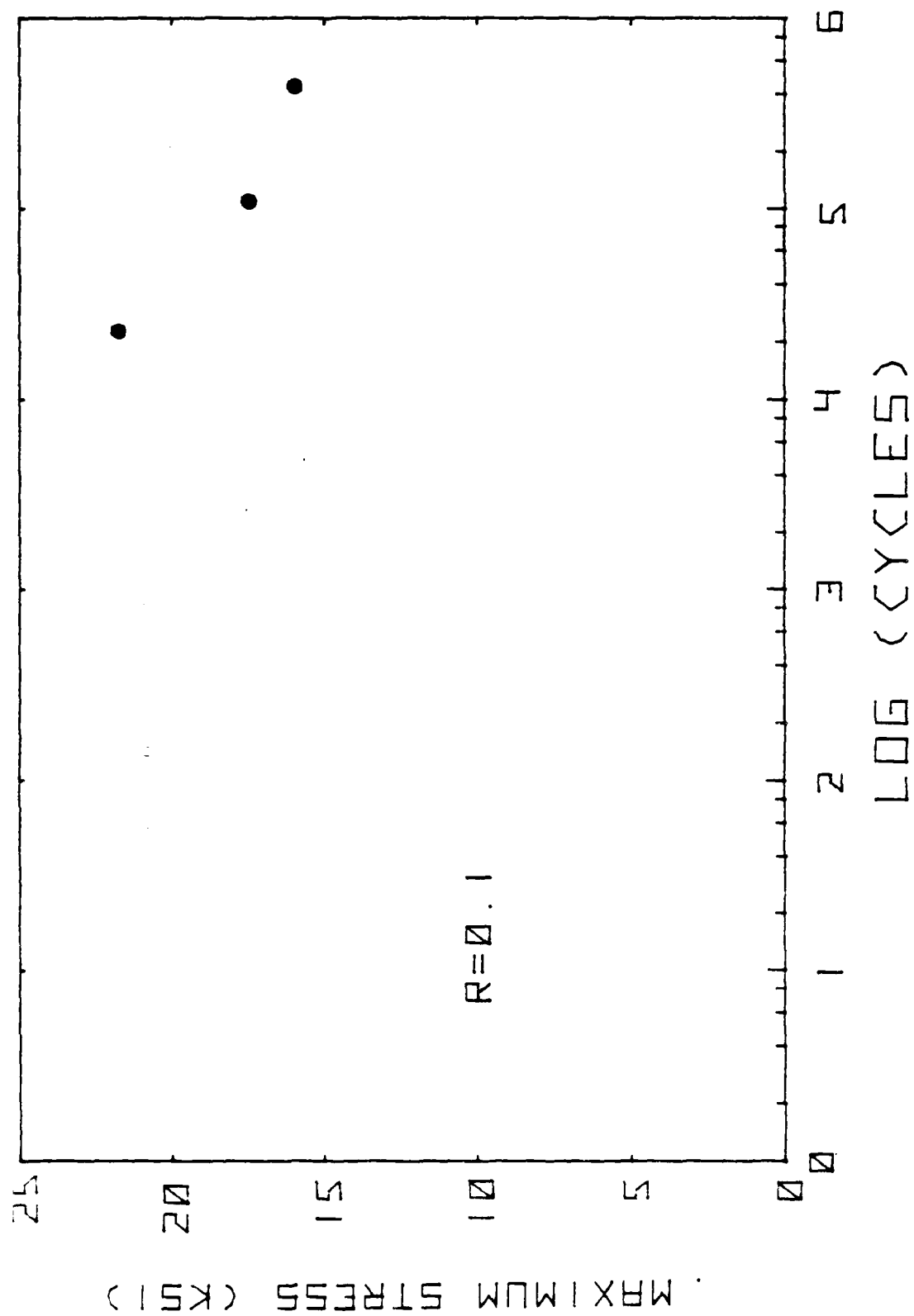
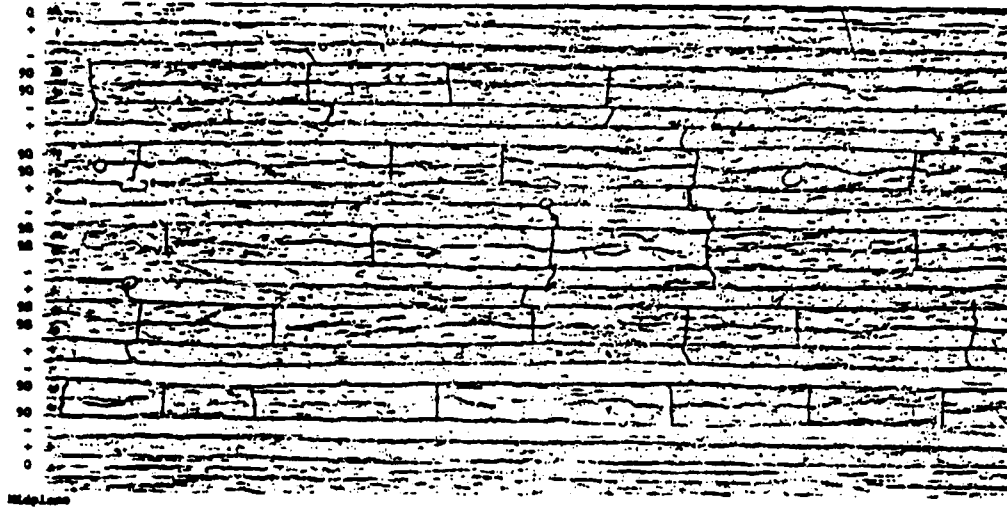


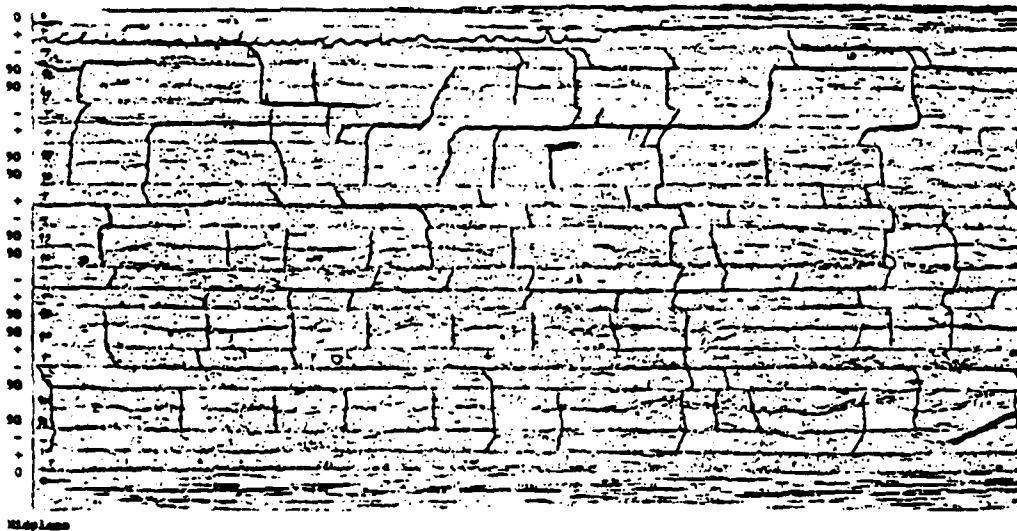
Figure 41 S-N Curve for Type D Coupons Under Tension-Compression Fatigue

TYPE D (T-C)

10K @ 4000 μ d



50K @ 4000 μ d



100K @ 4000 μ d

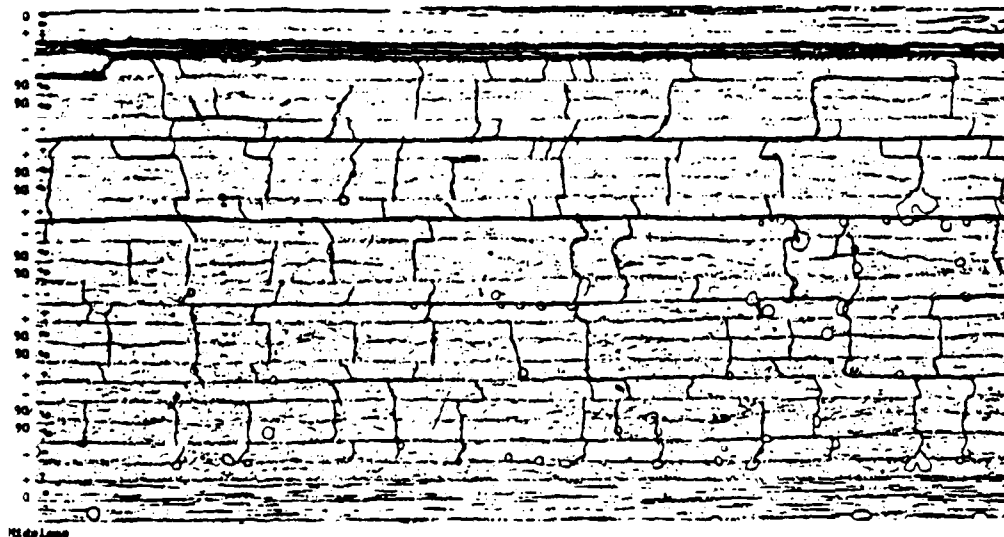


Figure 42 Edge Replicas of the Progression of Damage in Type D Coupons Under Tension-Compression Loading

TENSION-COMPRESSION FATIGUE

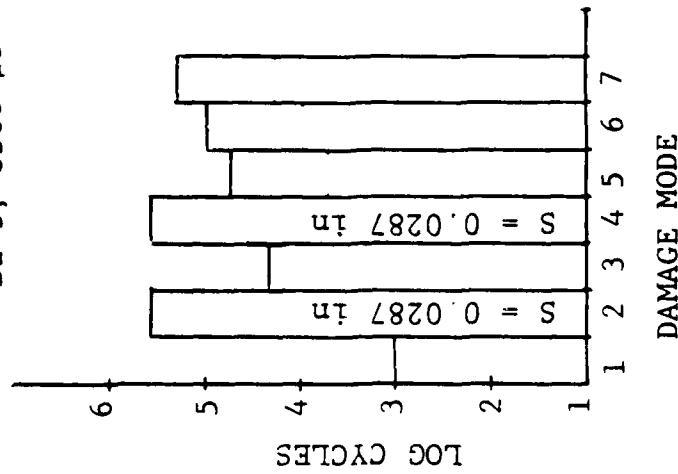
TYPE D

S = Saturation Spacing

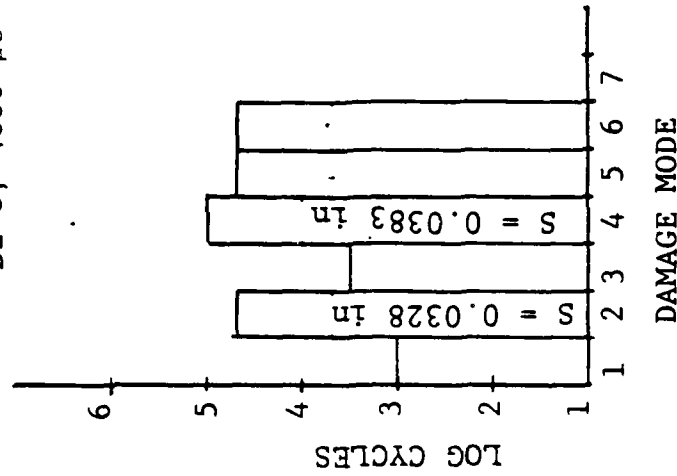
DAMAGE MODE

1. Initiation 90° Transverse
2. Saturation 90° Transverse
3. Initiation -45° Coupling
4. Saturation -45° Coupling
5. Initiation #1 +45 Interface
6. Initiation #2 +45 Interface
7. Initiation #3 +45 Interface

D2-5, 3500 $\mu\epsilon$



D2-8, 4000 $\mu\epsilon$



D1-10, 5000 $\mu\epsilon$

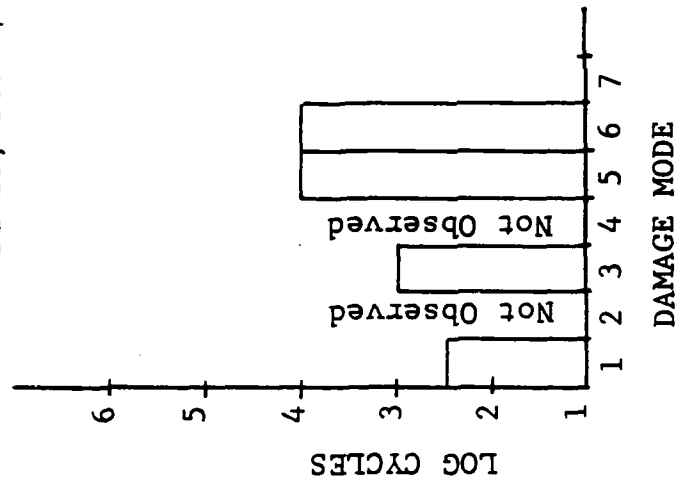


Figure 43 Damage Modes And Chronology - Type D - Tension-Compression Fatigue

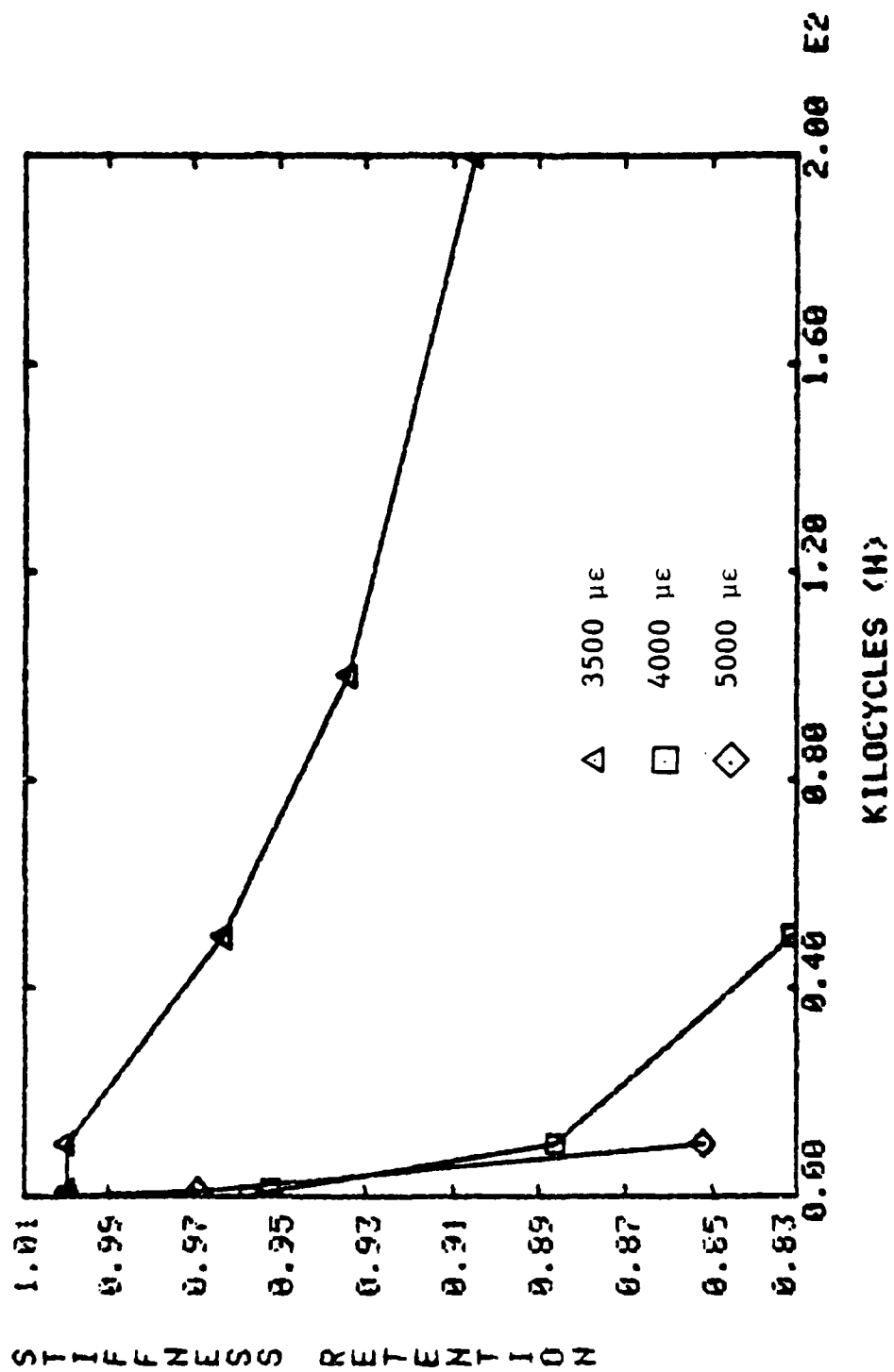


Figure 44 Longitudinal Stiffness Change - Type D, Tension-Compression Fatigue

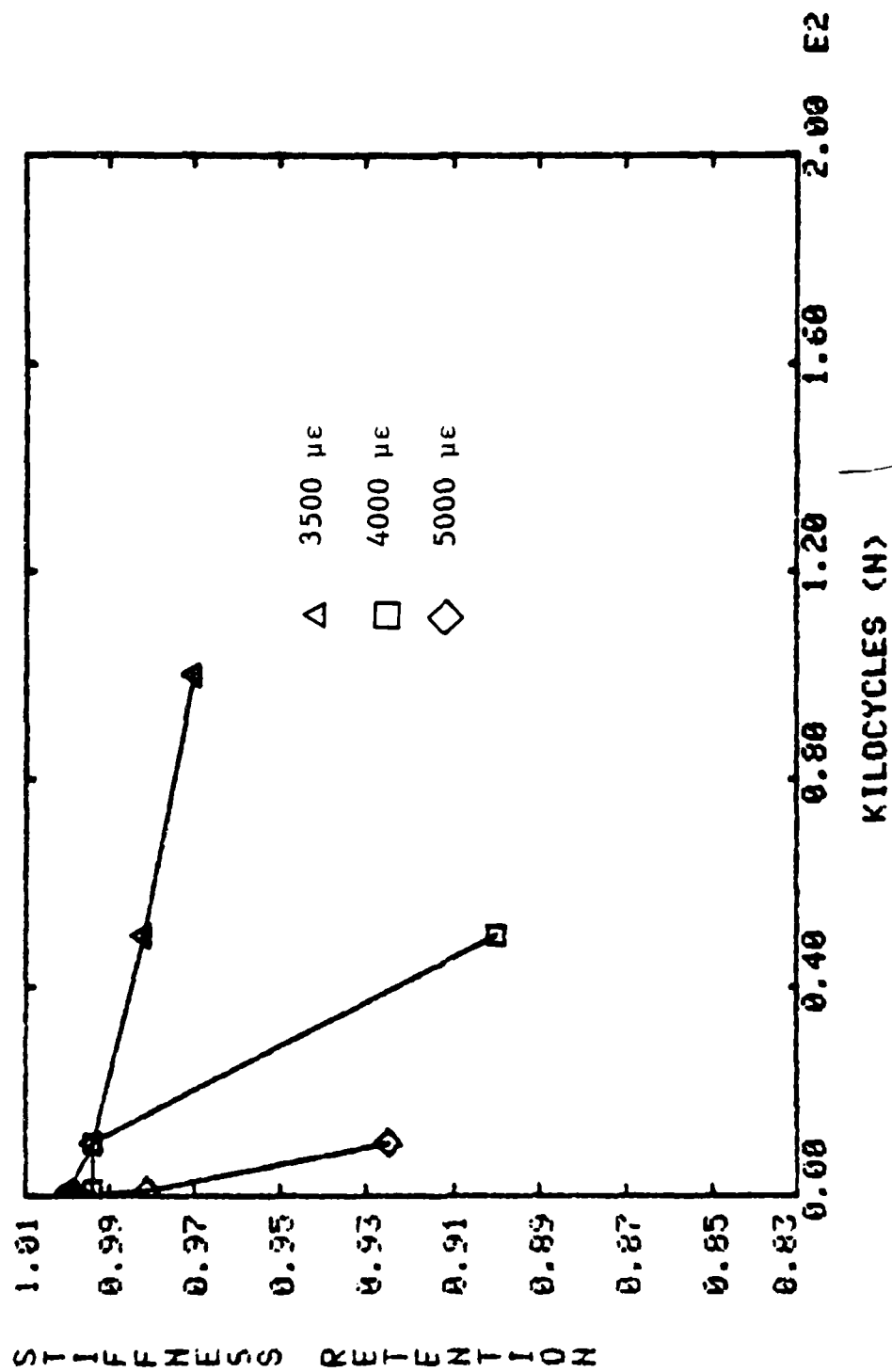


Figure 45 Transverse Stiffness Change - Type D, Tension-Compression Fatigue

initiated at 105K cycles in the 6500 microstrain test with final failure occurring after 846K cycles.

Tension-compression fatigue testing of Type D coupons at strain levels of 3500, 4000 and 5000 microstrain resulted in failures after 440K, 110K and 23K cycles, respectively. The S-N curve is shown in Figure 41. A sequence of edge replicas taken during the 4000 microstrain test are shown in Figure 42. The same progression of damage, transverse cracks in the 90° laminae producing cracks in the -45° laminae followed by interface cracks at the $\pm 45^\circ$ interface that was seen under tension-tension fatigue, was apparent here. The progressively earlier occurrence of initiation and saturation of damage as the strain level was increased is shown in Figure 43. The fact that saturation of transverse cracking was not observed in Specimen D1-10 (Figure 43) does not imply that it did not occur; only that the inspections that were made did not record it. The average saturation spacing observed in the tensile case was noted here for transverse cracking in tension-compression. The changes in longitudinal and Poisson stiffness are shown in Figures 44 and 45, respectively. The stiffness change with respect to strain level is consistent with what is expected. Longitudinal stiffness losses of 10% to 15% were observed prior to failure in tension-compression.

4.3.5 Summary of Test Results

In the previous sections, data for four different laminates subjected to five general loading conditions have been presented. In this section, similarities and differences in damage progression between the different laminates and loading conditions will be summarized.

In quasi-static tension, and tension-tension and tension-compression fatigue, the first sign of damage was always transverse cracking in the 90° plies. This was closely followed by cracking in the adjacent plus or minus 45° ply, depending on the stacking sequence. If transverse cracks appeared in +45° plies, they did not necessarily grow in -45° plies and vice versa. The saturation crack spacing was approximately the same within these loading modes. Transverse cracking was followed by interfacial cracks which linked the transverse cracks. This crack coupling occurred along all non-zero degree interfaces. The crack coupling tended to occur in the outermost plies first. Occasionally more transverse cracks would appear in the inner ply groups. Increasing the load level in the fatigue tests accelerated the damage accumulation process. Changes in stiffness due

to cracking of off-axis plies produced stiffness changes between two and five percent. Delaminations resulting from the crack coupling grew mainly along ± 45 interfaces. As the cracks coupled through interfacial damage, and delamination developed, stiffness changes on the order of 20% occurred. The laminate stiffness changes rapidly just prior to failure.

No damage or stiffness changes were observed in the quasi-static compression tests. Threshold fatigue levels were determined in the compression-compression tests. Transverse cracking was not observed in these tests and delamination was the mode of failure.

The most important observation that was made in all the testing was that tension-compression fatigue was the most damaging loading mode of all. Cracks which initiated due to tensile loading grew along interfaces and coupled at a greater rate in tension-compression fatigue than in either tension-tension or compression-compression at the same strain amplitude. The presence of transverse cracks under tension substantially reduced the delamination resistance in compression. Thus a possible source of delamination in the absence of stress concentrations has been identified, a fact which has implications for the integrity of larger structural elements.

The effect of stacking sequence was investigated through the use of the three quasi-isotropic laminates, Types A, B, and C. Recall from Figure 3 that the different stacking sequences gave rise to tensile and compressive interlaminar normal stresses of equal magnitude when coupons of Type A and B, respectively, were loaded in tension. For the same load, the type C coupons had smaller tensile interlaminar normal stresses.

Figure 46 summarizes the damage during the quasi-static tension testing. The effect of stacking sequence can be seen in the earliest initiation of all forms of damage in the Type A coupons which contained the largest tensile interlaminar normal stresses when a tensile load was applied. The damage rate in the Type C was greater than the Type B coupons which is consistent with the levels of interlaminar stresses that they experience. It should be also noted that no interfacial cracks were observed in the Type B coupons. The tension-tension fatigue test at 6000 microstrain results are summarized in Figure 47. Again a clear ordering of damage rates can be seen with damage modes occurring soonest in Type A coupons and latest in Type B. It should be noted that the strain levels in Figure 46 and

QUASI-STATIC TENSION TESTING QUASI-ISOTROPIC

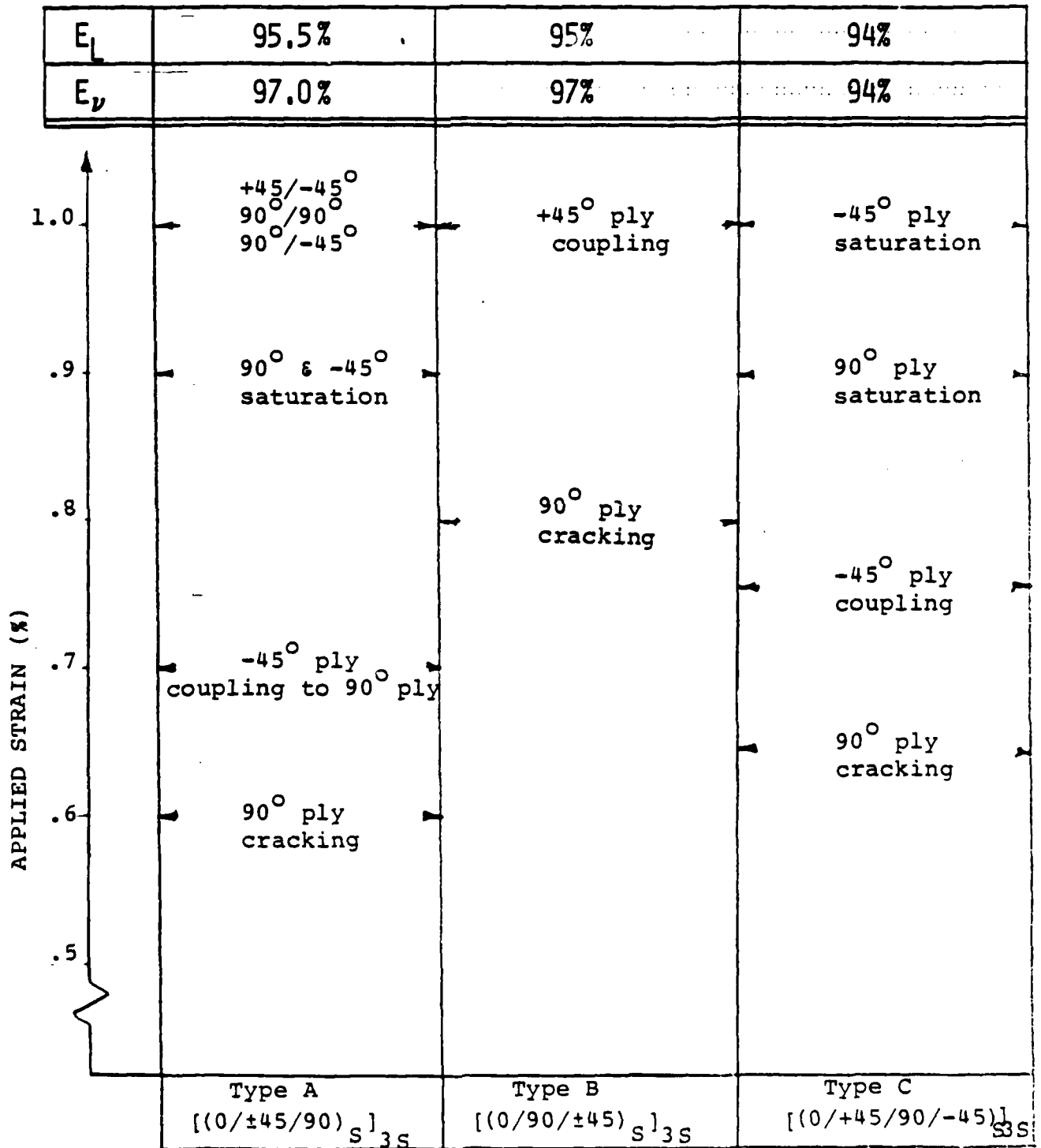


Figure 46 Summary of Quasi-Isotropic Quasi-Static Tension Results

TENSION-TENSION FATIGUE RESULTS
QUASI-ISOTROPIC
(6000 $\mu\epsilon$)

LOG CYCLES			
	TYPE A [(0/ \pm 45/90) $_S$] $_3$ S	TYPE B [(0/90/ \pm 45) $_S$] $_3$ S	TYPE C [(0/ \pm 45/90/ \pm 45) $_S$] $_3$ S
	\pm 45 & -45/90 INTER. GROUPS 1 - 6	\pm 45 INTER. -45 CRACKING 90 & \pm 45 SATURATION	-45 SATURATION \pm 45 CRACKING 90 SATURATION
	\pm 45 & -45/90 INTER. GROUPS 1 & 6	+45 CRACKING 90 CRACKING	-45/90 INTER. -45 CRACKING 90 CRACKING

Figure 47 Summary of Quasi-Isotropic Tension-Tension Fatigue Results

LIFE AND RESIDUAL STRENGTH DATA

QUASI-ISOTROPIC

LOAD MODE/LEVEL	TYPE A [(0/±45/90) _s] _{3s}	TYPE B [(0/90/±45) _s] _{3s}	TYPE C [(0/±45/90/-45) _s] _{3s}
T-T 4500 $\mu\epsilon$ 6000	NO FAILURES (90% RETENTION) NO FAILURES (82% RETENTION)	NO FAILURES (100% RETENTION) NO FAILURES (85% RETENTION)	NO FAILURES (100% RETENTION) NO FAILURES (97% RETENTION)
C-C 4500 $\mu\epsilon$ 5000 5500 6000 7000 8000	NO FAILURES ±45° CRACK NO FAILURE ±45° CRACK	NO FAILURES FAILURE @ 500K FAILURE @ 50K FAILURE @ 5K	NO FAILURE NO FAILURE FAILURE @ 360K
T-C 4000 $\mu\epsilon$ 4500 6000	FAILURE @ 50K	FAILURE @ 50K FAILURE 1K	FAILURE @ 650K FAILURE @ 100K

Figure 48 Quasi-Isotropic Life and Residual Strength Data

the cycles in Figure 47 indicate where damage was observed, not where it initiated. Finally, life and residual strength data (Figure 48) indicate that under compression-compression loading (which reverses the interlaminar normal stresses), lifetimes at a given load level were shortest for the Type B coupons. Figure 48 also shows that Type A and B coupons had the same lifetime under tension-compression loading at 4500 microstrain. The interlaminar stress levels in Type C coupons were lower (at 4500 microstrain) and they had longer lifetimes.

SECTION V

ENVIRONMENTAL FACTORS AND EFFECTS

The inclusion of environmental effects into the cumulative damage model stems from the recognition that the epoxy matrix material is polymeric and potentially viscoelastic. Moisture and temperature changes in the environment can therefore be expected to affect the response of the composite. In its present state, the shear lag model accounts for the effects of moisture and temperature through the lamina properties input to the model. The experimental investigation conducted was used to verify this concept.

As an initial step in investigating environmental effects, the Type A, $[0/\pm 45/90/90/\mp 45/0]_{3S}$ coupons were tested in tension, compression, and tension-compression fatigue at 250°F, dry. Section 5.1 describes the procedures that were used and measurements that were made. The results are presented and discussed in Section 5.2, along with some of the technical difficulties encountered.

5.1 Elevated Temperature Testing

The method that was originally intended to provide the 250°F, dry environment was to use an environmental chamber which surrounded the hydraulic grips in addition to the specimen. This was abandoned when it was discovered that the hydraulic fluid and seals in the grip mechanism could not withstand 250°F. If hydraulic grips are to be used, a localized method of environmental control which affects only the specimen must be effected. The method that was used in these tests was to wrap the 4" test section of the coupon with aluminum foil and then wind electrical resistance heating tape on top of the aluminum. Three thermocouples were mounted on the specimen to check the uniformity of the temperature distribution. Two were mounted one centrally but on opposite faces of the specimen and the third was mounted one inch from the center. The voltage to the heating tape was manually controlled by VARIAC transformer and it was found that the temperatures sensed by the thermocouples were within 0.5°C of one another.

Longitudinal and Poisson stiffness measurements were made using two strain gages mounted longitudinally on either side of the specimen and a third gage mounted across the width of the specimen. The gages were bonded to the coupon surface using a 350°F cure system in an attempt to minimize

gage creep. It was not considered advisable to lower the specimen temperature in order to perform other NDE due to the possibility of inducing damage by thermal stresses. In the quasi-static tension and compression tests, the stiffness was measured in each test as the maximum load was increased until failure occurred. The tension-compression fatigue tests were conducted at 4500 microstrain, constant amplitude, $R = -1.0$ and at a frequency of 10 Hz. Stiffness measurements were taken by stopping the tests at 1K, 5K, 10K and 20K cycles and loading from 0.5 Pmin to 0.5 Pmax.

5.2 Elevated Temperature Results

Quasi-static tensile testing of the Type A coupons was conducted at successively higher loads to a maximum applied strain of approximately 1%. The longitudinal and Poisson stiffness changes were measured at each load level and are plotted in Figure 49. The stiffness changes are of the same order (5%) as those measured in the room temperature tests but are more gradual. Although the curves do fit the data in an average manner, the data points indicate an increase in stiffness which may not be real but more a malfunction in the strain gage system.

The results of the quasi-static compression tests are shown in Figure 50. Room temperature compression tests resulted in no changes in stiffness. Figure 50 indicates that (buckling) failure occurred at approximately 0.50% strain and was accompanied by longitudinal and Poisson stiffness retentions of 97% and 93%, respectively.

Three tests were conducted under tension-compression fatigue at the 4500 microstrain maximum applied strain level. Failure occurred after an average of 23.753K cycles compared with no failure by 40K cycles in Type A coupons at room temperature. The longitudinal strain gages usually broke after 1K cycles and the transverse gages indicated, if anything, increases in stiffness, which must again be attributed to malfunctions in the strain gage system at elevated temperature.

These tests indicate that damage monitoring of elevated temperature fatigue testing cannot be approached as an afterthought. The techniques must be functional at the elevated temperature because cooling to room temperature to perform inspection could itself induce damage. This criterion rules out the use of surface replication and enhanced X-ray techniques in their present forms and means that any displacement measurement techniques should be

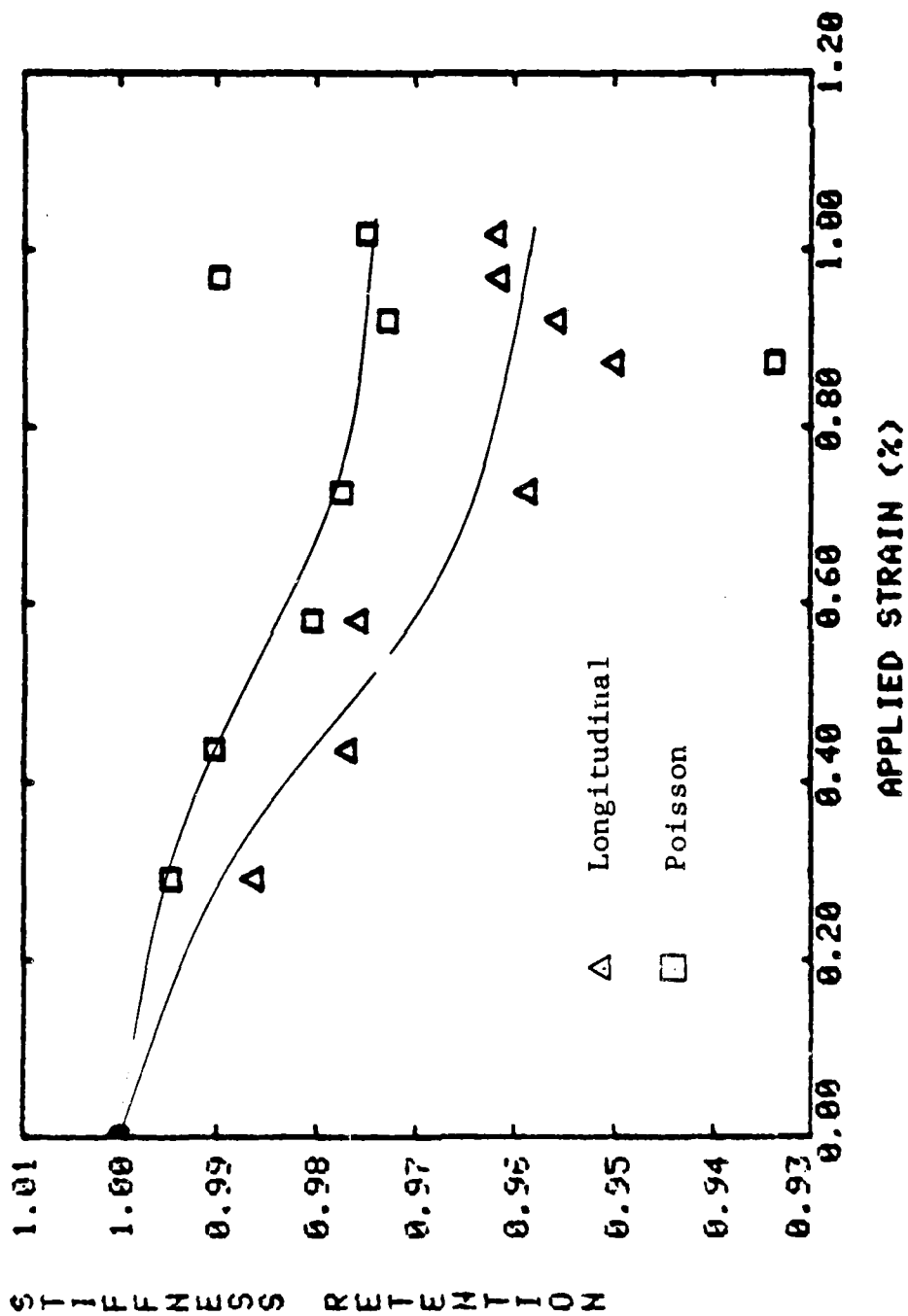


Figure 49 Stiffness Change - Type A, 250°F, Quasi-Static Tension

AD-A126 048

CUMULATIVE DAMAGE MODEL FOR ADVANCED COMPOSITE
MATERIALS(U) GENERAL DYNAMICS FORT WORTH TX FORT WORTH
DIV K M LIECHTI ET AL JUL 82 F2M-7074

2/2

UNCLASSIFIED

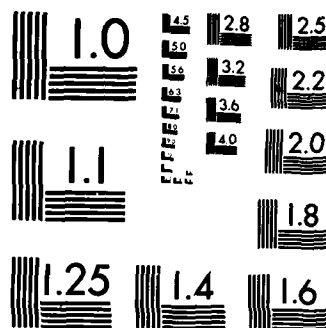
AFWAL-TR-82-4094 F33615-81-C-5049

F/G 12/1

NL

END

FILMED
+ (P)
DTIC



MICROCOPY RESOLUTION TEST CHART
NATIONAL BUREAU OF STANDARDS-1963-A

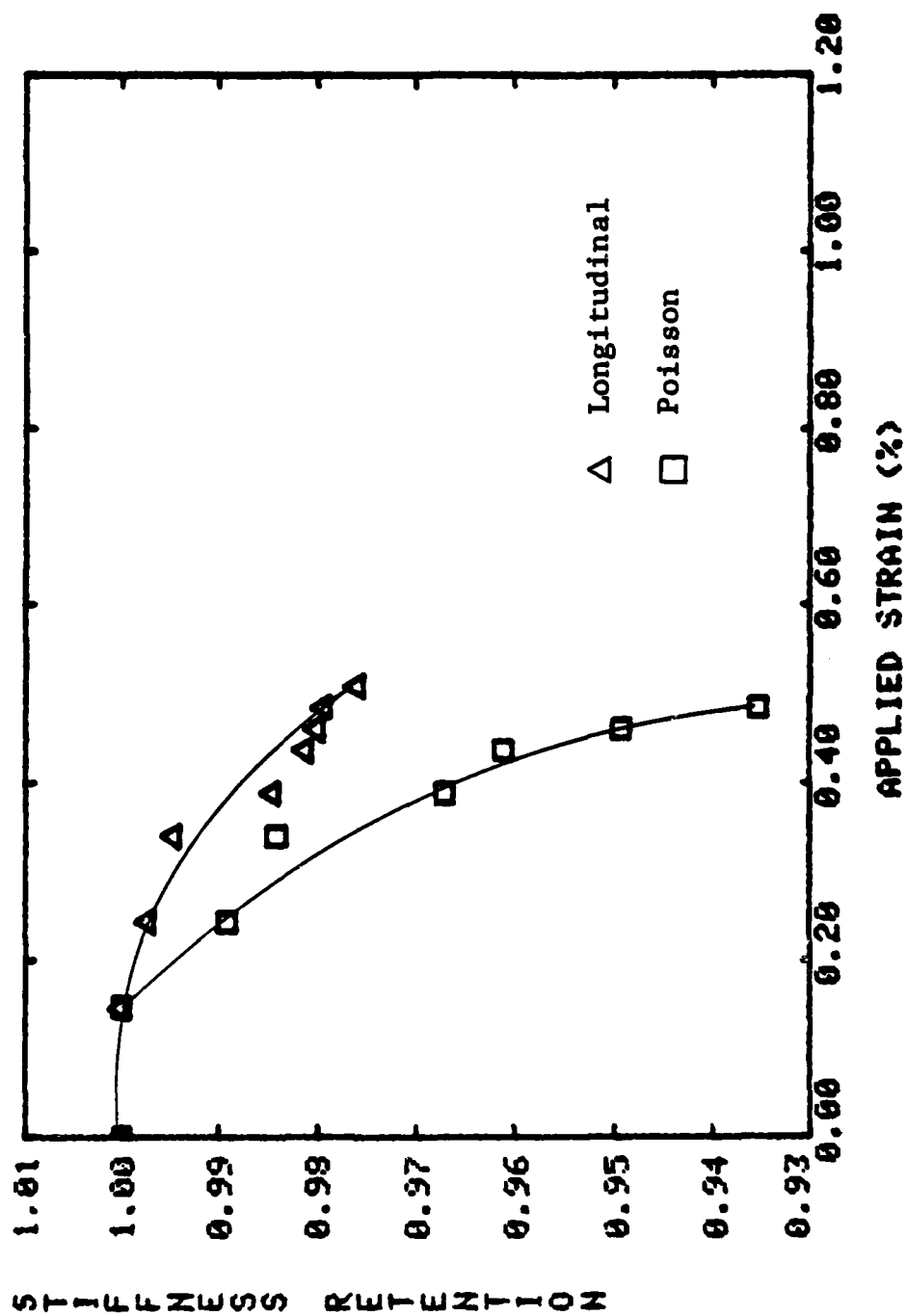


Figure 50 Stiffness Change - Type A, 250°F, Quasi-Static Compression

noncontacting. However, failing these, there remains the possibility of conducting tests at the room temperature, wet condition.

SECTION VI

MODEL DEVELOPMENT

Cumulative damage of composite laminates was already the subject of some controversy in 1966 when Boller observed that he was unable to confirm or refute the applicability of Miners rule based on his tests of E-glass epoxy laminates (five different types) using two-step loadings.

(1) A similar conclusion was reached by Hofer and Olsen (2) based on their tension-tension testing of uniaxial glass roving reinforced epoxy laminates and 181/S901 glass cloth reinforced epoxy.

The first real progress in characterizing cumulative damage appears to have been made by Broutman and Sahu. They developed larger data sets than their predecessors and tried to follow some of the physical details of fatigue damage in composite laminates. In particular, they noticed that strength appeared to decrease continuously during fatigue life in apparent contrast to the corresponding case for the fatigue of metals wherein the strength degradation is generally quite small until late in the fatigue life sequence (3). Perhaps their best known work was published in 1972. In that paper they introduced a linear equation for residual strength as a function of fatigue cycles. The attendant "theory" was compared to residual strength and two-stress level life data which they developed from extensive tests on 13-ply Scotchply type 1002 (E-glass reinforced epoxy) cross-ply specimens. The general agreement of their residual-strength and life expressions with the data was good. More significantly, however, many of the "modern" damage rules or residual strength expressions can be traced, in one way or another, to Broutman and Sahu's 1972 paper.

The well-known "wear-out model" of Halpin and Waddoups appeared at about the same time, representing a similar damage concept but taking a more phenomenological and fracture mechanics approach to the interpretation of the relationships used (5,6). Subsequently, Hahn and Kim published two papers which formed the basis for another major part of "modern" cumulative damage philosophy (7,8). Although they used a modified version of the same rate equation discussed by Halpin, et al., they introduced a new concept which came to be known as the "equal rank assumption." Simply stated, the concept says that, given a population of specimens having a specific distribution of strength and a specific distribution of life at stress amplitude S , a given specimen from that population will have the same statistical rank in the strength distribution of specimens having strength greater than S as it has in the life distribution (at stress amplitude S).

This equal rank concept is used in virtually all of the current models that deal with the statistical character of residual strength and life for composite laminate fatigue loading. As Chou and Croman have noted (9), that concept is implied by all deterministic degradation equations. If it is not valid then degradation must be considered as a random variable, degradation of strength cannot be deterministic.

Continuum theories of cumulative damage appear to have originated about the same time the equal rank postulate was made. Perhaps the best known such theory has been proposed by Tateishi (10). He applied several general kinetic models, including such things as bimolecular reaction rate equations and "pure birth" probabilistic nucleation rate concepts, to the damage accumulation process by means of a convolution

integral of the probability density of defects and the nucleation rate of the defects. The effect of defects on material properties was handled by introducing appropriate internal state variables. His theory was applied to certain thermodynamical (and mechanical) stability of equilibrium problems to obtain descriptions of the pertinent stability conditions.

More recent work falls into at least two general categories, extensions and generalizations of previous work and new approaches to cumulative damage. The use of deterministic strength degradation equations with the equal rank assumption to estimate the distributions of residual strength and life, as discussed initially by Hahn and Kim (7), has been one of the most active areas. For example, Yang and co-workers (11) have introduced a strength degradation equation which states

$$R^V(n) = R^V(o) - \frac{R^V(o) - \sigma^V}{R^C(o) - \sigma^C} KS^b n \quad (1)$$

where $R(o)$ is the initial and $R(n)$ the current strength (normalized by the scale parameter of the two-parameter Weibull fit of the quasi-static strength distribution), S is the current stress range, σ is the current maximum stress level, n is the current cycle count, and K , c and b are defined by the equations

$$c = \frac{\gamma \text{ (shape factor of static ultimate strength distribution)}}{\gamma_f \text{ (shape factor of fatigue life distribution)}} \quad (2)$$

and

$$KS^{\hat{N}} = 1 \quad (3)$$

where \hat{N} is the characteristic life of the life distribution. The

degradation of strength depends on the parameter v . If $v=c$ and $b=c+2$, equation (1) becomes identical to the so-called "wear-out" model of Halpin and Waddoups, (5,6). Equation (1) also is a more general form of earlier models proposed by Yang, et al. (12-15). For constant amplitude stress, and if $v=c$, equation (1) becomes identical to the model introduced by Hahn and Kim (16). And if one assumes that the values of $R(0)$, $R(n)$, \hat{N} are approximated by their median values, $v=1$ and $R^C(0) - \sigma^C = 1$, equation (1) reduces to the Broutman-Sahu linear relationship mentioned at the onset of this discussion (4).

A similar approach has been taken by Chou and co-workers (9,17). These theories have their greatest utility in the assessment of the statistical characteristics of residual properties when some data is available for a limited number of test cases.

A somewhat newer approach has been taken by Hashin (18). He introduces the concept of "damage curves" which define equal damage contours in the sense that any loading to that damage curve (in S-N space) will result in equal residual life (and, therefore, "equal damage" up to that point) at some second given stress amplitude. It is important to notice that "equivalent damage" in Hashin's model is defined by "equal life." Parenthetically, this is a minority point of view. The damage curves must, presumably, be established by extensive testing.

Other newer approaches include a probabilistic approach to the strength of unidirectional laminates based on the rule of mixtures (19). That theory includes a variety of effects peculiar to short fiber composites. Of course, the literature on probabilistic approaches to the general problem of strength and life is extensive. Our purpose is not served by a review of that literature here.

In the view of the present authors, at least one major deficiency is common to all of the models of cumulative damage discussed above. The models which represent the degradation of strength and life, whether they are deterministic or probabilistic, are not directly, precisely, and quantitatively associated with the micro-mechanisms and processes which define the physics and mechanics of damage accumulation. Stated in another way, we do not have a replacement for classical fracture mechanics in composite materials, for example, whereby the length of a single crack propagating in a self-similar way (damage accumulation) is related to residual strength and life through a well-set boundary value problem (fracture mechanics) and some experimentally determined damage rate information (Paris law or equivalent), respectively. This is the primary point of departure of the present modeling effort from foregoing work.

It should be noted that it is not difficult to find observables which might be candidates for representation efforts. Our principal effort is directed towards finding a systematic and rational set of observables that are directly, precisely and quantitatively associated with the micro-details of damage and just as directly, precisely and quantitatively associated with the governing equations of mechanics and the constitutive relationships. Our choice, for our basic set of observables, was the elastic moduli of the materials involved, a tensor array that we have, over more than four years of research work, been able to relate to the micro-details of many of the damage modes observed in composite laminates, and which has been clearly related, by a myriad of writers since the days of Newton, to the basic equations of mechanics.

Experimentally, these moduli also have the advantage of clear and universally familiar definitions and interpretations established by dozens of writers following Thomas Young in 1807. A disadvantage of stiffness as a damage indicator is that, while it is well established how a given modulus should be interpreted, it is not well established how all of the modulus components for a damaged anisotropic material should be measured. And such measurements are not always easy to make. However, our choice is made based on the balance of qualities which we feel is overwhelmingly positive.

Picking a basic set of observables does not a model make. The details of how damage is related to elastic modulus changes and how, in turn, the residual strength and life are anticipated are complex. A discussion of some of those details follows. The models are based on the experience of our Materials Response Group over the last twelve years, (20-30) and on the experience of others as described in the literature.

6.1 Modeling Approach

The present approach to modeling is based on the following precepts.

1. The models are mechanistic; the mechanisms are defined by generic damage modes and failure modes.
2. Models are developed at the engineering level.
3. The models are based on philosophy which has been checked against physical data.
4. Edge-related failure is not addressed.
5. Residual strength is the basis for equivalency of damage states.

It should be emphasized that these models and, indeed, the general approach, is a first effort at a very early stage of development of the understanding of behavior of composite laminates. A great number of questions regarding the strength, stiffness and life of composite laminates are unanswered; the determination of damage states in these materials is difficult and damage development is incompletely understood. Therefore, we present these models as "state of the art work" in a field where much must still be done by art in the absence of absolute or complete science.

We will be concerned with the long-term behavior of laminated composite specimens made from high-modulus fibers and polymer matrix materials. We take the terminology of "long-term behavior" to mean behavior associated with cyclic loading histories and amplitudes which cause specimen (or component) fracture after periods of time that are adequate for most engineering service requirements. Most of the modeling

effort focuses on situations which are produced by cyclic load levels (in tension or compression) which can be sustained for lifetimes of the order of one million cycles. Such situations are typified by the information presented in Fig. 51 which shows a schematic representation of a classical SN curve with damage development and residual strength variations superposed. The cyclic loading amplitude is represented as 60 percent of the static ultimate strength which is a typical level for long-term behavior.

It is important to note that the damage associated with low-load long-life failures is very great in the sense that residual strength and stiffness values are reduced to lower values before failure. In fact, the greatest possible damage corresponds to the longest possible finite life.

The approach we have taken to the modeling of these changes is to model the internal stress redistributions that are associated with the damage mechanisms observed, and to anticipate residual strength when these internal stress states are associated with failure criteria identified by observed failure modes. The life of the specimens (or components) is predicted by associating the rate of strength reduction with the remaining difference between the loading level and the current strength level, using observed damage rates to establish interim strength reduction rates. Hence, life is treated simply as the coincidence of the residual strength curve with the applied load level-actually life is locus of those coincidences. Hence, our general scenario is to observe the damage and damage rates associated with generic loading types, model the appropriate micromechanisms associated with that damage, and predict the remaining residual strength and life for a given situation.

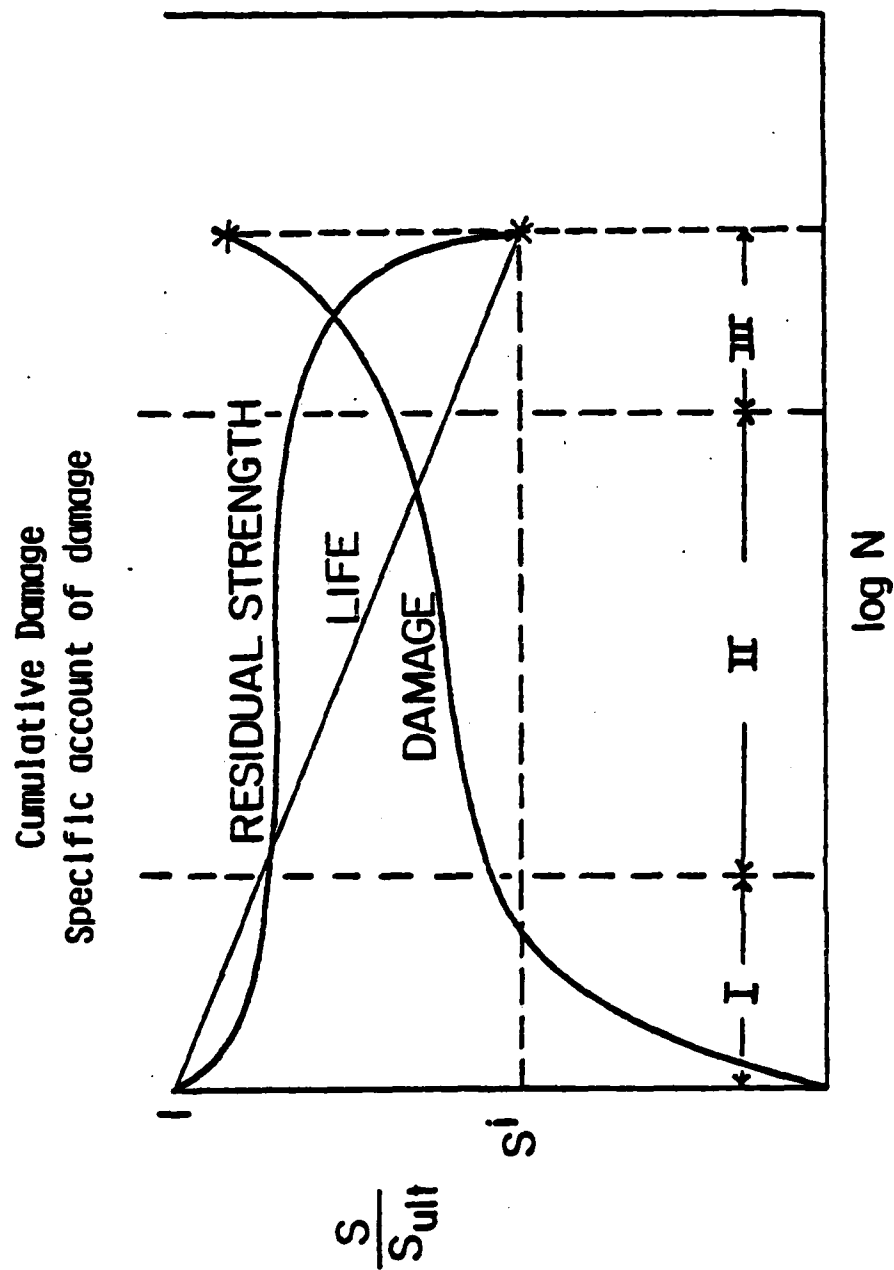


Figure 51. Schematic of the long-term fatigue behavior of composite laminates.

Since the ultimate user of these models will not, in general, wish to make laboratory investigations of micro-damage in a given component in order to establish its residual properties, it is necessary to establish some means of measuring the degree of damage development (nondestructively) in an arbitrary specimen for which the applied load history is unknown. Change in stiffness is used for that purpose in the present case. The concept, in one dimension, is illustrated in Fig.52. As the figure indicates, if the laminate fails at the applied stress amplitude of 0.7 of the ultimate strength, then the final stiffness, E_1 , must be $0.7E$ in magnitude or less if the strain to failure is equal to or less than the quasi-static value, ϵ_f , as the literature suggests (34,37). Figure53 shows an example of these changes for a $[0/\pm 45/0]_s$ graphite epoxy specimen and a $[0/90_2]_s$ glass epoxy specimen. In each case the reduction in longitudinal stiffness (Young's modulus) was quite close to the value implied in Fig.52. Stiffness is a well defined engineering property, routinely measured, clearly interpreted, and directly involved in mechanics (stress analysis) calculations through the constitutive relations. Stiffness changes are directly related to internal stress redistributions since the same events produce both results in proportion. In a sense, stiffness change replaces the (measurable) crack length in a comparable fracture mechanics treatment in homogeneous materials. We know of no other nondestructive measurement that has comparable utility and quantitative value for composite laminate damage monitoring.

A discussion of some of the specific models follows.

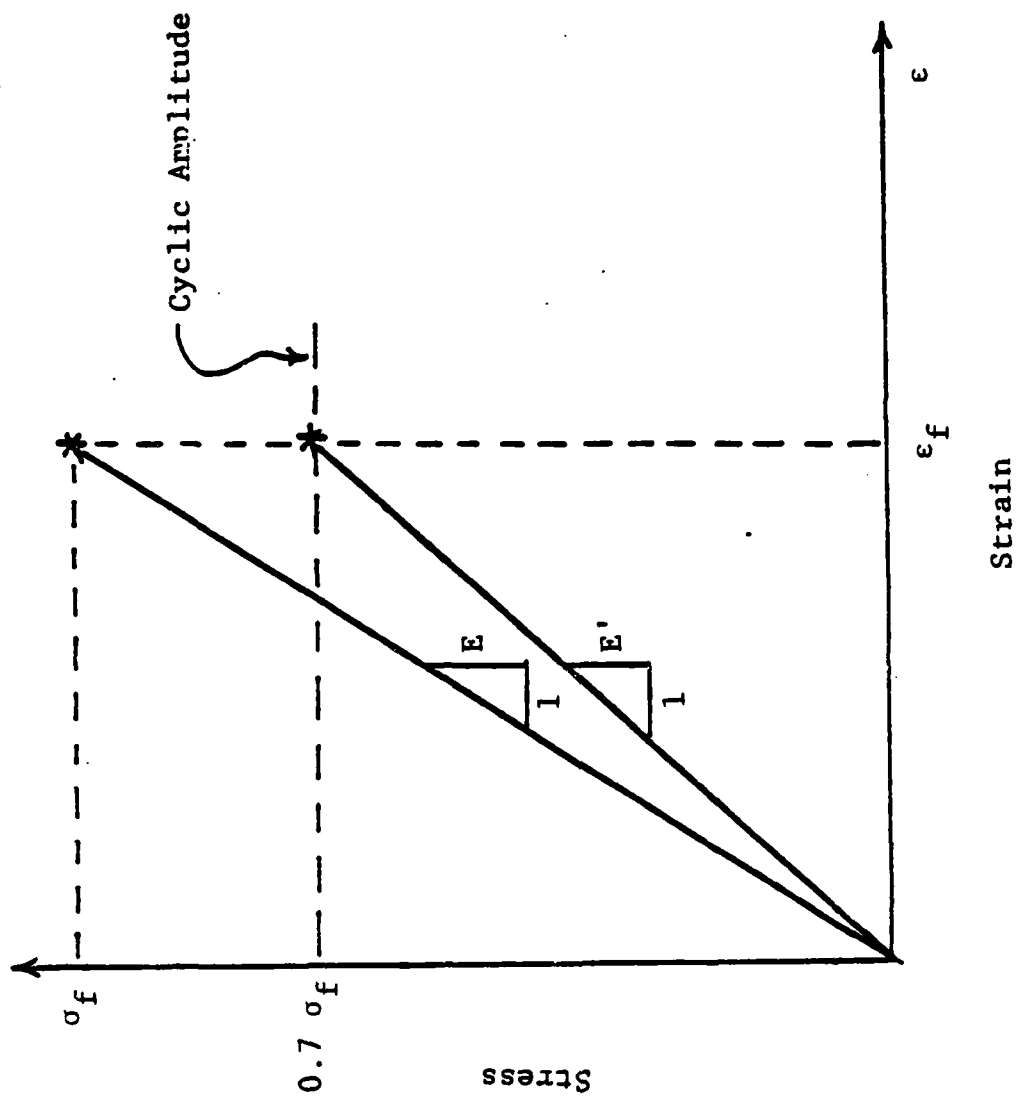


Figure 52. Stiffness reduction for a fatigue specimen loaded at an amplitude of 70% of the ultimate strength.

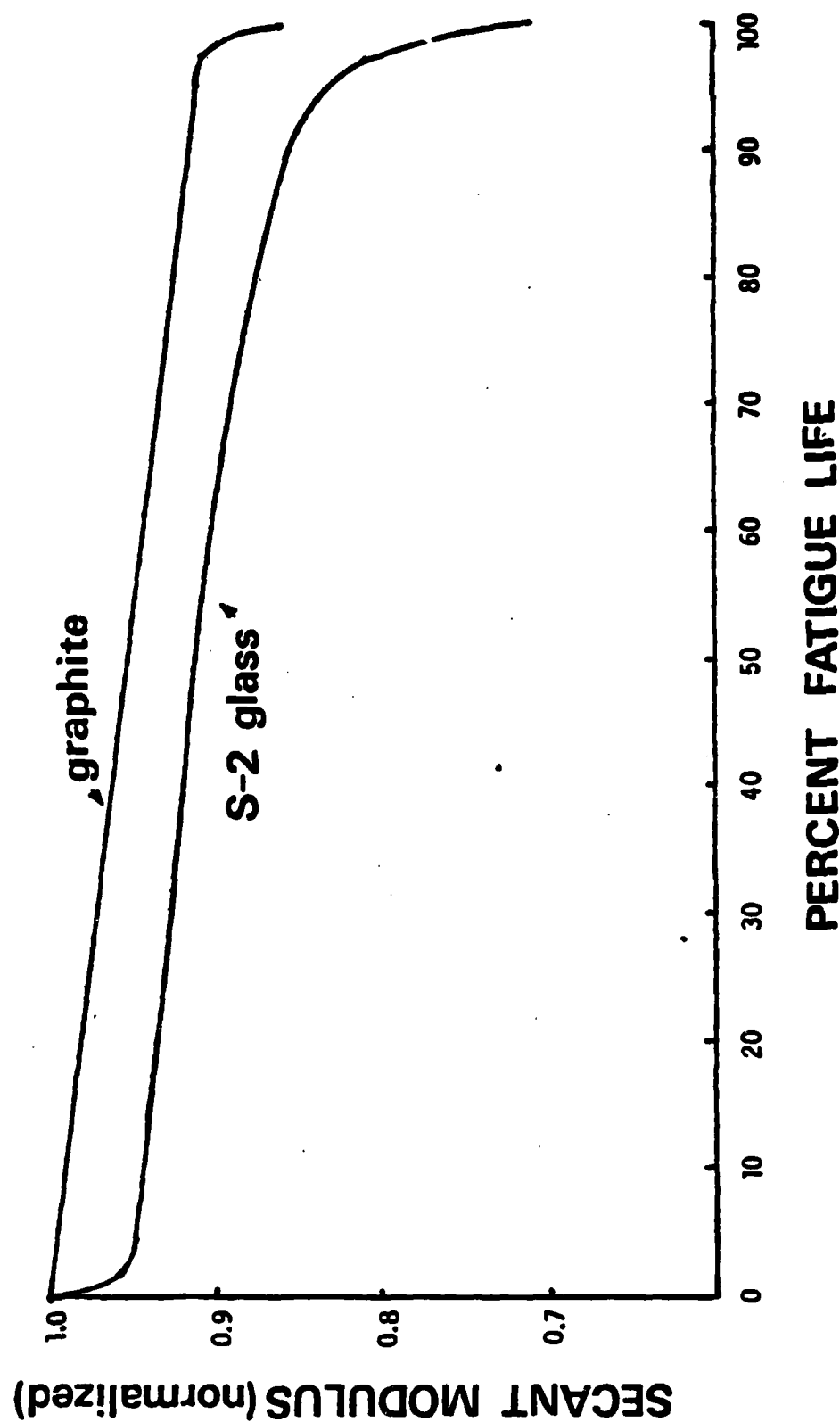


Figure 53. Longitudinal Young's modulus reduction for a $[0/+45/0]_s$ graphite epoxy laminate cycled at 0.85 of the static ultimate strength, and a $[0/90_2]_s$ glass epoxy specimen cycled at 0.6 of the static ultimate strength.

6.2 Models for Tensile Loading

As suggested in Fig.51, there is an early "stage of adjustment" to cyclic loading which is characterized by a rapid (and rapidly decreasing) rate of damage development. For laminates which have off-axis plies, such as the common $[0/90/\pm 45]_s$ quasi-isotropic stacking sequence, region I involves matrix cracking, usually by the formation of matrix cracks through the thickness of the off-axis (90 or 45 degree) plies parallel to the fibers and perpendicular (at least in transverse projection) to the dominant load axis (the 0 degree direction). This type of transverse crack formation has received a great deal of attention and is, by comparison to other micro-events, fairly well described and understood. Formation of the cracks can be reasonably well anticipated by laminate analysis coupled with a common "failure theory" such as the maximum strain, Tsai-Wu or Tsai-Hill concepts. The prediction of the occurrence (or absence) of such cracks is, however, of relatively little consequence in the engineering sense. It is possible, however, to anticipate the number and arrangement of such cracks, information which can be used for subsequent analysis of behavior.

Figure 54 shows the spacing between cracks in a -45 degree ply in a $[0/90/\pm 45]_s$ AS3501-5 laminate as a function of quasi-static load level and cycles of loading at about two-thirds of the ultimate strength ($R=0.1$). As one can see, cracks develop quite early in the life and quickly stabilize to a very nearly constant pattern with a fixed spacing. The same behavior occurs for quasi-static loading, in the sense that crack development occurs over a small range of load and quickly stabilizes into a pattern which has the same spacing as the fatigue crack

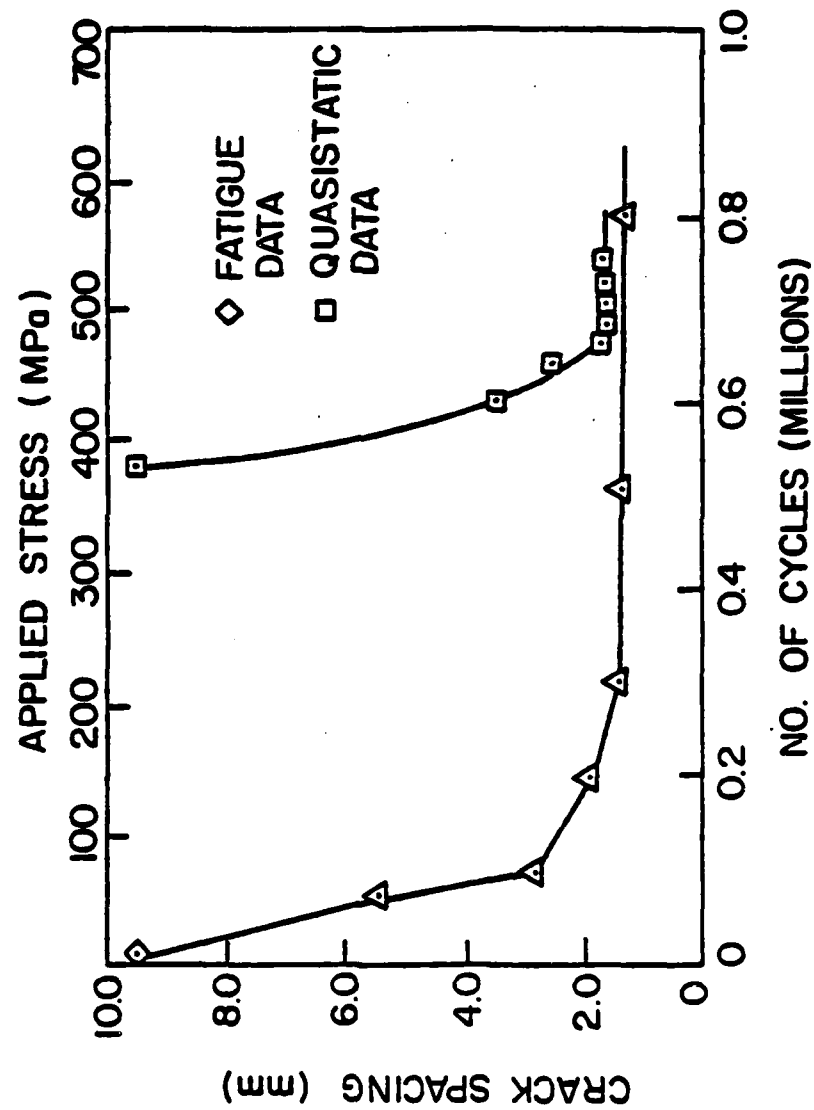


Figure 54. Crack spacing in -45 ply of $[0/90/\pm 45]_s$ graphite epoxy laminates under cyclic and quasi-static loading.

pattern. In fact, the two patterns are essentially identical regular crack arrays in that ply regardless of load history. Similar behavior is observed for the other off-axis plies and in other laminates. We have named these crack patterns "characteristic damage states" (CDS for short) for matrix cracking in laminates having off-axis plies. The CDS is a laminate property, i.e. it is completely defined by the properties of the individual plies, their thickness, and the stacking sequence of the variously oriented plies. The CDS is independent of extensive variables such as load history and environment (except as the ply properties are altered) and internal affairs such as thermal or moisture related stresses. A more thorough discussion of the CDS can be found in References 21,25,27,28,22.

The stability of the off-axis crack pattern, the CDS, is the reason for the sudden decrease in damage rate between regions I and II in Fig.51 and also accounts for the relatively flat nature of the damage development curve in region II. The regular crack patterns can be predicted with engineering accuracy as we show in the references just noted, and the stress state in the neighborhood of such cracks can be accurately anticipated (28). Using these predicted crack densities, the corresponding stiffness changes can be calculated. Such calculations have been made by the authors, and reasonable agreement with measured changes has been obtained (28).

The model for residual strength (and life) for cyclic tensile loading is based on the local stress state near the matrix cracks discussed above. A net section strength concept is used based on the following argument.

When calculating the quasi-static strength of an unnotched laminate, the common scheme is to calculate the ply stresses using laminate analysis, invoke some failure criterion to predict first ply failure (usually matrix cracking), reduce the moduli in the broken ply (usually E_2 perpendicular to the fibers and the in-plane shear stiffness G_{12}), recalculate ply stresses, test for second ply failure, etc. until "last ply failure" is predicted. This scheme, commonly referred to as the ply discount method, has been widely used over a period of at least fifteen years and is known to provide good engineering estimates of laminate strength when edge effects do not dominate the failure process. Table 7 shows the stresses in the individual plies of an example laminate before and after matrix cracks form in the 90 degree and ± 45 degree plies (for which E_2 and G_{12} are then set equal to zero). The stress in the fiber direction of the 0 degree plies (which control final fracture) is increased from 2631 to 2993 MPa, a jump of 14% which is then used in a failure analysis of some type to predict the "correct" strength (if both off-axis plies fail before laminate failure). In general, failure of the off-axis plies will cause stress redistribution of this type which, based on some 15 years of literature, must be properly accounted for to predict "good" values of laminate strength.

It is easy to forget, however, that these stress redistributions (and the stiffness reductions that caused them) are not, in reality, uniform. They exist only near the matrix cracks in the off-axis plies. The first direct proof of that (to our knowledge) was provided by Highsmith and Jamison (38,39) who (with the able help of Prof. Post at Virginia Tech) constructed a very high resolution moiré diffraction

Table 7

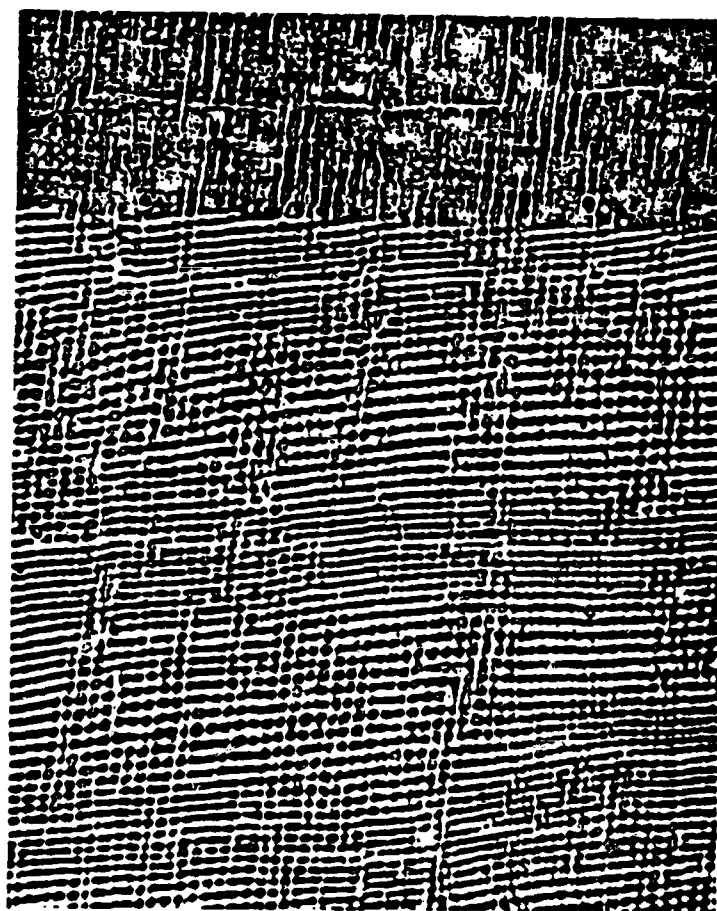
Example: $[0/90/+45]_s$ T300-5208

Applied stress $\sigma = 1000$

Ply	σ_x		σ_y		σ_{xy}	
	Before	After	Before	After	Before	After
0	2631	2993	- 2.3	- 4.7	0	0
90	167	0	-796	-1000	0	0
+45	600	503	400	503	417	503
-45	600	503	400	503	-417	-503

device which was used to resolve strain distributions in the 0 degree ply of several different laminates in regions near cracks in adjacent off-axis plies during quasi-static loading. An example of their results is shown in Fig.55. That figure was produced by the interference between a reference beam and a beam which was incident on a diffraction grating having about 800 lines per mm which was bonded to the specimen surface. The cracks in the off-axis 90 degree plies of the $[0/90_3]_s$ glass epoxy specimen can be seen as white horizontal bars having a spacing of about 4mm in the original photograph. The constant displacement diffraction lines are more dense in the region of the off-axis cracks, indicating a strain concentration in the 0 degree plies which are being observed. The strain distribution between two of the cracks is shown in Fig.56 along with strain plots from a simple one-dimensional model for three choices of the (only) parameter in that model.

Figure57 is general schematic representation of the situation shown in Figs.55 and56. The most important point to be made has to do with the local nature of the stress redistribution discussed above. The increased stresses (as discussed in Table 7) and increased strains (as discussed in Figs.55 and56) exist only in the region of the off-axis cracks as indicated by the dotted circle in Fig.57, and are in fact the average or net section values at the crack position. To that extent, then, some fifteen years of data appear to show that the net section strength of the 0 degree plies in the neighborhood of off-axis ply cracks controls the quasi-static laminate strength, at least to an engineering approximation level. Since this type of stress redistribution occurs if a specimen is quasi-statically loaded to failure or if



— 0.16 in.

↑
— 0.00 in.

Fig. 55. Moiré fringe pattern of a $[0/90_3]_5$ laminate between cracked sections in the 90° plies.

E-1 STRAIN DISTRIBUTION BETWEEN CRACKED SECTIONS

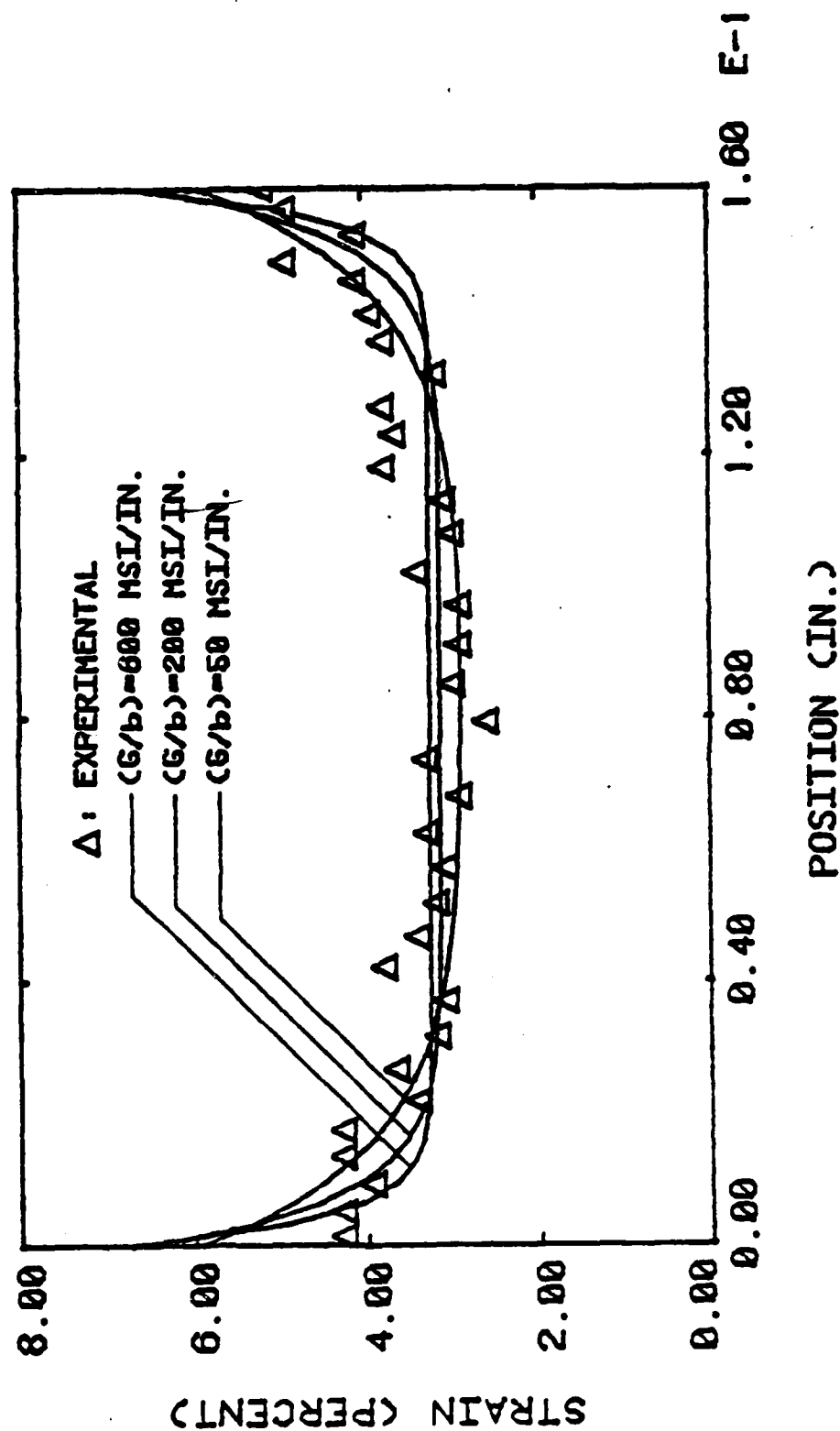
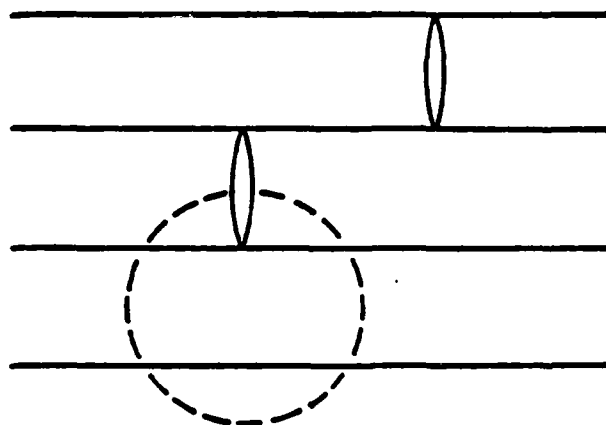


Fig. 56 Predicted and observed strain distributions in the 0° plies of a $[0/90_3]_s$ laminate between cracked sections of the 90° plies.

Global ply discount \Rightarrow
local net section mechanics



$0^\circ \quad \theta^\circ \quad \theta^\circ$

Figure 57 General schematic representation of local net-section stress situation near a matrix crack.

the cracks form during fatigue loading, no reduction of residual strength (during fatigue) is expected or observed due to CDS formation, as suggested by Fig.51. However, in region II of Fig.51, the matrix cracks begin to couple together by interlaminar crack growth.

The mechanics of this region are typified by the following scenario. Figure58 shows the interlaminar stress distributions that occur at the tip of a crack in the 90 degree plies of a $[0/+45/90]_s$ graphite epoxy laminate (from Ref. 12), as a function of distance through (half of) the thickness. For an uncracked material these stresses would vanish, but when a crack forms it creates an interlaminar tensile normal stress which tends to separate the plies and an interlaminar shear stress which tends to shear the plies along their interface in the neighborhood of the crack. These two stresses, demonstrated by the distributions in Fig.58, provide the basis for a mechanism of crack coupling and delamination. Cracks in the off-axis plies grow along the ply interfaces and, in some cases, couple up with cracks in other plies. This interfacial growth and crack coupling is the first distinctive feature of microdamage which separates fatigue damage from quasi-static loading damage. The nature of the interfacial growth is influenced by locality in the specimen and by the nature of the matrix cracks which precede it. The pattern of damage shown in Fig.59 is peculiar to the edge of that laminate, and typical of the edge of other laminates. The same stresses, illustrated by Fig.58 also operate in the interior of laminates, but the results are frequently different.

Figure 60 is a schematic diagram of the type of damage commonly found in the interior of a laminate (a cross-ply laminate for this

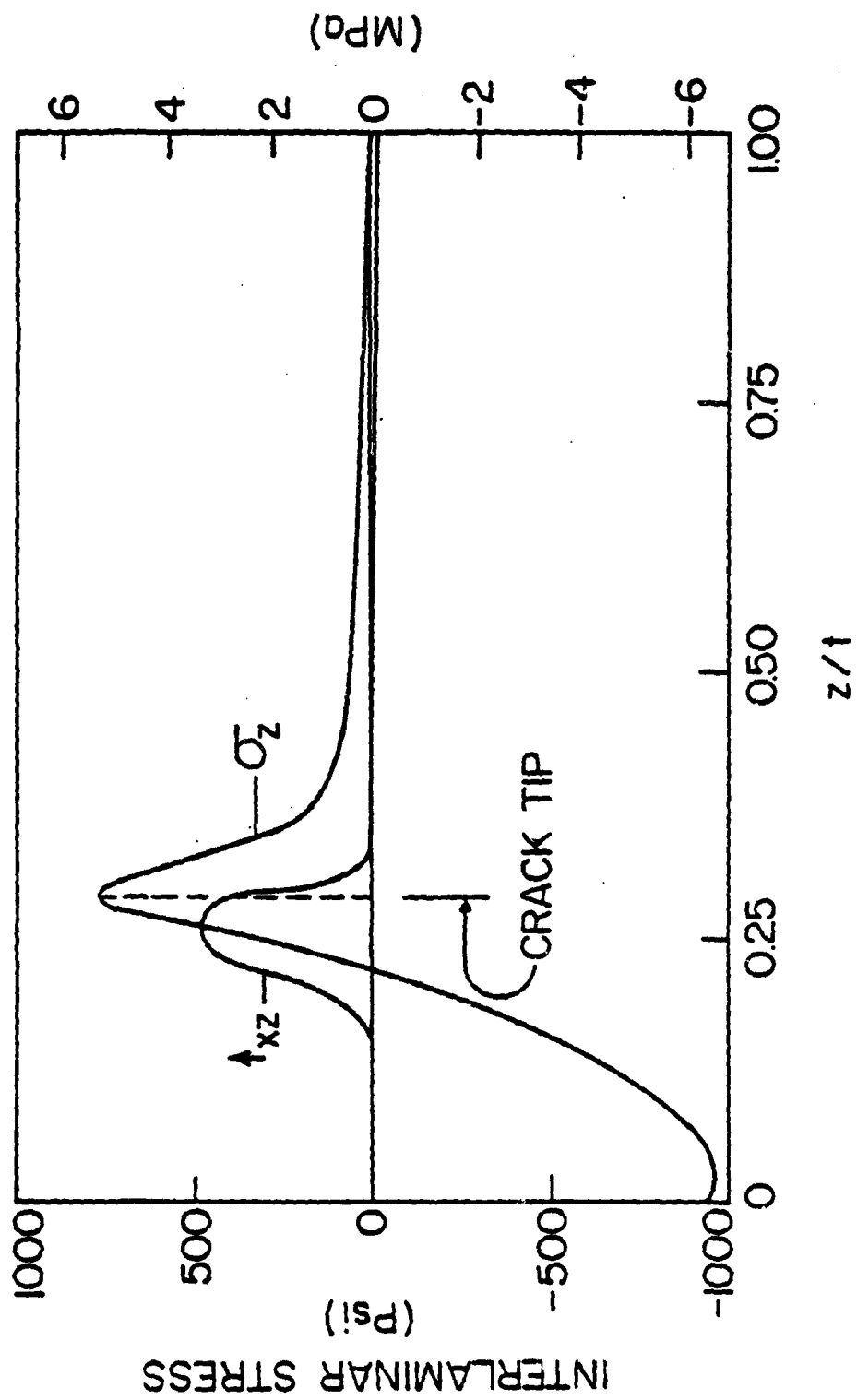
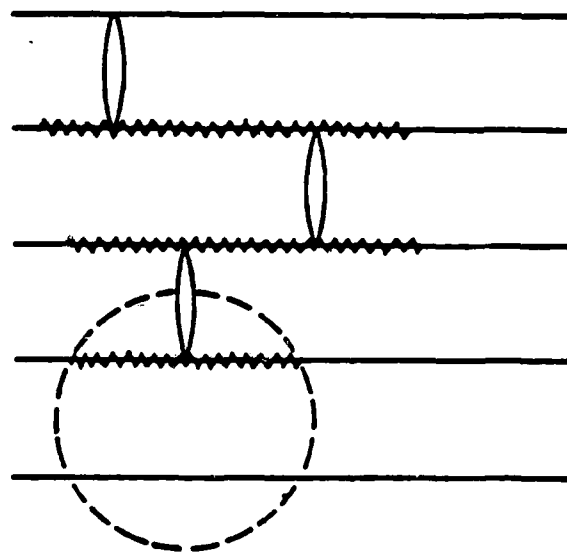


Figure 58. Interlaminar stresses near the tip of a matrix crack in a 90° ply of a $[0/+45/90]_s$ graphite epoxy laminate.



0° θ° θ° θ°

Figure 59 Local crack coupling and delamination near matrix cracks.

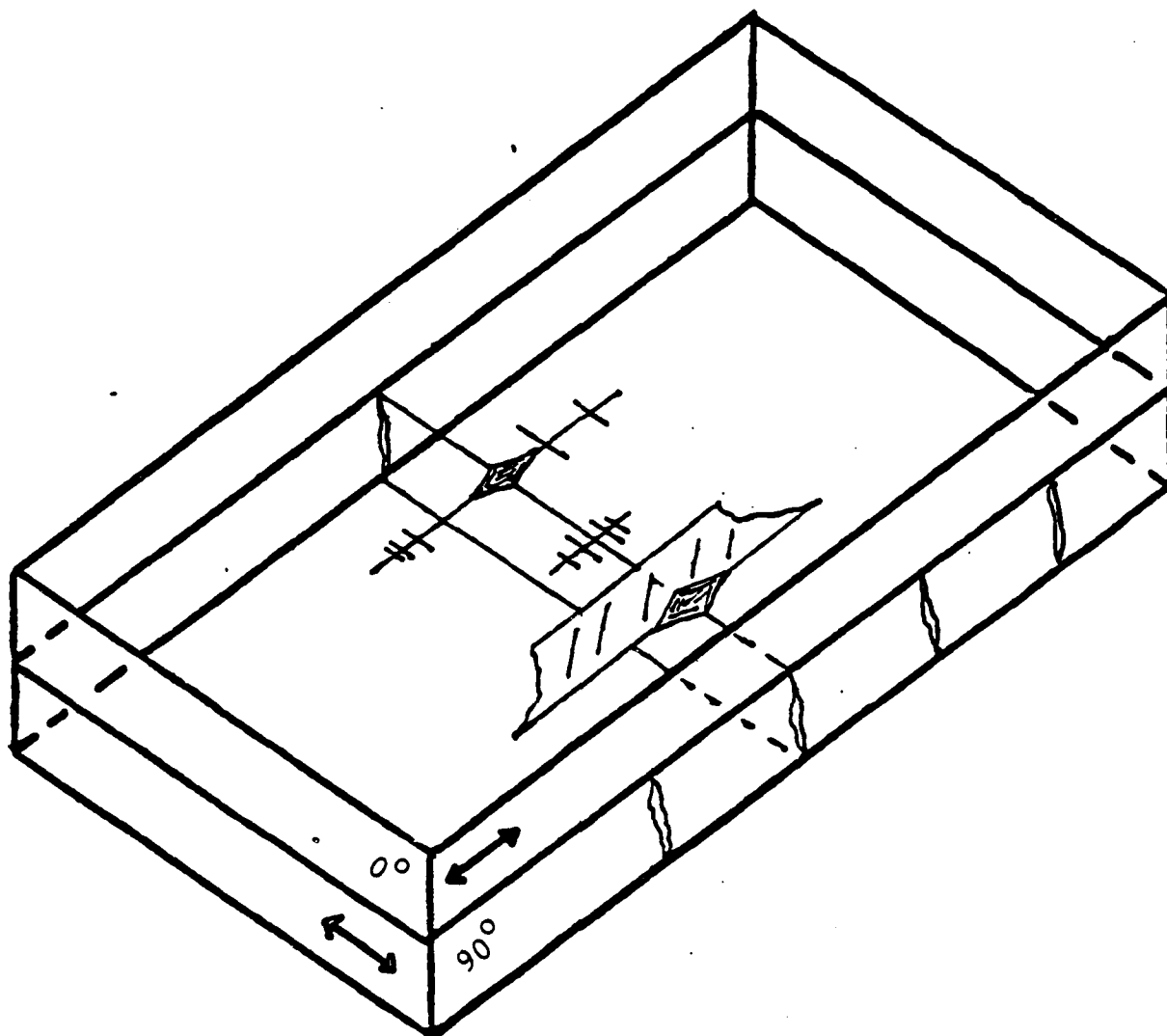


Figure 60.. Schematic of interior delamination and crack growth.

example). The details are generalizations of results obtained by X-ray radiography. Interfacial growth at a transverse matrix crack in the interior of a laminate is frequently constrained to a small region, at least in region II, and may also involve growth of the crack along 0 degree fiber directions into the 0 degree ply thickness as well as along the ply interface plane.

In region I (of Fig.51) we identified matrix cracking as the primary damage mechanism and discussed the associated internal stress redistribution. When the (local) E_2 and G_{12} of the cracked plies was reduced to zero we found that the axial stress in the 0 degree plies increased from 2631 MPa to 2993 MPa for a 1000 MPa input. At that point, the plies are all still bonded together and the cracked plies still influence the stress state in the 0 degree plies by supporting load in the fiber direction of the off-axis plies, i.e., by influencing the off-axis stresses (and load sharing) in the 0 degree plies. When ply separation occurs, however, that sharing is also relaxed so that the 0 degree plies act under completely uniaxial stress in that local region. The delaminated off-axis plies carry no 0 degree load and do not constrain lateral motion in the 0 degree plies. Under that situation, the uniaxial stress in the 0 degree plies becomes the only load bearing stress in the laminate. For the example discussed in Table 7 the σ_x stress in the 0 degree plies will revert to 4000 MPa in the local region where delamination is complete (using the net section value as motivated by our earlier discussion). If such a stress really occurs in the laminate, it should cause a corresponding reduction in strength. For the quasi-static loading case we say that such a reduction

(corresponding to the common discount scheme) does occur and forms the basis for the usual quasi-static laminate strength calculation. For fatigue loading at levels of stress corresponding to long lifetimes, the strength reduction (using Table 7) should be of the order of

$$\frac{4000 - 2993}{2631} \approx 0.34 \quad (4)$$

or approximately 30 percent. As we noted earlier, the strength reduction for long-term behavior is, in fact, of the order of 30-40 percent. So it would appear that crack coupling and (local) delamination or debonding (even in the interior of a specimen) near matrix cracks is a viable strength reduction mechanism for the long-term fatigue behavior of laminates. Our model is based on these stress redistribution and strength reduction concepts.

6.2.1 Cumulative Damage Model

The basic nature of the cumulative damage model proposed by the present authors is presented in the following section. Two major requirements were addressed in the formulation of this model and are responsible for most of the decisions that were made regarding complexity, generality, and approach. The two requirements are as follows.

1. It is required that the model predict strength and life of engineering composite laminates under complex load histories.
2. It is required that the model replace Miner's rule with an engineering model for cumulative damage based on the physical mechanisms of damage and failure.

Figure 61 illustrates a summary of some of the damage modes discussed in the previous section. There are, in general, numerous such

damage modes which develop in innumerable combinations depending upon load level, configuration of the laminate, and specimen or component geometry. However, in contrast to the complexity of the damage modes, there are relatively few failure modes. For example, under tensile loading, the zero degree plies (or nearest-on-axis plies) are responsible for the residual strength and life of composite laminates regardless of the complexity of damage that develops in the off-axis plies during fatigue loading. Although one may change the stacking sequence and, therefore, the general nature of matrix cracking, delamination, and debonding throughout a fatigue test, the final fracture event is still controlled by the zero degree plies in that case. Other similar examples can be cited for compressive loading and for combinations of tensile and compressive load excursions. Because of this observation we have elected to construct our cumulative damage model on the basis of "critical and subcritical elements." Critical elements are, quite simply, the parts of a composite laminate which control the strength and life of that laminate. Subcritical elements are the remaining parts of the laminate which, although they may be severely damaged during a fatigue loading situation, do not cause failure of the laminate per se, but rather introduce stress redistribution in the laminate which influences the strength or life indirectly. This philosophy affects our model in two ways. First of all, it introduces a new concept into the cumulative damage modeling process, namely that of internal stress redistribution at the micro level due to the formation of damage in off-axis plies. And second, it influences a major decision regarding the phenomenological input into the model. All strength and life models must include some phenomenological information, but it is desirable to maintain an absolute minimum of complexity and uncertainty associated

with that input. In view of these facts, we chose to represent the fatigue behavior of the critical elements in each laminate phenomenologically and to handle the fatigue damage that is observed in the other plies or elements of the laminate by stress redistribution as determined from models of the mechanics of those damage processes and of the resultant micro stress fields. That approach is summarized in Fig. 62 which also draws a parallel between the fracture mechanics approach commonly taken in the description of fatigue damage in metals with the present approach to the prediction of residual strength and life. As suggested by the figure, the mechanics associated with the philosophy of fracture mechanics is replaced by the mechanics associated with micro-damage for the case of composite materials and the phenomenological crack propagation equations usually associated with Paris and others becomes the degradation equation which we will propose shortly. The basis for the modeling is a prediction of residual strength with a consequent interpretation of life.

Figure 63 shows the proposed degradation equation with some definitions of terms included. A complete description of the details of that equation will be included in the discussion below. The equation is formulated in integral form so as to allow for cumulative damage computations in the presence of continuously varying load spectra. Figure 64 illustrates the contribution of mechanics analysis to the model. There are two major categories of input. A major part of the so-called "fatigue effect" in composite laminates is associated with damage development in the subcritical elements as described earlier. This damage development influences the critical element at the micro

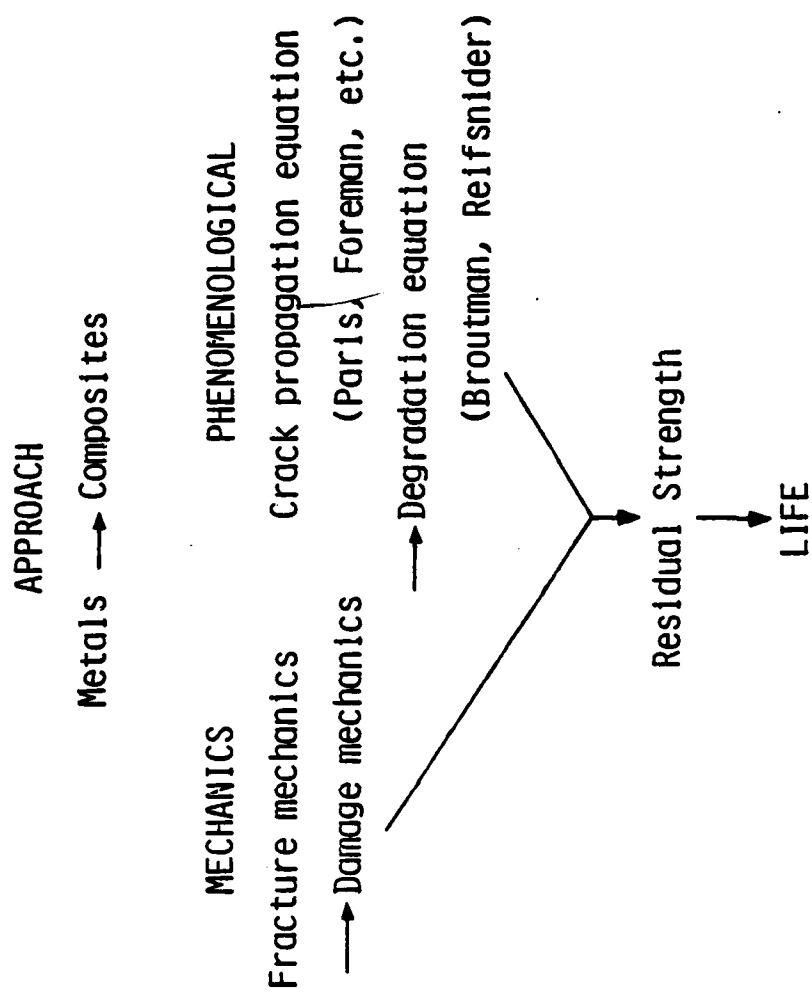


Figure 62. Approach to cumulative damage model development contrasted with fracture mechanics concepts.

Degradation Equation

$$(1 - F^r(n)) = \int_0^1 (1 - F^L(n)) f\left(\frac{n}{N}\right) d\left(\frac{n}{N}\right)$$

$F(n)$ - failure function

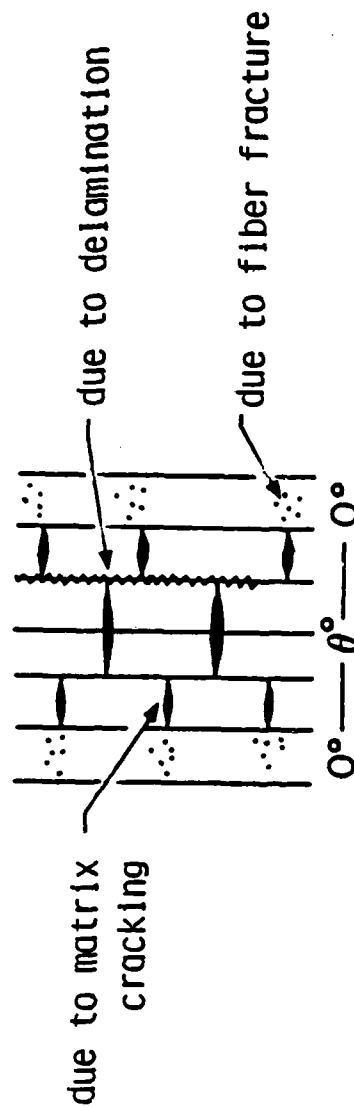
$N(n)$ - life locus

$f\left(\frac{n}{N}\right)$ - degradation function

Figure 63. Proposed degradation equation.

MECHANICS

1. Stress Redistribution



2. Failure Criterion

tensile fracture

$$\frac{\sigma_1^2}{X^2} + \frac{\sigma_2^2}{Y^2} - \frac{\sigma_1 \sigma_2}{X^2} + \frac{\tau^2}{S^2} = F \quad \text{etc.}$$

buckling failure

$$\frac{N_x}{N_{xc}} = F, \quad N_{xc} = N_{xc}(D_{ij}, a, b, m, n) \quad \text{etc.}$$

stress concentration

$$\frac{K}{K_c} = F, \quad K_c = \sigma_0 \sqrt{\pi a_0 \left(\frac{c}{2c + a_0} \right)} \quad \text{etc.}$$

delamination induced
tensile failure

$$\frac{\epsilon}{\epsilon_c} = \frac{E_c}{E} = F \quad \text{etc.}$$

Figure 64 Role of mechanics analysis in cumulative damage model.

level by virtue of the stress redistributions that occur because of that activity. These stress redistributions are computed from mechanics models of the micro-damage events themselves. The second major input to the model from mechanics is associated with the failure criterion, the F in Fig. 63. That criterion is dictated by one's choice of the critical element in a laminate and by the failure mode of that critical element. Under tensile loading, for example, perhaps a Tsai-Wu equation such as the first one suggested under category II might be appropriate. Under other situations perhaps a stress concentration condition involving a stress intensity factor might be appropriate, etc. While the criteria themselves are not derived from first principles and are in fact phenomenological, the manner in which they are used and the stress fields on which they are based must be determined from mechanics treatment.

The phenomenological inputs are summarized in Fig. 65. Again there are two categories. The critical element degradation rules, as discussed earlier, are phenomenological. For tensile loading of the zero degree plies a simple SN curve might suffice. In the case of self-similar flaw growth a crack propagation rate relationship might be necessary. The form of the summation equation which expresses the change in residual strength shown in the second category in Fig. 65 is also phenomenological and is, in fact, a postulate. All quantities in the equation are normalized and the choice of variable of integration is based on the observation that under spectrum loading the ratio of current number of cycles to expected life is generally a continuous function.

Phenomenological

1. Critical element degradation rules $f\left(\frac{n}{N}\right)$

- i. fatigue behavior of 0 degree plies

$$N = \log^{-1} \left[\frac{B}{A - S/S_u} \right]^{1/x} \quad S = S(n)$$

- ii. flaw growth $\frac{da}{dn} = C_1 \mathcal{L}^b \quad \mathcal{L} = \mathcal{L}(n)$

2. Form of residual strength equation:

change in residual strength =

$$(1 - F^r) = \int (1 - F^L) f\left(\frac{n}{N}\right) d\left(\frac{n}{N}\right)$$

F^r = normalized residual strength

F^L = local value of failure function for
redistributed stress state

Figure 65. Phenomenological inputs to the cumulative damage model.

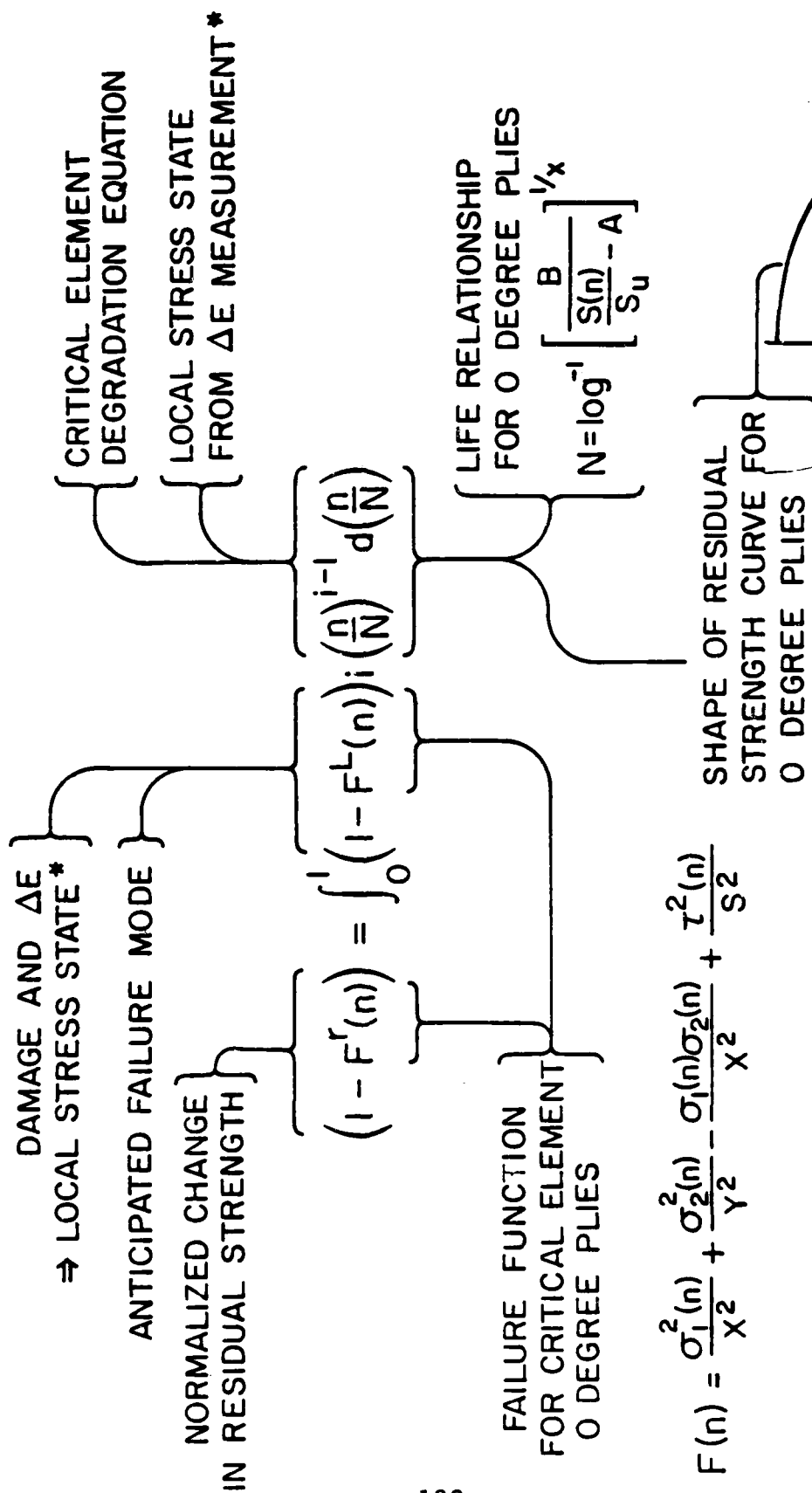
Experimental Inputs

1. Degradation parameters
2. Change in stiffness \Rightarrow
damage mode and extent \Rightarrow
local stress state as a
function of cycles which
determines current values
of F^L and N or critical
crack length, etc.

Figure 66. Experimental inputs to degradation model.

Figure 66 identifies the experimental inputs to the present model. The degradation parameters must, of course, be determined from baseline testing. For tensile load excursions, the tensile SN curve of the zero degree material might serve as the degradation parameter characterization. Under those conditions, that single characterization would provide sufficient phenomenological input for all laminates made from that material system. During the fatigue spectrum loading of a given composite laminate, the change in stiffness during the load process is suggested as a second experimental input from which the damage mode and extent of damage can be implied and from which, in turn, the local stress state and stress redistribution can be determined using the mechanics models alluded to earlier. Once the internal stress states have been determined the local failure function and predicted life locus can be established. Two simple demonstrative scenarios of this approach are illustrated in Figs. 67 and 68. The first scenario is for a tension-tension fatigue loading situation for a laminate which is not dominated by edge delamination. As the figure shows, the normalized change in residual strength depends upon the integral of the product of two expressions, one of which can be roughly interpreted as the current amplitude of possible residual strength change as determined from the internal stress state and the level of applied loading and the second of which can be associated with degradation of the critical element which is the zero degree plies in this case. As shown on the bottom right of Fig. 67, this latter part of the total equation depends upon the SN curve of the zero degree plies and the expected shape of the residual strength variation for those plies as determined from baseline experiments.

SCENARIO:
TENSION - TENSION, NO SIGNIFICANT DELAMINATION EFFECT:

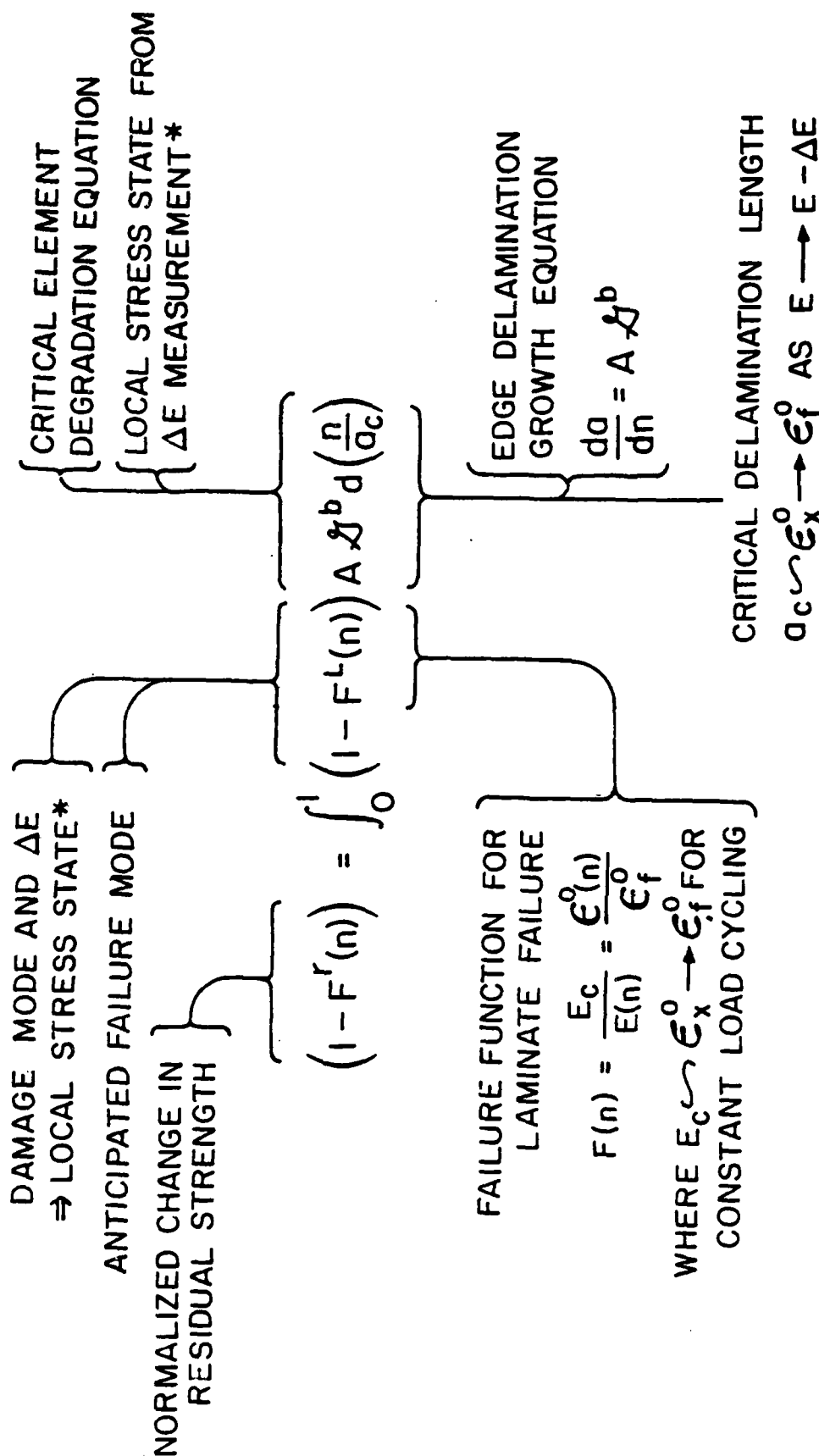


FROM MECHANICS MODELS OF DAMAGE

Figure 67. Scenario for tension-tension cyclic loading of a laminate which has no major edge

SCENARIO:

TENSION - COMPRESSION, EDGE DELAMINATION DOMINATES
TENSILE STRAIN TO FAILURE CONTROLS (O'BRIEN)



* FROM MECHANICS MODELS OF DAMAGE

Figure 68 Scenario for tension-compression cyclic loading of a laminate for which edge delamination

The former part of the integrand depends upon the failure function which has been postulated to be a Tsai-Wu equation as shown in the lower left of that figure. Figure 68 indicates a similar scenario for tension-compression loading of a laminate which does fail due to edge delamination. The degradation of the critical element is given by a simple rate equation for edge delamination growth as suggested by O'Brien (private communication) and the critical delamination length for that damage mode is established by associating failure with a reduction in stiffness of the laminate to the point where the resulting laminate strain reaches the quasi-static strain to failure for the load level being applied in the fatigue test. We have assumed in that scenario that tensile failure is responsible for the final fracture event. It is, of course, possible to assume that the failure function involves a buckling criteria of some sort for compressive failure.

Figure 69 shows a flow diagram of the model use procedure. One begins by establishing a critical element based on the anticipated failure mode for the laminate type and spectrum of loading to be used. It is, of course, possible to compute the expected residual strength and life reduction using several different critical element assumptions and to associate the actual situation with the most conservative of those estimates. The stress state in the element is determined and the phenomenological element properties are obtained from baseline testing. A failure function appropriate to the expected fracture mode of the critical element is also identified and the damage modes anticipated from quasi-static stress analysis. During cyclic loading of the component, stiffness measurements (or any other nondestructive evaluation

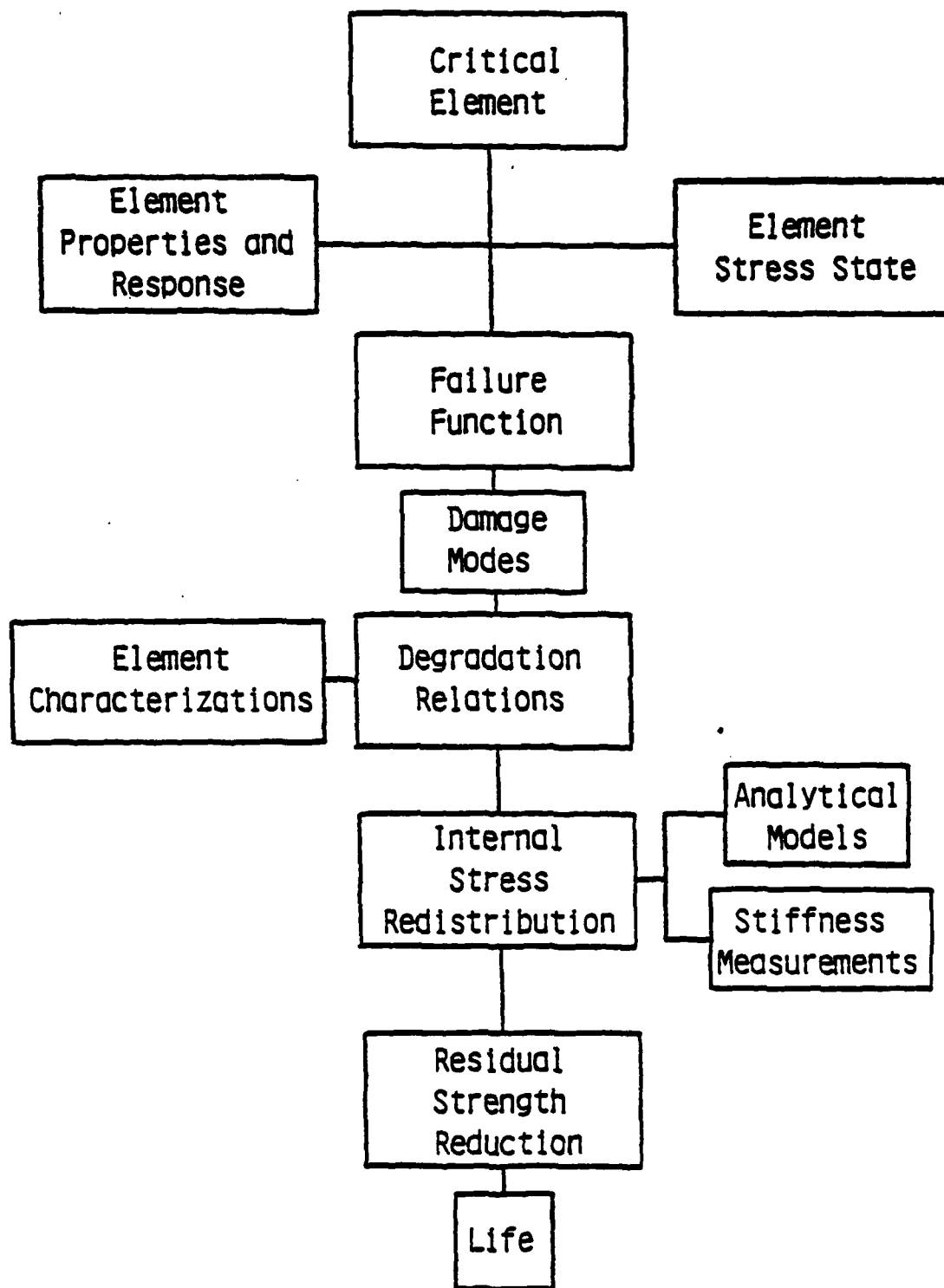


Fig. 69. Flow diagram of model use procedure.

measurement which can establish the nature and extent of internal damage development) is used along with analytical models of the damage observed to determine the internal stress redistributions which influence the rate at which life is expended in the critical elements. Finally, the cumulative damage equation is used to estimate the residual strength reduction and the coincidence of that value with the applied load levels--or more correctly the resultant internal current stress state at the micro level--is used to anticipate the life of the laminate.

6.2.2 Illustrative Example

In order to illustrate some aspects of the concepts outlined above, some simplified illustrative examples will be presented below. Some of the details of the examples will be taken from the data base available for T300-5208 material since only limited data is presently available for AS-3502. We will first present a simple linearized example for tension-tension fatigue loading to provide a demonstration of the approach. That application will not represent a final version of the modeling involved since the degradation will be linearized, the failure function will be one-dimensionalized, and block loading will be considered. It should be viewed as a special case of our model.

As mentioned earlier, residual strength is taken to be the basis for equivalency of damage states. Figure 70 shows a linear idealization of the residual strength at various stress amplitude levels, normalized by the static ultimate strength, as a function of the fractional life. The linear relationship

Cumulative Damage
Residual Strength is basis of equivalency
of damage states

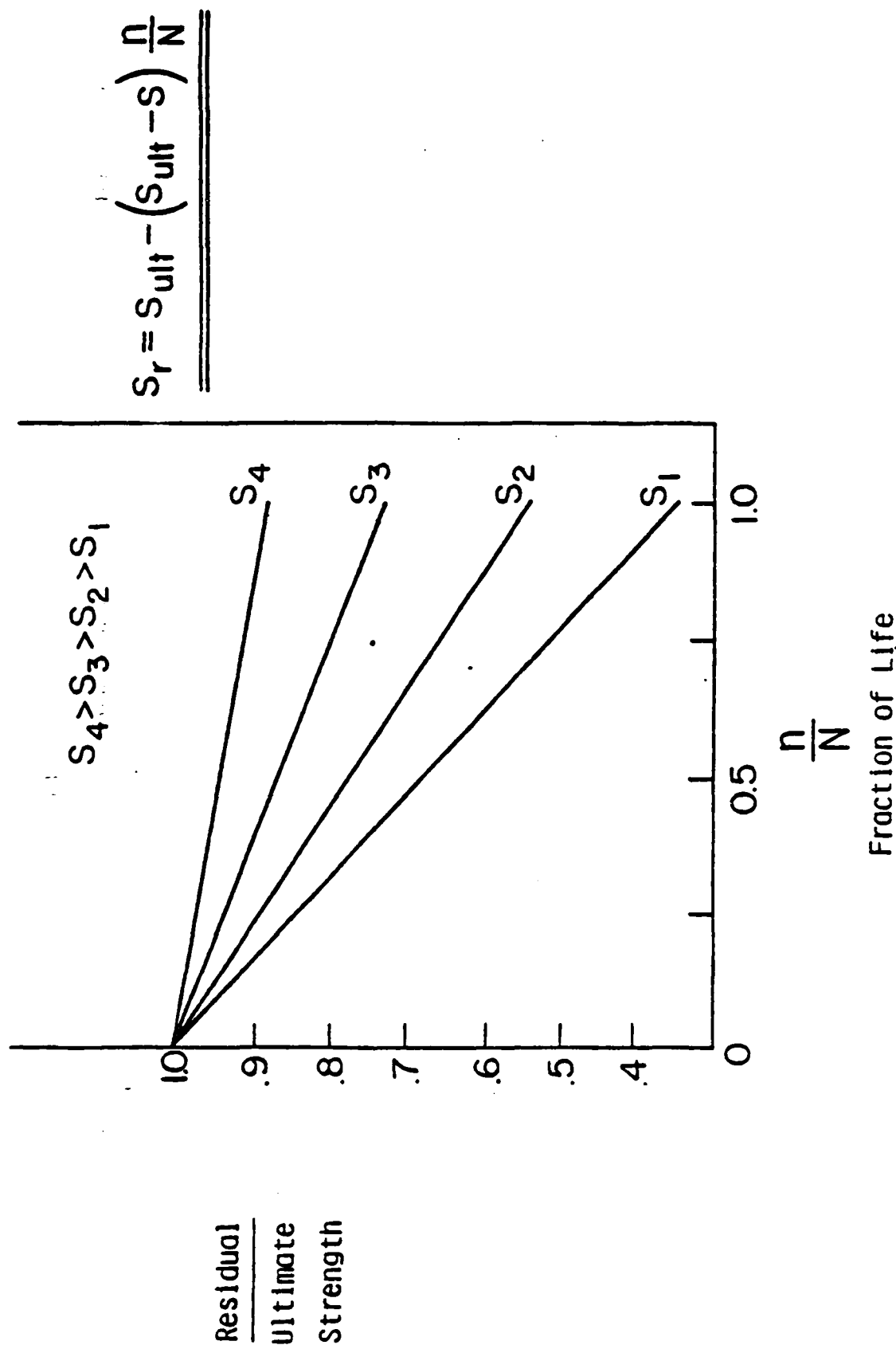


Fig. 70. Linear approximations of the reduction of normalized residual strength as a function of fraction of fatigue life.

$$S_r = S_{ult} - (S_{ult} - S) \frac{n}{N} \quad (5)$$

where S_r is the residual strength, S_{ult} is the ultimate strength, S is the stress amplitude, n is the current cycle count and N is the life, is identically satisfied for $n=0$ or $n=N$, but the variation of residual strength between these two points is not necessarily linear. Figure 7.1 shows a more commonly assumed nonlinear variation in residual strength superposed on the locus of the end points of the residual strength curves, the so-called SN curve. As suggested by the figure, these residual strength curves are related to observations of the accumulated damage and the rate of damage by the models to be discussed.

If a spectrum of loads, consisting of "k" blocks of constant amplitude, S^i , are applied in sequence to a specimen, the residual strength, S_r^k , again using the idealized linear form, is given by

$$\frac{S_r^k}{S_{ult}} = 1 - \sum_{i=1}^k \left(1 - \frac{S^i}{S_{ult}} \right) \frac{n^i}{N^i} \quad (6)$$

where n^i is the number of cycles applied at amplitude S^i and N^i is the corresponding life at that amplitude.

Expression (6) can be put into a form involving only the stress amplitudes, S^i , the number of cycles, n^i , and material constants by approximating the locus of the end points of the residual strength curve by

$$\frac{S^i}{S_{ult}} = A + \frac{B}{(\log N^i)^x} \quad (7)$$

where A , B and x are material constants. Then

$$\frac{S_r^k}{S_{ult}^k} = 1 - \sum_{i=1}^k \left(1 - \frac{S^i}{S_{ult}^i} \right) \frac{n^i}{\log^{-1} \left[\frac{B}{\frac{S^i}{S_{ult}^i} - A} \right]^{1/x}} \quad (8)$$

becomes the linear residual strength approximation for spectrum loading.

For our example, we consider the particular case of T300-5208 material in a $[0/90/\pm 45]_s$ laminate. Using data from an independent source (private communication from T. K. O'Brien, U.S. Army Research and Technology Labs, NASA Langley), we obtain

Lamina Strength = 1722 MPa

Laminate Strength = 551 MPa

and (for our residual strength calculations) we suppose that

$$\frac{S^i}{S_{ult}^i} = 1.054 - \frac{0.04}{(\log N)^{-1.3}} \quad (9)$$

which was obtained by curve-fitting the life data of the laminate. With equation (9) in equation (8) we calculate the predicted residual strength of eleven specimens which were subjected to the fatigue loadings shown in Table 8. (The stress ratio for all tests was 0.1.) The last column on the right of the Table shows the percent differences between the predicted and observed values.

Two points should be made. First, the values are generally close; the average variation is 12.5 percent. Second, the predicted values are consistently lower than the observed residual strengths, i.e., the residual strength curve is, in fact, nonlinear in the way suggested in

Table 8 Residual Strength Prediction

Specimen Number	Maximum Stress MPa	Number of (K) Cycles	Residual Strength Obs. (MPa)	Residual Strength Predicted (MPa)	Percent Difference
A29	370.5	150	545.5	493	10
B10	370.5	250	529.6	454	14
F21	370.5	275	478.9	445	7
F11	425.0	30	470.8	432	8
E11	425.0	25	498.4	452	9
D26	425.0	30	491.7	432	12
D21	354.2	1000	450.1	357	21
E5	452.2	8	530.9	447	16
F13	425.0	25	535.0	452	16
A35	397.7	70	528.4	465	12
B3	397.7	90	509.6	441	13

Av. Laminate ultimate strength 551 MPa

Av. percent discrepancy 12.5

Fig. 71. A displacement of the residual strength prediction curve "upward" by 7-10 percent would have brought all values quite close to those observed.

If a spectrum of loads is applied, equation (8) will predict the same residual strength regardless of the order of application of the block components since, as we have said, we have used residual strength as the basis for equivalency of damage states. An example of such a calculation is shown in Fig. 72. Under the low-high sequence a residual strength of 540 MPa was measured, and after the high-low sequence a value of 521 MPa was observed. The predicted value of 496.2 MPa differs from those values by an average of 6.5 percent. Even in this simple linear form the residual strength model seems to agree reasonably well with single-level and two-level fatigue loading residual strength observations for the cases examined.

Having taken residual strength as the basis for equivalent damage, we can extract residual life predictions by observing that the life at stress amplitude S^k following $k-1$ blocks of spectrum fatigue loading will be defined by the point at which the residual strength is reduced to that stress (amplitude) value, i.e., the specimen will fail when $S_r^k = S^k$. Then, for example, equation (8) will become

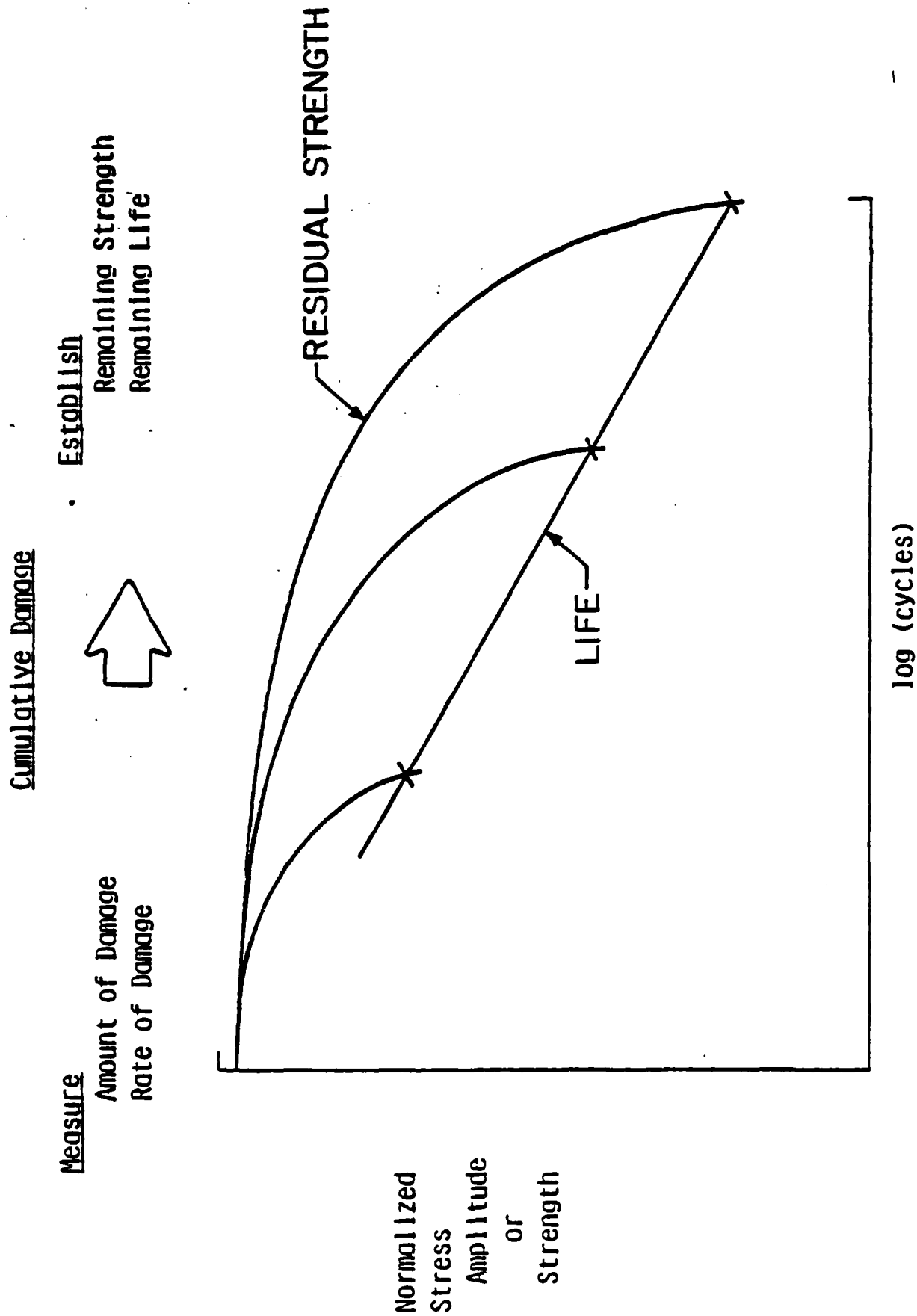


Fig. 71. Nonlinear approximations of the reduction of normalized residual strength.

Residual Strength Under Spectrum Loading

Low - High Sequence:

Low - 381.4 MPa for 90,000 cycles

High - 435.9 MPa for 7,000 cycles

Average measured residual strength 540 MPa

Predicted value

496.2 MPa

Percent discrepancy

8

High - Low Sequence

Reverse of above

Average measured residual strength 521 MPa

Predicted value

496.2 MPa

Percent discrepancy

5

Fig.72 . Residual strength observations and calculated values for two-step spectrum loading.

$$n^k = \left\{ 1 - \frac{\sum_{i=1}^{k-1} (S_{ult} - s^i) \frac{n^i}{\log^{-1} \left[\frac{B}{\frac{s^i}{S_{ult}} - A} \right]^{1/x}}}{S_{ult} - s^k} \right\} \log^{-1} \left[\frac{B}{\frac{s^k}{S_{ult}} - A} \right]^{1/x} \quad (10)$$

As stated in Fig. 73, the general consequence of this linear approximation, assuming that the SN relationship is nearly linear also, is that the sum

$$\sum_{i=1}^k \frac{n^i}{N^i} = \begin{cases} >1 & \text{for high-low sequences} \\ <1 & \text{for low-high sequences} \end{cases} \quad (11)$$

of spectrum loads. For more general forms of equation (10) it can be said that the sum of the cycle ratios will always be sequence dependent, i.e., will depend on the order of application of various blocks or components of the fatigue spectrum.

Figure 74 shows an example of residual life predictions for the two sequences discussed in Fig. 73. For the low-high sequence the calculated residual life is 9,375 cycles, 2,375 cycles greater than the cycles applied at that (final) stress level in the residual strength tests. The life for a constant amplitude of 381.4 MPa is about 276,200 cycles, and at 435.9 MPa it would be about 18,035 cycles. Hence, the sum of the cycle ratios is about 0.85. For the high-low sequence the predicted residual life at the second level of 381.4 MPa is 203,446 cycles, which is 113,446 cycles greater than the 90,000 cycles applied in the

FOR LIFE
After k-1 segments, Life at $s^k \rightarrow s^k_f \rightarrow s^k$
whereupon

$$n^k = \left\{ 1 - \frac{\left[\sum_{i=1}^{k-1} (S_{ult} - s^i) \frac{n_i}{\log^{-1} \left[\frac{B}{\frac{s^i}{S_{ult}}} - A \right]^{1/x}} \right]}{S_{ult} - s^k} \right\} \log^{-1} \left[\frac{B}{\frac{s^k}{S_{ult}}} - A \right]^{1/x}$$

which is sensitive to sequence

$$\sum_{N_1}^{N_1} = \begin{cases} > 1 & \text{for high-low sequence} \\ < 1 & \text{for low-high sequence} \end{cases}$$

Fig. 73. Linear approximation of residual life for spectrum loading.

Two-Step Spectrum

Low - High:

Stress Amplitude (MPa)

381.4

435.9

Cycles

90,000

9,375 predicted

$$\sum_1^n \frac{1}{N_1} = 0.85$$

High - Low

Stress Amplitude (MPa)

435.9

381.4

Cycles

7,000

203,446 predicted

$$\sum_1^n \frac{1}{N_1} = 1.12$$

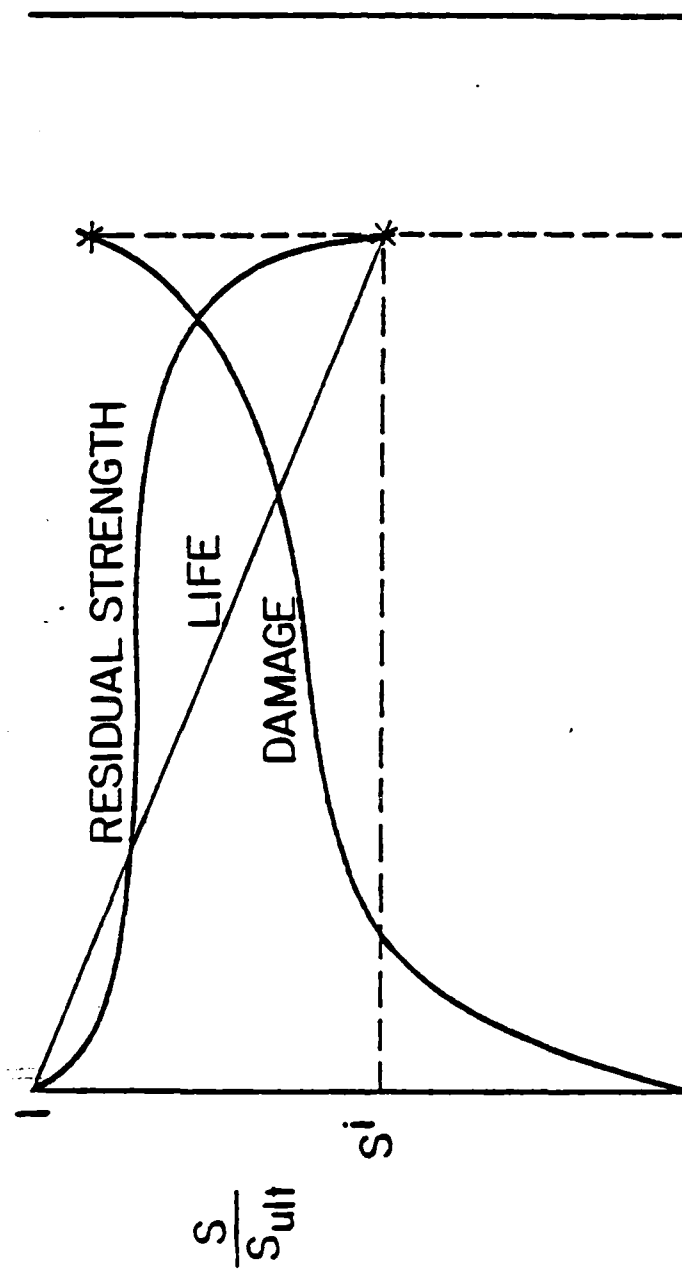
Fig. 74. Predicted residual lives for high-low and low-high spectral fatigue loading.

residual strength tests for this sequence. The sum of the cycle ratios for that sequence is predicted to be about 1.12. Unfortunately, no residual life data yet is available for direct comparison with these predictions. However, the predictions are consistent with the residual strength spectrum loading results in the sense that the calculated residual lives exceed the applied cycles by significant margins. The predicted cycle-ratio sums are also consistent with literature values (4). These sums are, of course, influenced by the relationship which describes the residual strength curve end points through the values of A, B and x, and by the form of the residual strength variation relationship. As we have said, the most basic pursuit of this research effort is to establish the residual strength variation with applied cycles. A more general form of such a relationship is

$$S_r^i = S_r^{i-1} - f(S^i, n^i, S_{ult})(S_{ult} - S^i) \frac{n^i}{N^i} \quad (12)$$

where S_r^{i-1} is the residual strength after $i-1$ blocks of spectrum loading have been applied and $f(S^i, n^i, S_{ult})$ is a "damage rate modifier," a normalized function that is an explicit function of the number of cycles, the applied stress amplitude and some set of material properties (S_{ult} has been used for illustration). Figure 75 shows a schematic representation of the concept involved in the damage rate modifier. For purposes of discussion, (examples will be provided later), the damage development is assumed to follow the curve marked "damage" in Fig. 75. For the situation shown, damage develops rapidly at the beginning of the test at amplitude S^i , levels off over some mid-range of cycles, and

Cumulative Damage
Specific account of damage



$\log N$

$$s_r^i = s_r^{i-1} - \underbrace{f(s_i^i, n_i^i, s_{ult})}_{\text{Damage Rate Modifier}} (s_{ult} - s_i^i) \frac{n_i^i}{N_i^i}$$

Damage Rate Modifier

Fig. 75. Damage rate modifier schematic representation.

risers rapidly again near the end of the life of the specimen. For such a damage development it is assumed that the residual strength changes in a nonlinear way as suggested by the "residual strength" curve in Fig. 75. The residual strength is assumed to drop initially, level off, and then decrease at a rapid rate near the end of the test. It should be noted that the drops in residual strength are proportional to the consequences of the damage which develops, i.e., while the damage curve may increase by a large amount, the residual strength (which will drop synchronously) may change only a small amount if the consequences of the particular type of damage that develops is small. Other scenarios with similar logic can be developed.

We now turn our attention to the specific question of residual life determination. Figure 76 shows a graphical sequence that illustrates an application of the philosophy to be used. Reading from the top of that figure, as a fatigue test progresses the change in specimen stiffness is measured. From that measurement, and an observation of the type of damage that is occurring, (ultimately the damage mode will be anticipated from quasi-static calculations), the internal stress redistributions can be determined from various models that have been developed under earlier contract and grant activities. Let us say that we make the premise that the 0 degree plies will control the laminate life. The stress redistribution will be interrogated to determine the stress state in the zero degree plies as a function of cycles. The degradation of the zero degree ply is then determined by assuming that such degradation is generic, i.e., that the zero degree plies degrade the same under a known stress state in all laminates. (There is good evidence to support

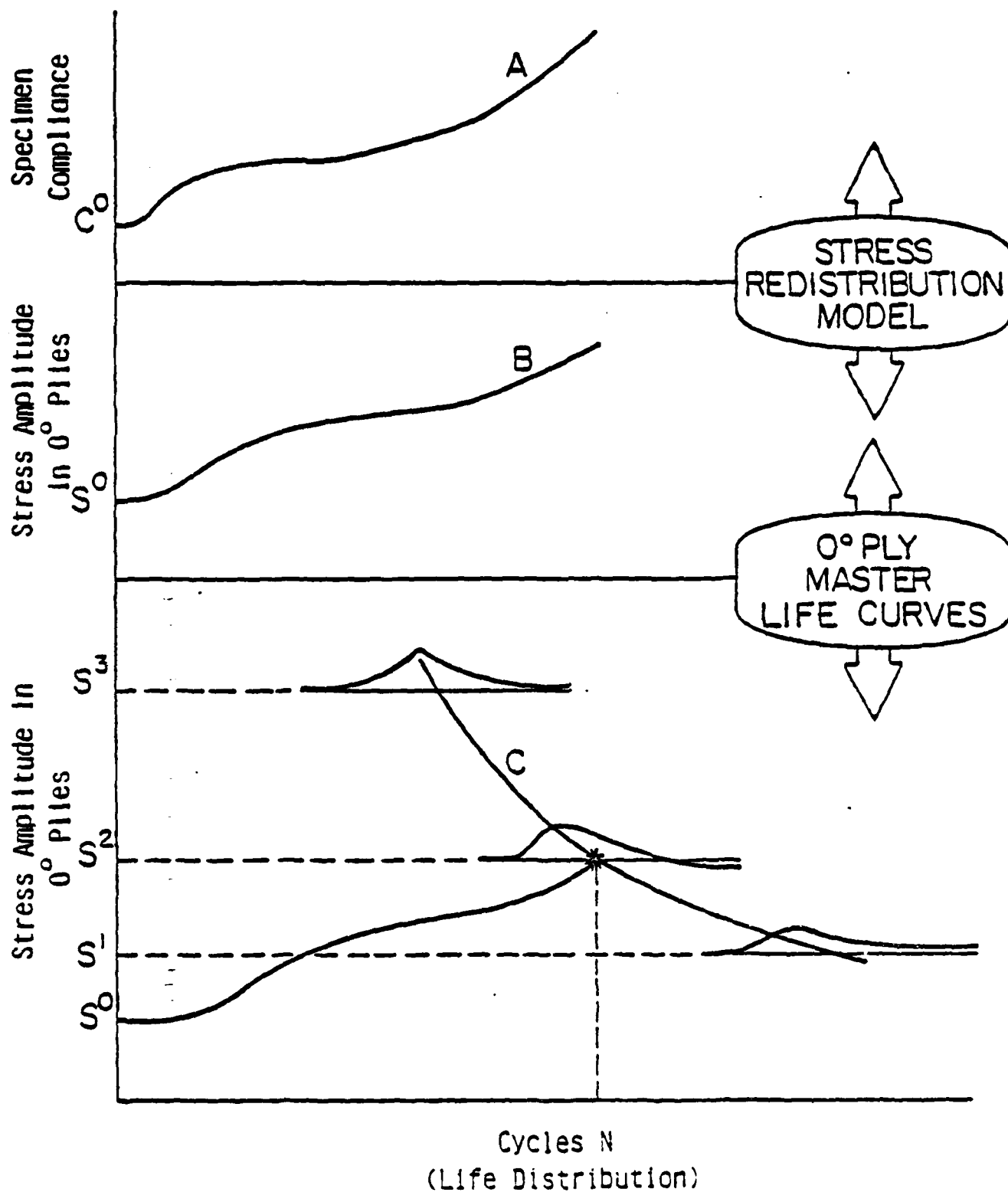


Fig.76. Modeling concepts for residual life determinations.

this assumption from our data and from the work of others (35,36). Then a life determination can be made as shown in the bottom of Fig. 76. A special-case reduced computational sequence is illustrated in Fig. 77. During the course of this investigation, precise and complete determinations of the type and amount of damage that occurs for several laminates during cyclic loading will be determined and correlated with the observed stiffness changes as part of the model development. When the development and refinements are complete, such details will be anticipated or "calculated" from the model itself.

Figure 78 is an expanded version of Fig. 76 showing the equation and relationships to be used in the residual strength and life calculations for our example calculation. Based on literature data and our experience, we assume that the 0 degree plies degrade according to the expression

$$S/S_{ult} = 1 - 0.07 \log N \quad (16)$$

Two points should be made regarding this assumption. Over the range of life between 3,000 and about 1×10^6 cycles this relationship is close to virtually all the data the authors have seen, for T300-5208; the variations from this expression are not large regardless of who obtained the data or how it was obtained. Second, if the final failure process of the 0 degree ply or plies was well established and understood it would not be necessary to use an assumed locus of the end points of the residual strength curves since we could proceed from fundamental developments. But such an understanding, or even a consistent and general representation, of the failure processes are not yet available. We are

TENSION-TENSION FATIGUE

Generic Information

S-N behavior of 0 degree plies

Static Calculations

Damage mode $\longrightarrow \Delta E_{IJ} \longrightarrow \Delta \sigma_{IJ}$ in 0 degree plies

Fatigue Observations

Damage rate (direct or from ΔE_{IJ} of laminate)

Fatigue Calculations

Residual Strength

Residual Life

Fig.77. Computational sequence for tension-tension fatigue.

TENSION-TENSION FATIGUE

Generic Information

$$S^o/S_u^o = A + \frac{B}{(\log N)^X}$$

Static Calculations

Matrix Cracking $\rightarrow E2, \delta \rightarrow 0$ in off-axis plies $\rightarrow \Delta S^o$ in fiber direction.

Fatigue Observations

Damage rate modifier $f(n, S^o(\text{applied})) = a + bn + cn^2 + dn^3 + en^4$

$$f(n, S^o) \Big|_{\max} = 1$$

143

For other stress levels $n \rightarrow S_t^{ns^o}(\text{test level})$

Fatigue Calculations

Stress in 0 degree ply as function of cycles

$$S^o = S^{\phi} + \Delta S^o f(n, S^o)$$

Residual Strength \rightarrow Life

$$\int_{S^r}^{S^u} dS = \int_0^n (S_u^o - S^o(n)) \frac{dn}{\log^{-1} \left[\frac{S^o(n)}{S_u^o} - A \right]^{1/X}}$$

Fig. 78 Computational relationships in sequence for residual property determination in tension-tension fatigue.

working very hard on that problem, as are numerous other investigators, but the philosophy is not yet available. Until such representations can be made with reliable and general applicability, we believe it is appropriate to use the fatigue response of the zero degree plies as a starting point. Our experience has shown us that it is relatively easy to obtain such a starting point and, in fact, we have developed schemes (to be discussed at a later time) for estimating the 0 degree fatigue response (at least in one dimension) from quasi-static data.

Having started with that generic information, we see (from Fig. 78) that the next step is to determine the magnitude of the stress change (in the fiber direction) in the zero degree plies as matrix cracking occurs in the off-axis plies of our $[0/90/\pm 45]_s$ laminate. We take these numbers from the simple ply-discount method for our example, a method which is known to give results that correlate well with experimental data for quasi-static strength calculations. The fiber-direction stress in the zero degree plies, normalized by the applied stress, is 2.73 initially. After all matrix cracking has occurred (and ply discount has been made) the normalized fiber-direction stress is 2.99. Hence, we take the magnitude of the stress redistribution to be 10 percent. Then, in Fig. 78, ΔS^0 will be equal to 10 percent of the initial stress in the zero degree plies when the stress amplitude is first applied to the laminate.

Referring again to Fig. 78, the next quantity that is needed is the damage rate function $f(n, S)$. As we mentioned earlier, during our model development we will make precise measurements of damage development to obtain the rate function $f(n, S)$. Subsequently, it will be implied from

stiffness change measurements. As suggested in Fig. 77, we make two assumptions for our example. We assume that $f(n,S)$ has some polymeric form (although a fourth order equation is shown, we ultimately used an exponential in the present example for added simplicity) and we normalize the function so that it becomes the modifier that determines the rate at which the maximum variation in internal stress occurs as a function of fatigue cycles.

For our example, we determine the damage rate modifier from crack density measurements as shown in Fig. 79. In that figure the (normalized) number of transverse matrix cracks in the 90 degree plies of a $[0/90/\pm 45]_S$ laminate under a constant stress amplitude of 289.5 MPa ($R=0.1$) was determined by two different investigators at different times, and are shown as the two broken curves in the figure. For simplicity, an exponential curve was fit to that data (with a correlation of 0.9) and is shown as the solid curve in Fig. 79. The equation so determined is

$$f(n, 289.5 \text{ MPa}) = \frac{\ln n + 1.67}{6.391} \quad (17)$$

As suggested in Fig. 78, a fourth order polynomial fit will give added fidelity to the experimental data. Then, the fiber direction stress in the zero degree plies of the $[0/90/\pm 45]_S$ laminate can be written as

$$S^0(n) = S^0 + \Delta S^0 f(n,S) \quad (18)$$

$$S^0(n) = S^0 \left(1 + 0.1 \left[\frac{\ln n + 1.67}{6.391} \right] \right) \quad (19)$$

where S^0 is the initial value of the stress (determined from quasi-static undamaged laminate analysis).

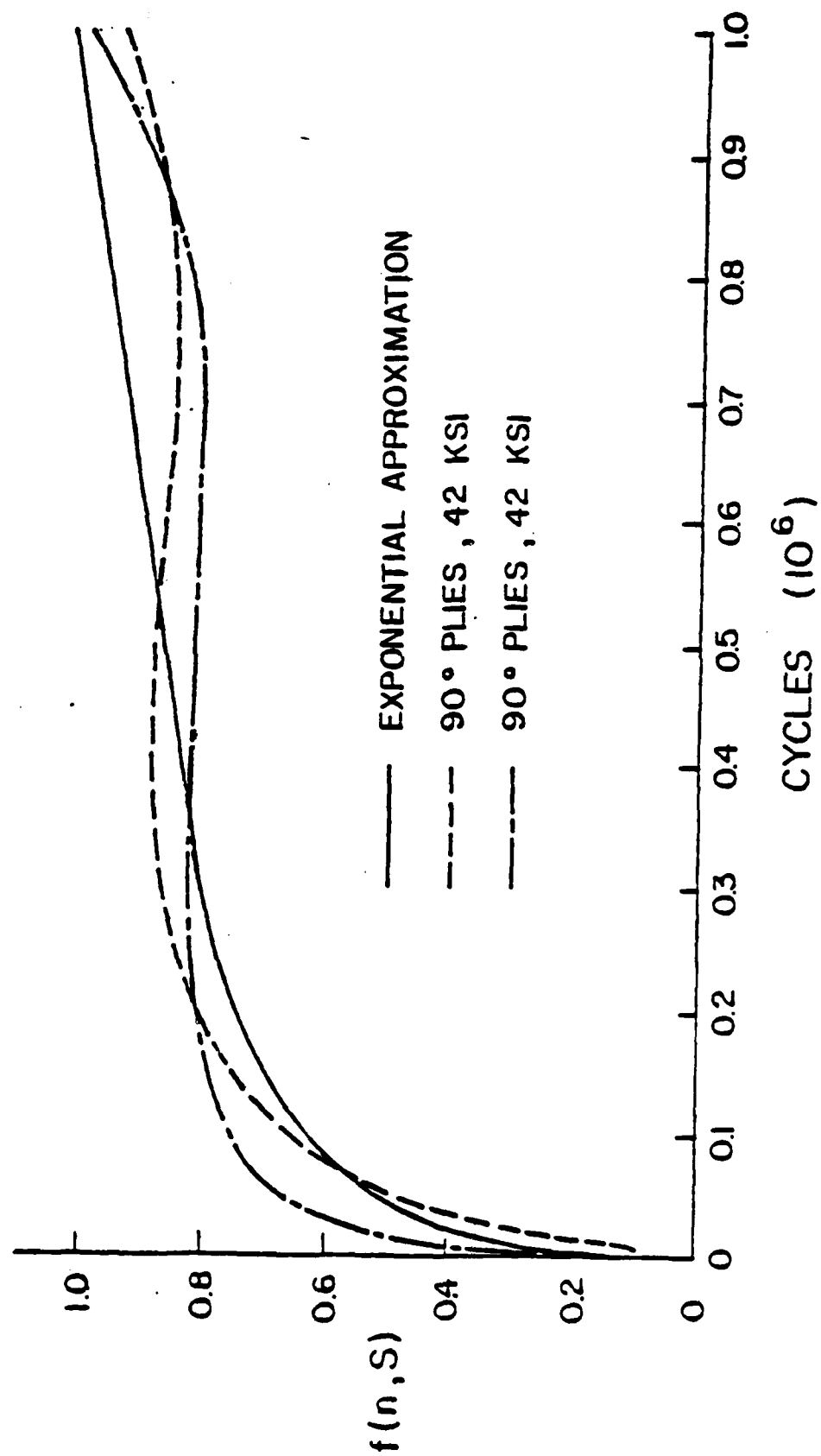


Fig. 79. Damage rate function as a function of cycles.

Since we now have a continuous function for the stress component in the 0 degree plies that we assume controls failure, we need an integral form for the residual strength equation, expression (5). Such an equation can be written as,

$$\int_{S_r^0}^{S_{ult}^0} dS = \int_0^n (S_{ult}^0 - S^0(n)) \frac{dn}{\log^{-1} \left[\frac{\frac{B}{S^0(n) - A}}{S_{ult}^0} \right]^{1/x}} \quad (20)$$

where $S^0(n)$ is given by equation (18). The right-hand side of equation (20) is difficult to integrate in closed form. Numerical integration was used for the present calculations.

For purposes of demonstration, let us say that a stress amplitude of 347.5 MPa is applied to our laminate, and we ask, "what is the residual strength curve and what is the life of the laminate?" We assume that the damage rate function is the same for this applied stress level as it was for the case for which damage was determined. (We chose 347.5 MPa arbitrarily, but with the idea of looking at results for shorter life tests.) Then the stress in the 0 degree plies in the fiber direction is initially 903.1 MPa. The strength of that ply is taken to be about 1496 MPa, so that $S^0/S_{ult}^0 = 0.6$. The integral equation (20) then becomes

$$\frac{S_r^0(n)}{S_{ult}^0} = 1 - \int_0^n \frac{1 - \left[0.6 + 0.06 \frac{(\ln n + 1.67)}{6.391} \right]}{\log^{-1} \left[\frac{1 - \left[0.6 - 0.06 \frac{(\ln n + 1.67)}{6.391} \right]}{0.07} \right]} dn \quad (21)$$

which is evaluated by numerical integration. The results are shown in Fig. 80. The residual strength curve is convex upward in a manner that had been anticipated earlier. However, the curvature is small since the magnitude of the stress redistribution was only 10 percent. The curve is also rather regular, not showing a distinct plateau in the mid-range as we might have expected. This, of course, is entirely controlled by the shape of the damage rate function which we took to be a very simple exponential, and the shape of the generic strength-life locus curve that is used for the 0 degree plies, which we took to be a very simple linear (in $\log N$) relationship.

The predicted life of 1.9×10^5 cycles compares well with the observed life of about 2×10^5 cycles at that applied stress level.

Although these sample calculations have been simplified for brevity, and although only tension-tension fatigue has been discussed in detail, the basic concepts are illustrated by the examples. We have generated a computer code which enables us to apply the general form of our model as described in Fig. 69. Preliminary calculations indicate that the model is realistic and workable.

6.3 Models for Compressive Loading

The damage which develops under compression-compression (C-C) loading has also been modeled as part of the present effort. Two types of damage modes dominate damage development under cyclic C-C loading. Both are delamination modes with one mode consisting of longitudinal growth and the other mode consisting of growth across the width of the specimens. In both instances, delaminations are seen to initiate at high interlaminar stress positions near the edge of the laminates as

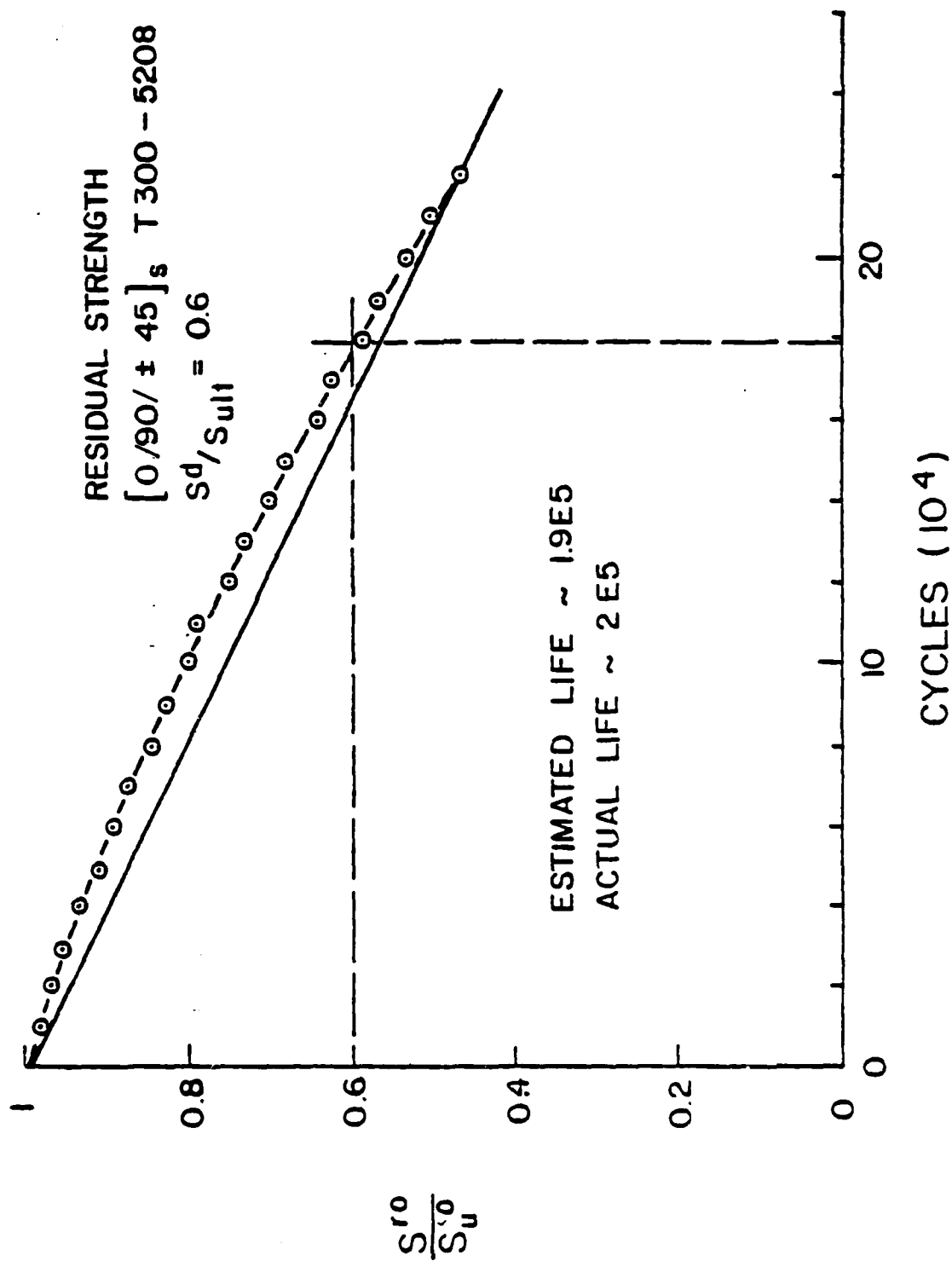


Fig. 80 . Residual strength curve and life calculation for T300-5208 $[0/90/\pm 45]_s$ laminate under tension-tension fatigue loading at a constant amplitude of 347.5 MPa.

schematically indicated in Fig. 81. The longitudinal and across-the-width growth of those delaminations is represented by two different models as described below.

The model used for longitudinal delamination growth is an adaptation of a philosophy generated by Chai, Babcock, and Knauss (private communication). The philosophy is based on the idealization of a delaminated region as sketched in Fig. 82. For an orthotropic strip, the critical strain for buckling to occur, using a wide column with clamped ends as an approximation to the buckled geometry, is given by equation (22)

$$\epsilon_{cr}^o = \frac{4\pi^2}{\ell^2} \frac{D_{xx}}{A_{xx}} \quad (22)$$

where the matrix D_{xx} and the matrix A_{xx} are the usual stiffness matrices of the buckled laminate portion. If a sinusoidal mode shape such as

$$w = \frac{A}{2} \left(1 + \cos \frac{2\pi x}{\ell} \right) \quad (23)$$

is assumed, the amplitude A of the buckling displacement can be determined from the condition that the difference between the strain in the buckled and unbuckled portions of the laminate times the length of the delaminated region must equal the difference in length between the buckled strip and the original length ℓ , as indicated in equation 24.

$$(\epsilon_x^o - \epsilon_{cr}^o) \ell = \int_{\ell/2}^{\ell/2} \sqrt{dx^2 + dy^2} - \ell \quad (24)$$

That identity produces an equation in the square of the magnitude A ,

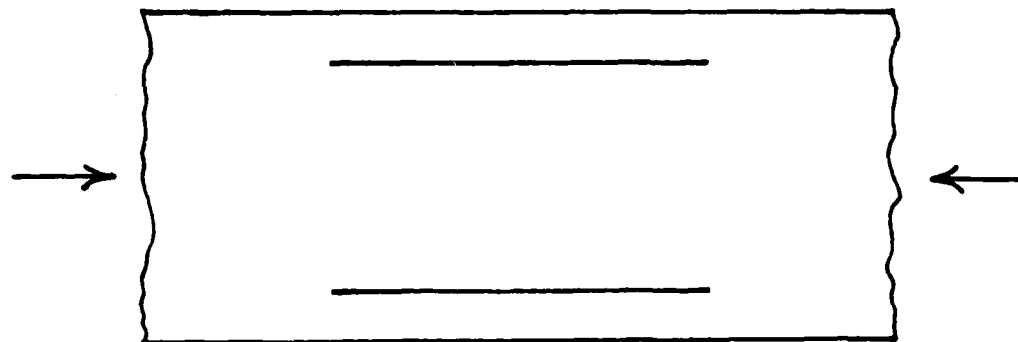


Figure 81. Edge view of laminate loaded in cyclic compression showing delamination near the specimen surfaces.

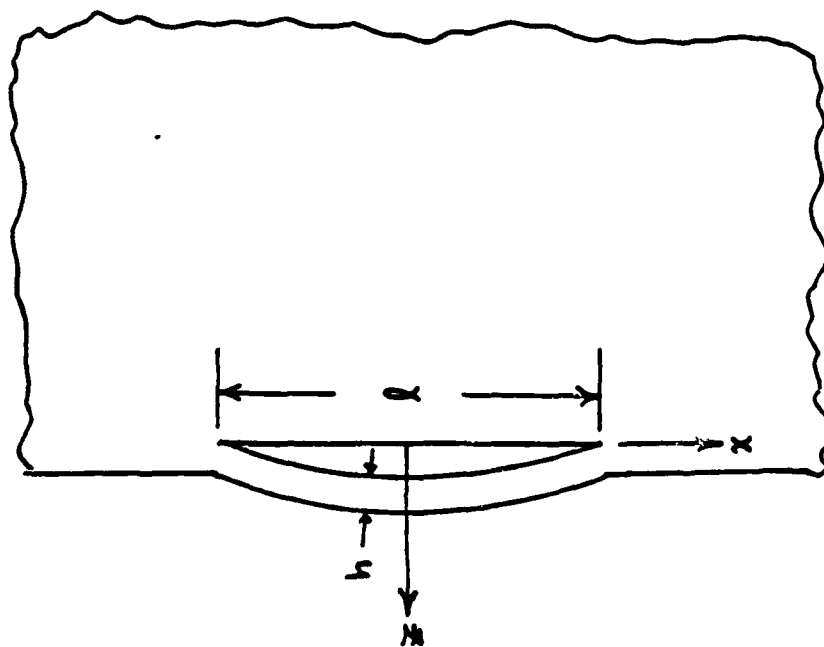


Figure 82 Idealized longitudinal delamination schematic.

$$A^2 = (\epsilon_x^o - \epsilon_{cr}^o) \left(\frac{2l}{\pi} \right)^2 \quad (25)$$

One can write the energy in the buckled strip as

$$\begin{aligned} U &= \frac{1}{2} \int_{Area} A_{xx} \left(\frac{du^o}{dx} \right)^2 d Area + \frac{1}{2} \int_{Area} D_{xx} \left(\frac{d^2 w}{dx^2} \right)^2 d Area \\ &= \frac{4D_{xx}}{l} \frac{2\pi^4 D_{xx}}{l^2 A_{xx}} + (\epsilon_x^o - \frac{4\pi^2 D_{xx}}{l^2 A_{xx}}) \end{aligned} \quad (26)$$

where the A and D matrices are the same stiffness matrices mentioned earlier, and u^o and w are the x and z displacements, respectively. Considering the energy stored before buckling, one can then write the energy release for an increment of increase, dl , of buckled strip length as

$$\frac{dU}{dl} = \epsilon_x^{o2} \frac{A_{xx}}{2} + \epsilon_x^o \frac{4D_{xx}}{l^2} + \frac{1864D_{xx}^2}{l^4 A_{xx}} \quad (27)$$

where ϵ_x^o is the unbuckled laminate applied strain.

Some of the general features of this model are illustrated by Figs. 83 and 84. Figure 83 indicates that as the buckled ligament grows in length, the buckling load required to cause the ligament to buckle away from the remainder of the laminate decreases. Figure 84 indicates that the buckling load increases for an increase in the ligament thickness. Equation 27 suggests that the driving force for longitudinal delamination growth is proportional to the uniaxial extensional stiffness and bending stiffness of the buckled ligament, and is a quadratic

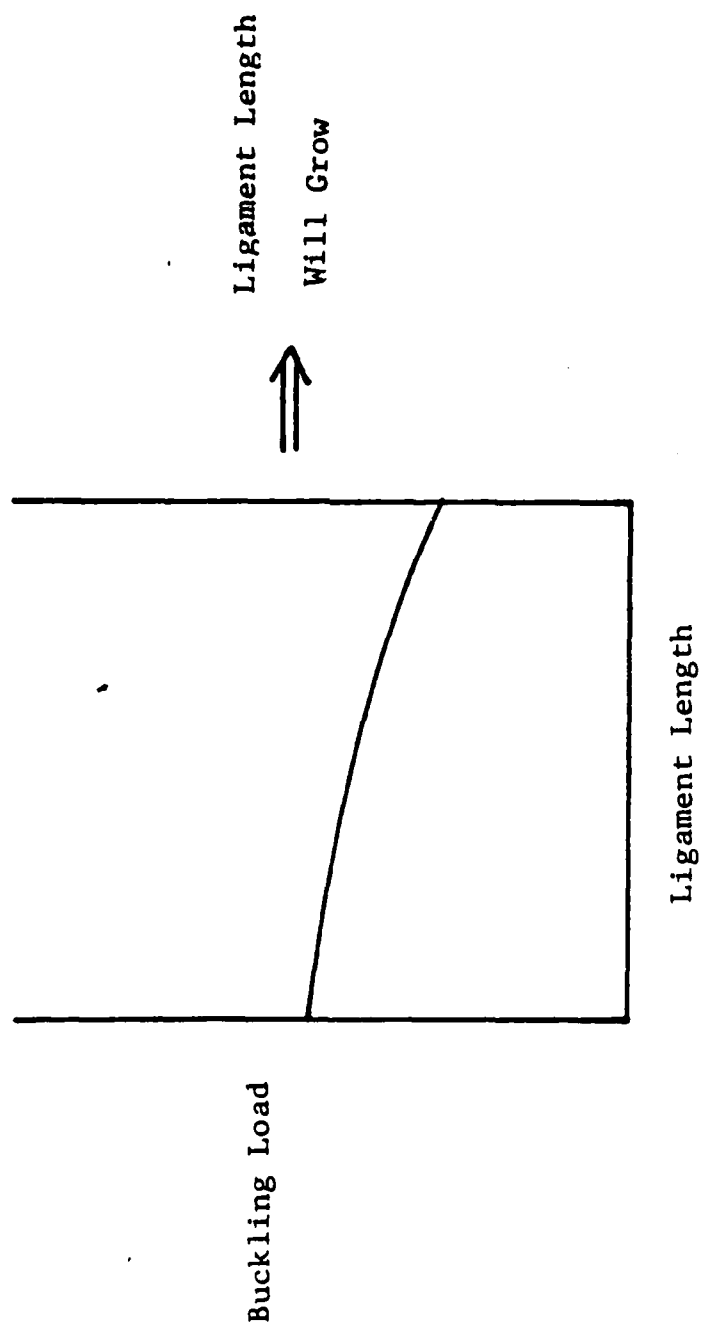


Figure 83. Dependence of longitudinal delamination growth on ligament length.

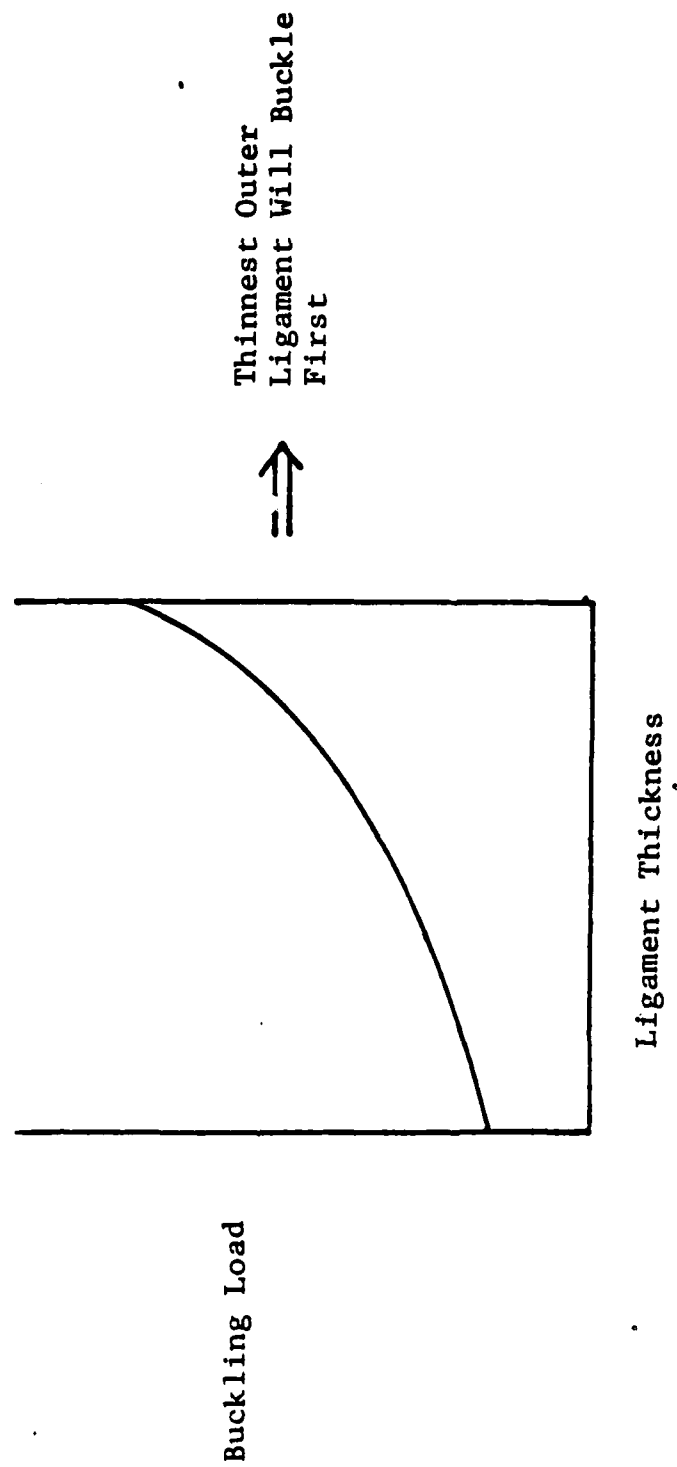


Figure 84. Dependence of longitudinal delamination growth on ligament thickness.

function of the applied laminate strain ϵ_x^0 . Taken together, the implications of the model can be interpreted as a prediction of delamination growth that is shown in Fig. 85. Reading from left to right in that figure, it is expected that delamination will initiate in the thinnest possible ligament which terminates in the first high-interlaminar stress interface in from the exterior surface of the laminate as suggested by the diagram on the left of Fig. 85. The first delamination will grow along the length driven by the strain energy release for that growth and by the fact that the longer delaminated ligament length will buckle more easily than their shorter predecessors. At the same time, new delaminations will initiate at the next high-interlaminar stress interface in from the exterior surface of the specimen as suggested by the middle diagram in Fig. 85. This process will continue with initiation continuing to grow into the interior of the thickness and delamination growth continuing to occur along the length of the specimen. These predictions are quite consistent with the observations of damage growth and initiation that we have made under C-C cyclic loading.

The delamination problem is complicated by the fact that delamination grows in both the longitudinal and the across-the-width direction. We shall call this latter type of growth transverse growth. The model of delamination growth in the transverse direction is an adaptation of the model provided by O'Brien (40), which is based on two concepts illustrated in Figs. 86 and 87. O'Brien found that there was a linear relationship between the length of edge delamination growth and longitudinal stiffness (Young's modulus) change as illustrated by the simple analytical relationship and experimental data in Fig. 86. Hence, it is

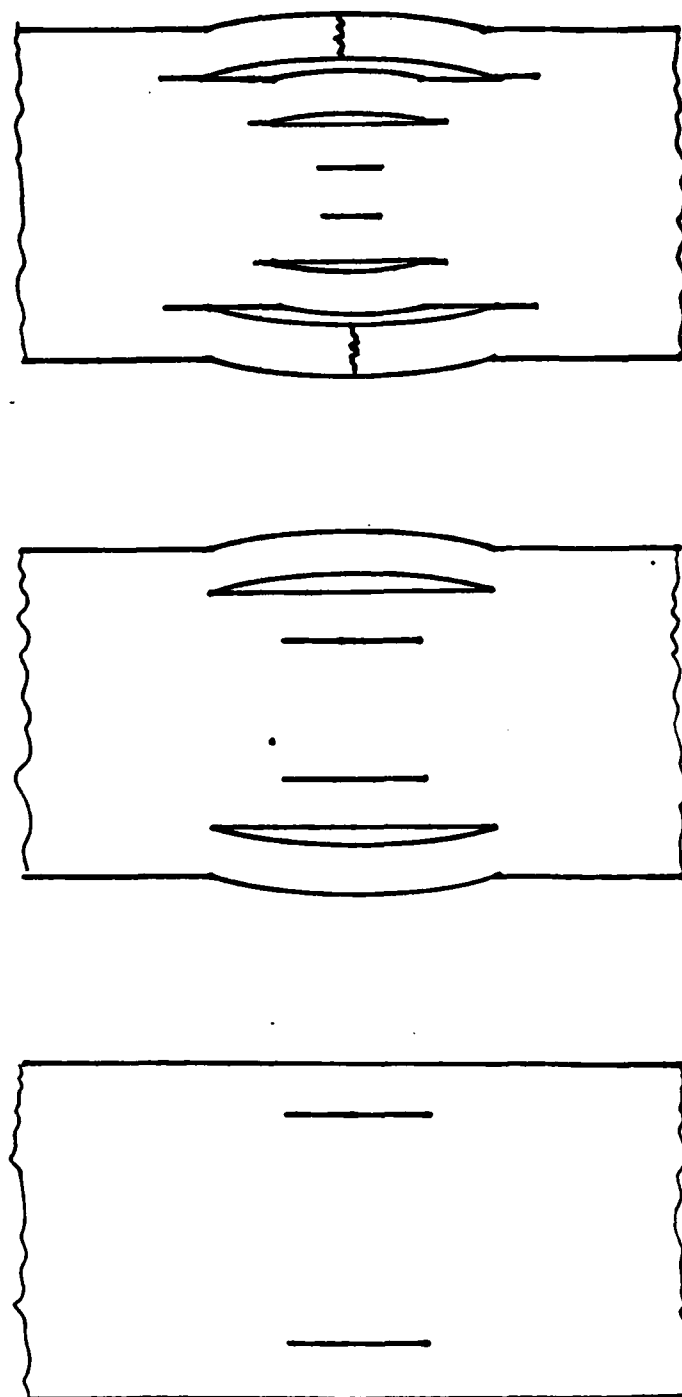


Figure 85 . Schematic of predicted longitudinal delamination growth pattern.

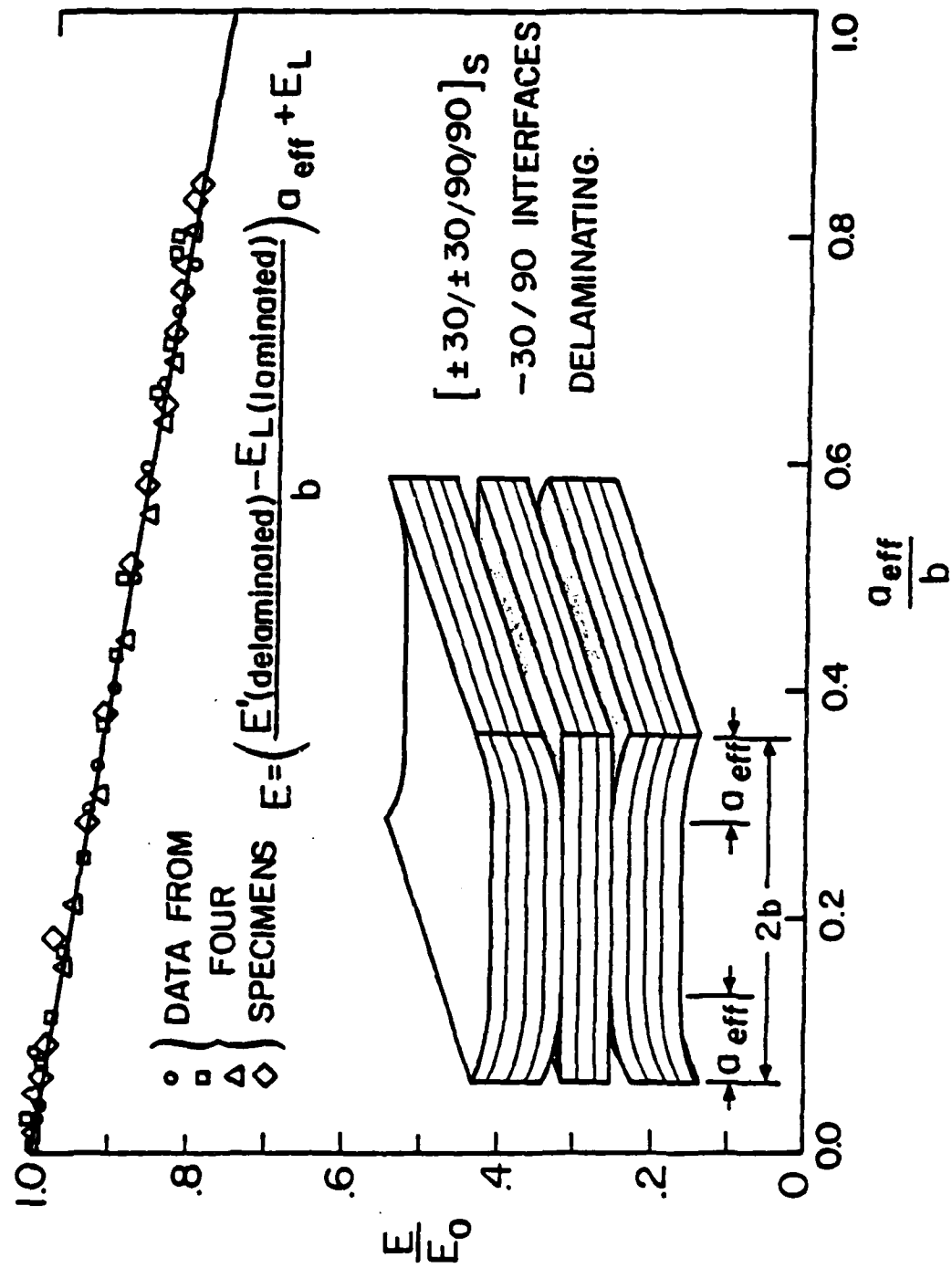


Figure 86. Delamination growth across the specimen width and the attendant stiffness change as described by O'Brien.

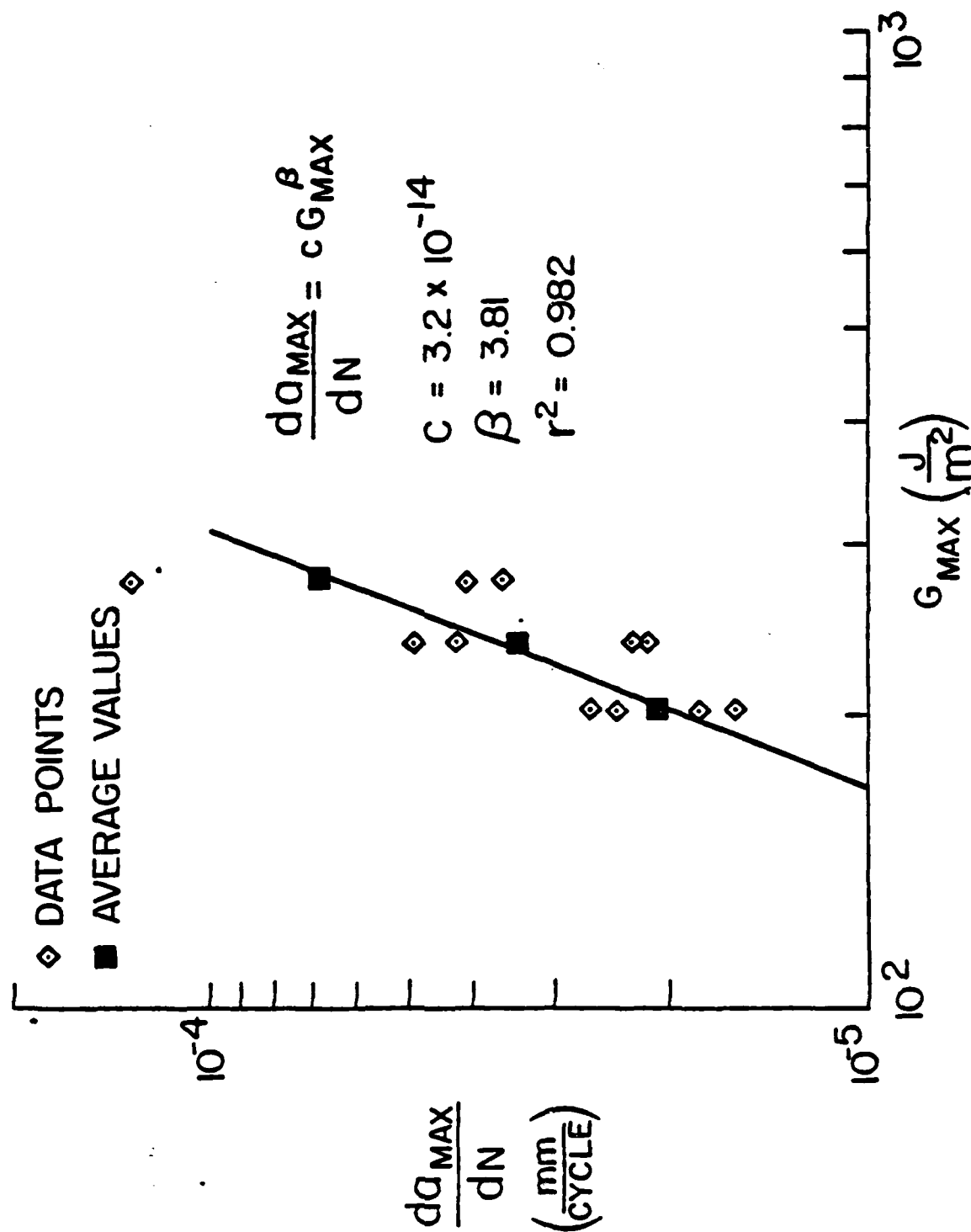


Figure 87 . Proportionality between total strain energy release rate and across-the-width delamination growth rate as described by O'Brien.

possible and feasible to follow the growth of edge delamination by following longitudinal stiffness. O'Brien also found that the rate of transverse delamination growth was proportional to the total strain energy release rate as portrayed in Fig. 87. The material constants, C , and β , in Fig. 87 apply to the graphite epoxy laminate described in Fig. 86. O'Brien has shown that the correlation between the analytical predictions based on this model and several sets of experimental data are excellent.

These equations, along with our basic model (Fig. 69) are used to anticipate longitudinal and transverse delamination growth based on information regarding delamination initiation. The eventual "failure" of the unbuckled laminate is assumed to occur by buckling instability or by tensile fracture. The delamination that occurs is used to anticipate the remaining buckling resistance of the laminate by altering the elements of the D matrix in an appropriate fashion and using the resulting values in an appropriate buckling criteria such as that shown in equation (28):

While the results of this modeling effort correlate well with the observations presently available, a development of the models for C-C fatigue loading is not yet complete. One of the most difficult questions yet to be addressed is the nature of the coupling of growth in the longitudinal direction and the transverse direction. While it is certainly possible to assume at the onset that each of those growth processes can be treated independently, it is hardly likely that such is the case for real situations. It is also true that the complexity of the general situation for arbitrary laminates is very great, and it is

difficult to view even a successful effort at modeling laboratory specimens in the context of the fatigue performance of large structural components where edge effects are certainly less generic to the fatigue behavior and performance. Nevertheless, the basic elements of a rational model appear to be available and progress in the interpretation of that part of the model and the experimental results can be reported.

REFERENCES

1. Boller, K. H., "Effect of Single Change in Stress on Fatigue Life of Plastic Laminates Reinforced with Unwoven E Glass Fibers," Technical Report AFML-TR-66-220, (Dec. 1966).
2. Hofer, K. E., Jr. and Olsen, E. M., "An Investigation of the Fatigue and Creep Properties of Glass Reinforced Plastic for Primary Aircraft Structures," AD-652415, IIT Research Institute, Chicago, IL.
3. Broutman, L. J. and Sahu, S., "Progressive Damage of a Glass-Reinforced Plastic During Fatigue," 24th Annual Technical Conference, Reinforced Plastics/Composites Dir., SPI, (1969).
4. Broutman, L. J. and Sahu, S., "A New Theory to Predict Cumulative Fatigue Damage in Fiberglass Reinforced Plastics," Composite Materials: Testing and Design (Second Conference), ASTM STP 497, ASTM (1972) pp. 170-188.
5. Halpin, J. C., et al., "Characterization of Composites for the Purpose of Reliability Evaluation," AFML-TR-77-289, (1972) WPAFB, OH.
6. Halpin, J. C., Johnson, T. A. and Waddoups, M. R., "Intern. J. of Fracture Mechanics, Vol. 8 (1972) pp. 465-472.
7. Hahn, H. T. and Kim, R. Y., "Proof Testing of Composite Materials," J. Comp. Mat., Vol. 9 (1975) pp. 297-311.
8. Hahn, H. T. and Kim, R. Y., "Fatigue Behavior of Composite Laminate," J. Comp. Mat., Vol. 10 (1976) pp. 156-179.
9. Chou, P. C. and Croman, R., "Residual Strength in Fatigue Based on the Strength-Life Equal Rank Assumption," J. Comp. Mat., Vol. 12, (April 1978) pp. 177-194.
10. Tateishi, Tatsuya, "Continuum Theory of Cumulative Damage," Bulletin of the JSME, Vol. 19, No. 135 (1976) pp. 1007-1018.
11. Private correspondence.
12. Yang, J. N. and Liu, M. D., Journal of Composite Materials, Vol. 11, (1977), pp. 176-203.
13. Yang, J. N., Journal of Composite Materials, Vol. 12, (Jan. 1978), pp. 19-29.
14. Yang, J. N. and Jones, D. L., Journal of Composite Materials, (Oct. 1978) pp. 371-389.

15. Yang, J. N. and Jones, D. L., Proc. AIAA/ASME/ASCE/ASH 20th Structures, Structural Dynamics and Materials Conference, (April 1979), pp. 232-239.
16. Hahn, H. T., "Fatigue Behavior and Life Prediction of Composite Materials," AFML-TR-78-43, (1978), WPAFB, OH.
17. Chou, P. C. and Croman, R., "Degradation and Sudden-Death Models of Fatigue of Graphite Epoxy Composites," Proc. Symposium on Composite Materials: Testing and Design, ASTM, (March 20, 1978) New Orleans, LA.
18. Hashin, Z. and Rotem, A., "A Cumulative Damage Theory of Fatigue Failure," Materials Science and Engineering, Vol. 34 (1978), pp. 147-160.
19. Fukuda, H., Chou, T. W. and Kawata, K., "Probabilistic Approach on the Strength of Fibrous Composites," Composite Materials, K. Kawata and T. Akasaka, Eds., Proc. Japan-U.S. Conf., (1981) Tokyo.
20. Reifsnider, K. L. and Highsmith, A., "The Relationship of Stiffness Changes in Composite Laminates to Fracture-Related Damage Mechanisms," Proc. of 2nd USA-USSR Symposium on Fracture of Composite Materials, Lehigh University (March 1981), pp. 9-12.
21. Reifsnider, K. L., Proceedings, 14th Annual Meeting of Society of Engineering Science, Lehigh University, Bethlehem, PA, (Nov. 14-16, 1977) pp. 373-384.
22. Kriz, R. N., Stinchcomb, W. W. and Tenney, D. R., "Effects of Moisture, Residual Thermal Curing Stresses and Mechanical Load on the Damage Development in Quasi-Isotropic Laminates," VPI-E-80-5, College of Engineering, Virginia Polytechnic Institute and State University (Feb. 1980).
23. Stinchcomb, W. W., Reifsnider, K. L., Yeung, P. and O'Brien, T. K., "Investigation and Characterization of Constraint Effects on Flaw Growth During Fatigue Loading of Composite Materials," Final Report, NASA Grant NSG-1364, Virginia Polytechnic Institute and State University (March 1979).
24. Reifsnider, K. L. and Talug, A., "Analysis of Fatigue Damage in Composite Laminates," International J. of Fatigue (Jan. 1980), pp. 3-11.
25. Reifsnider, K. L., Stinchcomb, W. W. and Henneke, E. G. II, "Defect-Property Relationships in Composite Laminates," AFML-Technical Report 76-81, Part III (April 1979).
26. O'Brien, T. K. and Reifsnider, K. L., "Fatigue Damage: Stiffness/Strength Comparisons for Composite Materials," J. of Testing and Evaluation, Vol. 5, No. 5 (1977), pp. 384-393.

27. Yeung, P. C., Stinchcomb, W. W. and Reifsnider, K. L., "Characterization of Constraining Effects on Flaw Growth," Nondestructive Evaluation and Flaw Criticality for Composite Materials, STP 696, P. B. Pipes, Ed., American Society for Testing and Materials (1979).
28. Highsmith, A. and Reifsnider, K. L., "Stiffness Reduction Mechanisms in Composite Laminates," Proc. ASTM Conf. on Damage in Composite Laminates, Bal Harbour, FL (Nov. 12-14, 1980).
29. O'Brien, T. K., "An Evaluation of Stiffness Reduction as a Damage Parameter and Criterion for Fatigue Failure in Composite Materials," Ph.D. Dissertation, Virginia Polytechnic Institute and State University (1978).
30. Reifsnider, K. L., Stinchcomb, W. W. and O'Brien, T. K., "Frequency Effects on a Stiffness-Based Fatigue Failure Criterion in Flawed Composite Specimens," in "Fatigue of Filamentary Composite Materials," K. L. Reifsnider and K. N. Lauraitis, Eds., ASTM STP-636, American Society for Testing and Materials, Philadelphia (1977).
31. Whitney, J. M. and Nuismer, R. J., "Stress Fracture Criteria for Laminated Composites Containing Stress Concentrations," J. of Comp. Mat'l's., Vol. 8, No. 2 (1974) p. 253.
32. Hofer, K. E. Jr., Larson, D. and Humphreys, V. E., "Development of Engineering Data on the Mechanical and Physical Properties of Advanced Composite Materials," AFML-TR-74-266, Air Force Materials Laboratory, Wright Patterson AFB, OH (1975).
33. O'Brien, T. K., "Stiffness Change as a Nondestructive Damage Measurement," Mechanics of Nondestructive Testing, W. W. Stinchcomb, Ed., Plenum Press (1980) pp. 101-122.
34. O'Brien, T. K. and Reifsnider, K. L., "Fatigue Damage: Stiffness/Strength Comparisons for Composite Materials," J. of Testing and Evaluation, Vol. 5, No. 5 (1979) pp. 384-393.
35. Highsmith, A. and Reifsnider, K. L., "Stress Redistribution in Composite Laminates," Composites Technology Review, Vol. 3, No. 1 (1981) pp. 32-34.
36. Hahn, H. T. et al., "Flywheel Materials Technology: Design Data for Composite Materials," UCRL-15365, Vol. 7, Lawrence Livermore National Laboratory (1981).
37. Hahn, H. T. and Kim, R. V., "Fatigue Behavior of Composite Laminates," J. Composite Materials, Vol. 10 (April 1976) pp. 156-180.
38. Highsmith, A. L., "Stiffness Reduction from Transverse Cracking in Fiber Reinforced Composite Laminates," Thesis for Master of Science, College of Engineering, Virginia Polytechnic Institute and State University, (Aug. 1981).

39. Jamison, R. D., Highsmith, A. L. and Reifsnider, K. L., "Strain Field Response of 0° Glass/Epoxy Composites Under Tension," Composites Technology Review, Vol. 3, No. 4 (1981) pp. 158-159.
40. O'Brien, T. K., "Stiffness Change as a Nondestructive Damage Measurement," Mechanics of Nondestructive Testing, W. W. Stinchcomb, Ed., Plenum Press, N.Y. (1980).

APPENDIX A

Quality Assurance Plan

Uniformity in specimen material quality and minimization of property variations due to unknown defects in materials and processes are key elements for the successful achievement of the objectives in this program. These prerequisites are a paramount condition for the observation and monitoring of damage accumulation as well as the subsequent model development. General Dynamics has developed quality control (QC) procedures and nondestructive evaluation (NDE) techniques that permit continuous surveillance of the manufacture of graphite epoxy composite components from incoming raw material to the stage of finished specimens ready to be tested. The quality assurance plan proposed for use in the Cumulative Damage Model program is outlined below.

Procurement Quality Assurance (PQA) Inspection

The established PQA procedures for incoming graphite-epoxy composite materials in the F-16 production will be followed in the QA plan for the specimens fabricated for this program. General Dynamics Specification FMS-2023C establishes the minimum requirements for graphite-fiber-reinforced epoxy laminating materials for primary aircraft structure. Prepreg inspection and mechanical property requirements on the supplier and on General Dynamics for acceptance will be controlled by that specification and FPS-2003, "Advanced Composite Materials Test Specification".

Under these procedures, the material is dated for age control, inspected for in-transit damage, and inspected for transit temperatures by means of a thermograph. The batch roll and test report numbers are recorded. Procurement acceptance tests include chemical and mechanical characterizations. In the chemical characterization, the tack, gel time and moisture content are measured. In addition to this data, the in-coming materials are characterized via high pressure liquid chromatography (HPLC) for formulation, resin advancement, and contaminants. The mechanical characterization consists of measuring the following properties: 0° flexural strength at room temp. (R.T.) and 450°K (350°F), 0° flexural modulus at R.T., 90° flexural strength at R.T. and 450°K, and horizontal shear strength at R.T. and 450°K.

In-Process Control/Inspection Plan

A set of rigid QA procedures used in F-16 production to track the processing of laminates and specimens through all the manufacturing steps will be applied to the laminates investigated in this program. The major monitoring steps are: (1) Sensing of pre-preg tape flaws and foreign materials during tape layup, (2) Curing of composite part with recording of cure cycle parameters, and (3) production-type ultrasonic inspection.

General Dynamics Specification FPS-2021C establishes the requirements for lay-up, inspection, and cure of laminates using FMS-2023 materials. Ply inspection, lay up, preparation for cure, storage, cure cycle temperature and pressure profile control, and documentation will be controlled by that specification and FPS-2002B, "Process and Quality Control of Adhesive Bonded Boron and Graphite Composite Assemblies."

As a first step of processing after the raw materials leave the cold storage, they are allowed to warm for eight hours minimum at room temperature before use. During the lay-up, room temperature will be maintained at $75^{\circ} \pm 5^{\circ}\text{F}$ and relative humidity maintained below 45 percent. In the tape laying operation, gaps (separation between two courses of tape) are monitored to ensure that there is no gap greater than .10 in. in width and in excess of 2 in. in length. Overlaps of adjacent courses of tape are generally acceptable in production practice provided they do not exceed 0.1 in. However, the overlaps are generally corrected by stripping off the overlap portion to eliminate a magnified seam buildup in succeeding plies. No wrinkles or protrusions exceeding 0.06 in. from the surfaces are permitted. Tape splices across the width of tapes are not allowed in the laminate. The orientation of each course in a ply must be within 5 degrees of the specified orientation. No foreign materials of any nature are permitted in the laminate. Possible solid and liquid contaminants include dust, tape, release agents, and separator paper. Lay-up of each ply is visually monitored to ensure that there are no inclusions in the laminates.

After the appropriate preparations are completed for the laminates, they are cured by the procedures depicted in Figure A1. The temperature and pressure values at various steps in the curing cycle are monitored automatically to form part of the laminate's record in the QA Plan. Upon completion of the curing cycles, the laminates are removed from the curing mold for a thickness check. Measurements

General Dynamics
Fort Worth Division

May 11, 1981
Engineering
Chemistry Lab.

COMPOSITE PANEL FABRICATION

Job Number: C 1425
Material: ASI/3502
Batch/Roll: B 1851/10A3+23A1
Panel No: 1
Panel Type: Thick Lam.
Cure Cycle: FPS 4589, Para. 6.4.2
Test Conductor: NJN
Time started: 13:46

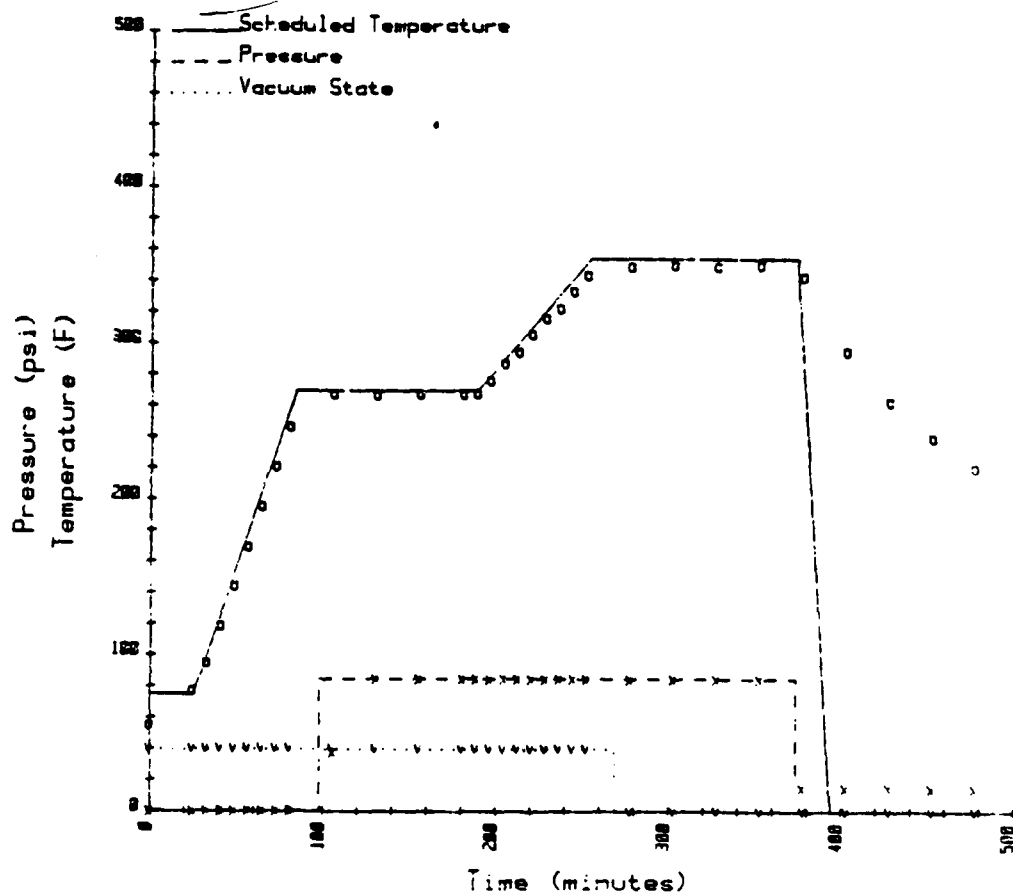


Figure A-1 Time-Temperature-Pressure Monitoring Results

will be made at 2-in. intervals to ensure a uniform laminate thickness. Each laminate is then visually inspected to ensure that it is free of blisters and wrinkles to the process specification.

Each laminate will be nondestructively tested over its entire surface area for anomalous indications that may be characteristic of internal planar voids, delaminations, foreign material, and porosities. An ultrasonic technique will be used in this in-process control step. This technique will employ the reflector plate pulse-echo method to provide a real time C-scan recording as a permanent record of the quality of the laminate. Anomalies revealed in the inspection will be resolved by a high-resolution ultrasonic technique which is a contact mode of inspection. Areas of the laminate which are of questionable quality will be outlined and specimens will be fabricated from the acceptance areas.

Post-Process NDT

In addition to the production-type inspection performed on the cured laminates as a part of the in-process QA plan, NDT techniques will be used to further characterize the initial quality of the specimens as a post-process inspection. This will further ensure that property variations due to unknown defects in the material and in the processing have been minimized. It will also clearly define the baseline damage state of the specimens so that a practical zero damage state may be established in accordance with the methodology in the cumulative damage model.

This will include visual and optical examination of each test specimen for:

- (1) General Appearance
 - Peel ply removal, disfiguration or distortion, uniform thickness and width, scratch or scribe marks, unusual discoloration
- (2) Edge Conditions
 - Smooth, parallel edges, no nicks or scratches, displaced or pulled-out fibers
- (3) Proper Lay-Up and Number of Plies

Two NDE techniques, edge replication and DIB enhanced X-ray radiography will also be employed to inspect the test

specimens. These techniques will define and characterize edge damage incurred while the specimens were being machined. This will also provide a baseline for NDE monitoring of the damage developed in the specimens when they are loaded.

An additional part of this post process NDE characterization will include specimen dimensional characterization. This will entail measuring the specimen width at three locations in the gage section and measuring the specimen thickness at six locations in the gage section. The fiber and resin content of the cured laminates will also be determined to further define the specimens.

Permanent records of all the QA inspection steps outlined above will be maintained in a manner such that each specimen can be traced back to the prepreg tape stage.

